



**INSTITUTO POTOSINO DE INVESTIGACIÓN  
CIENTÍFICA Y TECNOLÓGICA, A.C.**

**POSGRADO EN CIENCIAS APLICADAS**

**Dynamical Equivalence in Chemical Reaction Networks**

Tesis que presenta

**José Martín Méndez González**

Para obtener el grado de

**Doctor en Ciencias Aplicadas**

En la opción de

**Control y Sistemas Dinámicos**

**Director de la Tesis:**

Dr. Alejandro Ricardo Femat Flores

San Luis Potosí, S.L.P., Agosto de 2012



### *Constancia de aprobación de la tesis*

La tesis *Dynamical Equivalence in Chemical Reaction Networks*, presentada para obtener el Grado de Doctor en Ciencias Aplicadas en la opción Control y Sistemas Dinámicos fue elaborada por **José Martín Méndez González** y aprobada el **17 de Agosto de 2012** por los suscritos, designados por el Colegio de Profesores de la División de la División de Matemáticas Aplicadas del Instituto Potosino de Investigación Científica y Tecnológica, A.C.

---

Dr. Alejandro Ricardo Femat Flores  
(Director de la tesis)

---

Dr. Juan Paulo García Sandoval  
(Sinodal)

---

Dr. Eric Campos Cantón  
(Sinodal)

---

---

Dr. Edgar Moctezuma Velázquez  
(Sinodal)

---

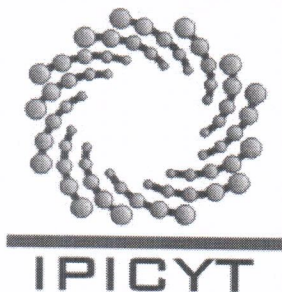
Dr. Juan Gonzalo Barajas Ramírez  
(Sinodal)



### *Créditos Institucionales*

Esta tesis fue elaborada en la División de Matemáticas Aplicadas del Instituto Potosino de Investigación Científica y Tecnológica, A.C., bajo la dirección del Dr. Alejandro Ricardo Femat Flores.

Durante la realización del trabajo el autor recibió una beca académica del Consejo Nacional de Ciencia y Tecnología No. 27142 y apoyos del Instituto Potosino de Investigación Científica y Tecnológica, A. C.



# Instituto Potosino de Investigación Científica y Tecnológica, A.C.

## Acta de Examen de Grado

El Secretario Académico del Instituto Potosino de Investigación Científica y Tecnológica, A.C., certifica que en el Acta 012 del Libro Primero de Actas de Exámenes de Grado del Programa de Doctorado en Ciencias Aplicadas en la opción de Control y Sistemas Dinámicos está asentado lo siguiente:

En la ciudad de San Luis Potosí a los 17 días del mes de agosto del año 2012, se reunió a las 17:00 horas en las instalaciones del Instituto Potosino de Investigación Científica y Tecnológica, A.C., el Jurado integrado por:

<b>Dr. Edgar Moctezuma Velázquez</b>	<b>Presidente</b>	<b>UASLP</b>
<b>Dr. Alejandro Ricardo Femat Flores</b>	<b>Secretario</b>	<b>IPICYT</b>
<b>Dr. Eric Campos Cantón</b>	<b>Sinodal</b>	<b>IPICYT</b>
<b>Dr. Juan Gonzalo Barajas Ramírez</b>	<b>Sinodal</b>	<b>IPICYT</b>
<b>Dr. Juan Paulo García Sandoval</b>	<b>Sinodal externo</b>	<b>UdG</b>

a fin de efectuar el examen, que para obtener el Grado de:

**DOCTOR EN CIENCIAS APLICADAS  
EN LA OPCIÓN DE CONTROL Y SISTEMAS DINÁMICOS**

sustentó el C.

**José Martín Méndez González**

sobre la Tesis intitulada:

*Dynamical Equivalence in Chemical Reaction Networks*

que se desarrolló bajo la dirección de

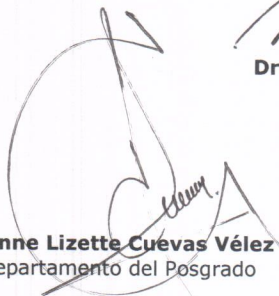
**Dr. Alejandro Ricardo Femat Flores**


El Jurado, después de deliberar, determinó

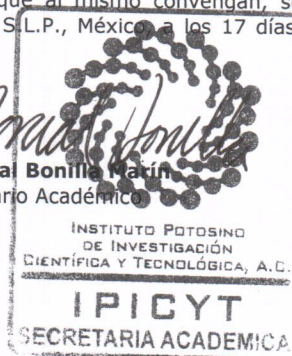
**APROBARLO**

Dándose por terminado el acto a las 19:00 horas, procediendo a la firma del Acta los integrantes del Jurado. Dando fe el Secretario Académico del Instituto.

A petición del interesado y para los fines que al mismo convengan, se extiende el presente documento en la ciudad de San Luis Potosí, S.L.P., México, a los 17 días del mes de agosto de 2012.

  
**Mtra. Ivonne Lizette Cuevas Vélez**  
Jefa del Departamento del Posgrado

  
**Dr. Marcia Bonilla Marín**  
Secretario Académico

  
INSTITUTO POTOSINO  
DE INVESTIGACIÓN  
CIENTÍFICA Y TECNOLÓGICA, A.C.  
**IPICYT**  
SECRETARÍA ACADÉMICA

---

Er lügt wie gedruckt.

Every attempt to employ mathematical methods in the study of chemical questions must be considered profoundly irrational and contrary to the spirit of chemistry... If mathematical analysis should ever had prominent place in chemistry - an aberration, which is happily almost impossible - it would be a rapid and widespread degeneration of that science.

—Auguste Comte, *Philosophie Positive* (1830)

---

*To my Mother and absent father.*

---

## *Acknowledgements*

More than four years ago I faced the blank page of my MSc Thesis, with the clear idea in my mind to pursue a PhD. I was not satisfied with the topic of neural networks and their applications. I wanted something more than a nonlinear fitting of raw data. By the middle of my Masters studies, I found on Google the topic of Chemical Reaction Networks and their capacity to display a wide variety of nonlinear phenomena. I collected all the papers about the subject I was able to get.

I was hooked.

Then, the name of Dr. Femat came up during a talk with Dr. Roberto Leyva, who encourage me to arrange a meeting with him. I did it. Our first face-to-face interview was minutes later after CNS opening ceremony. I still remember our short talk while we head for the Beta building... “I am everywhere excepting in church”, he said because his busy agenda. “Maybe because you do not want to be saved”, I replied without thinking. We look each other for a second. I thought, “That’s it. No PhD with him ”. I wonder what we was thinking at that moment.

We reached the Office and I showed him all I got about chemical reaction networks. He scanned the more than five hundred pages of printing papers and I ask me: “Have you ever read about the Belousov-Zhabotinsky reaction? ”. Silence. “It is a chaotic reaction-he continued. Back in the eighties it was a huge controversy concerning which chemical mechanism was the right one...The question I am interested to answer is what property do they share? If the kinetics can be written in terms of complex



---

networks<sup>1</sup>, what topological properties would they share, if any?”.

I did not ask myself about the use of a PhD, anyway. Neither I asked whether or not if that particular topic will pave the way to new questions. I was haunted by the question itself and its possible answer. I have found it my PhD thesis project.

After many diffeomorphisms later, here it is the result. It was not easy. It required a lot of discussions with reviewers, not to mention the constant fight against our very particular stubbornness. Among the discussions and constant ringing of the (cell)phone, incoming e-mails and people knocking at the door, somehow it was a time to let our thoughts to wander around many topics. For example, the possible composition of diffeomorphic maps as a time/space-traveling machine using the human consciousness. Or the explanation of how a scientific genius is conceived. Such an explanation was so clear to me that... I forgot it!. Or the cryptic expression, “Human beings are funny”, after hanged up the phone. Words of wisdom were lurking around our discussions too, such as a very useful one: “Explicación no pedida, condenación manifiesta ”. Or the missattributed words “Lo ven a uno y creen que es fácil...”. Besides these moments, I found in Femat a man of his word, who provided me with the best scientific environment he could. Thank you.

I would like to thank Dr. Moran, IPICYT’s founder. Without him, probably this thesis would not exist.

During the course of this project, I met really wonderful people. Inside the Biomathematics’ group I would like to thanks, specially: Dra. Griselda Quiroz, who point me out the existence of Guinness beer, Dra. Aurora Espinoza, who was my first L<sup>A</sup>T<sub>E</sub>X teacher. I got so many compilation errors that the L<sup>A</sup>T<sub>E</sub>X editor showed the message “Too many compilation errors-get human help”. The technician *par excellence*, MSc. Crescencio Hernández, for his big hearth and constant drive towards

---

<sup>1</sup>Dr. Barajas was in the Office too

---

Mexican education. Also, all those who, during my group presentations, made fruitful comments about my research, improving it: Dr. Barajas and his *koan* questions, Dra. Bonifas, Dr. Campos and Dr. Héctor González, to name a few. Outside the Biomathematics' group I would like to thank my office mates: Fanny Méndez and her "Pan de Dios", Karla Cuellar and Rocío, who speaks in binary code (Yes...No). Thanks for all the jokes and laughs. Special thanks to Dr. David Lizárraga, his patience while answering my doubts about any mathematical concept belongs to  $\aleph$ . Thanks also to Victor Mata, who obtained so many references for my thesis. Elizabeth, Ivone and Edith were always kind with me to orient me around the IPICYT bureaucracy.

Overseas, in Belgium, I thank Prof. Dr. Deni Dochain along with all the members at the Catholic University of Louvain-la-Neuve. Mrs. Bahia and family for having me for two months. Emile and Bob for those delightful talks during lunch and coffee breaks. Thanks to my cousin Adrian for the good weekend, the muffins and funny people I met at Amsterdam.

Since my arrival to San Luis Potosí, I found very good friends. Manuel Díaz de León is one of them, it was always there for a moment of peace when reality seemed too much real. People who has treated me as a family member: Mrs. Carolina, Mrs. Lourdes and Rod. The Santos' family: Mrs. Esther, Dr. Manuel, Dra. Griselda and Sandra, Gus and their heirs: Lucas and Frida. A special member of Santos' family is engraved in my heart since the moment I saw her blue/green eyes shining for one second, the most beautiful (*frau*) Prof. I ever met: Leticia. She has an uncanny laugh able to sweep the worries in me.

Back in Coatzacoalcos, my brother Daniel and his constant jokes at the phone were a relief. It is inspiring the way you look life. Thanks, Brother. My uncles Adrian, Cecilia and Teresa, for their support at any moment. Last but not least, I would like to thank again my Mother, for her unlimited support. Madre, tu corazón es más grande que la palabra gracias. Un abrazo.

# Contents

<b>List of Figures</b>	<b>xiv</b>
<b>List of Tables</b>	<b>xix</b>
<b>1 Introduction</b>	<b>1</b>
1.1 Motivating examples . . . . .	2
1.1.1 A heterogeneous catalytic example . . . . .	3
1.1.2 A biochemical reaction network example . . . . .	9
1.1.3 The Belusouv-Zhabotinsky reaction . . . . .	11
1.2 State of knowledge . . . . .	16
1.3 Description of the thesis . . . . .	18
1.3.1 Hypothesis . . . . .	18
1.3.2 Objectives . . . . .	19
1.3.3 Methodology . . . . .	19
<b>2 Mathematical Framework</b>	<b>22</b>
2.1 Chemical reaction networks . . . . .	22
2.2 Reaction kinetics . . . . .	26
2.3 Differential equations associated to CRNs . . . . .	27
2.4 Chemical reaction network theory . . . . .	30

## Contents

---

2.5	Stoichiometric network analysis . . . . .	32
2.6	Change of coordinates via Lie derivatives . . . . .	37
2.7	Concluding comments . . . . .	40
<b>3</b>	<b>Dynamical Equivalence Between CRNs</b>	<b>42</b>
3.1	Graph approaches . . . . .	42
3.1.1	Chemical reaction network theory . . . . .	42
3.1.2	Mechanistic classification of chemical oscillators. . . . .	45
3.2	Change of coordinates . . . . .	51
3.2.1	Illustrative example . . . . .	53
3.2.2	Brusselator and Oregonator dynamical equivalence. . . . .	59
3.3	Concluding remarks . . . . .	63
<b>4</b>	<b>Dynamical Equivalence: BZ reaction</b>	<b>64</b>
4.1	Deficiency and stoichiometric analysis . . . . .	64
4.2	Dynamical equivalence analysis . . . . .	66
4.3	Concluding remarks . . . . .	73
<b>5</b>	<b>An autocatalytic CRN for Prion replication</b>	<b>75</b>
5.1	Proteins might attack . . . . .	75
5.2	Proposed Kinetic Model . . . . .	77
5.2.1	MAK-ODES induced by $\mathcal{N}$ and $\tilde{\mathcal{N}}$ CRNs . . . . .	79
5.3	Dynamical scenarios . . . . .	82
5.3.1	Dynamics for $\mathcal{N}$ . . . . .	82
5.3.2	Dynamical scenario of $\tilde{\mathcal{N}}$ . . . . .	88
5.4	Bifurcation analysis . . . . .	88
5.5	Concluding remarks . . . . .	93

<b>6</b>	<b>Conclusions and Further Research</b>	<b>96</b>
	<b>Bibliography</b>	<b>99</b>
<b>A</b>	<b>Research articles</b>	<b>106</b>

# List of Figures

1.1	Experimental dynamics of the BZ reaction. Upper panel: oscillations in color under batch and well stirred conditions. Lower panel: pattern formation in a Petri dish where the solution is not well stirred. . . . .	12
1.2	$GF_A$ CRN, taken from [1]. Chemical species in curly braces are held constant during the course of reaction. . . . .	14
1.3	$GF_B$ (upper panel), $GF_C$ (middle panel) and $GF_D$ (lower panel) CRNs were taken from [1]. Chemical species in curly braces are held constant during the course of reaction. . . . .	15
2.1	CRN associated to the full Brusselator. . . . .	24
2.2	The convex cone formed by reaction rates in a CRN. . . . .	34
2.3	Simple current cycles adapted from [2]. (a) weak (2,1; $\kappa_{exit} = 2, \kappa_{cycle} = 1$ ); (b) critical (1,1); and (c) strong (1,2). . . . .	36

**List of Figures**

---

2.4 Oscillatory dynamics of the reduced Brusselator for both chemical and transformed spaces. Kinetic constants  $k_1 = k_2 = k_4 = 1, k_3 = 2$ . Initial conditions  $\mathbf{x}(0) = (1, 1)$ . (a) Time evolution of  $x_1$  (solid line) and  $x_2$  (dotted line); (b) Chemical species concentration state space; (c) Time evolution of  $x_1$  (solid line) and  $x_2$  (dotted line) after change of coordinates, i.e.  $z_1$  and  $z_2$  as in Equation (2.45); (d) Dynamics in transformed state space. . . . . 41

3.1 Brusselator extreme current diagram, where  $X = X_1, Y = X_2$ . Adapted from [2]. . . . . 46

3.2 Oregonator extreme current diagram where  $X = \tilde{X}, Y = \tilde{X}_2, Z = \tilde{X}_3$ . Adapted from [2]. . . . . 47

3.3 Weighted directed pseudograph for Brusselator.  $X = X_1, Y = X_2$  . . . 49

3.4 Weighted directed pseudograph for Oregonator.  $X = \tilde{X}, Y = \tilde{X}_2, Z = \tilde{X}_3$  . . . . . 50

3.5 Composition of diffeomorphic functions for Brusselator and MMAKWLC CRNs, using as observable functions  $y = h(\mathbf{x}) = x_1$  and  $\tilde{y} = \tilde{h}(\tilde{\mathbf{x}}) = \tilde{x}_2$ . Upper panel: Brusselator's states as function of MMAKWLC's states. Lower panel: MMAKWLC's states as function of Brusselator's states. Initial conditions and kinetic parameters for the Brusselator:  $\mathbf{x}_{BR}(0) = (2, 2), k_1 = 1, k_2 = 2, k_3 = 1, k_4 = 1$ . Initial conditions and kinetic parameters for the MMAKWLC:  $\mathbf{x}_{MMAKWLC}(0) = (2, 2), k'_1 = 1, k'_2 = 27, k'_3 = 3$ . . . . . 55

**List of Figures**

---

3.6 Composition of diffeomorphic functions for Brusselator and MMAKWLC CRNs, using as observable functions  $y = h(\mathbf{x}) = x_1 + x_2$  and  $\tilde{y} = \tilde{h}(\tilde{\mathbf{x}}) = \tilde{x}_1 + \tilde{x}_2$ . (a) MMAKWLC state phase. (b) Brusselator's states as function of MMAKWLC's states. (c) Brusselator state phase. (d) MMAKWLC's states as function of Brusselator's states. Initial conditions and kinetic parameters for the Brusselator:  $\mathbf{x}_{BR}(0) = (2, 2)$ ,  $k_1 = 1, k_2 = 3.2, k_3 = 2, k_4 = 1$ . Initial conditions and kinetic parameters for the MMAKWLC:  $\mathbf{x}_{MMAKWLC}(0) = (2, 2)$ ,  $k'_1 = 1, k'_2 = 8.5, k'_3 = 2$ . 57

3.7 Dynamical chirality phenomenon between Brusselator and the MMAKWLC is found for  $(k_3, k_4) = (k'_3, k'_1) \in \mathbf{P}^* = \mathbb{R}_+^4 \cap \mathbb{R}_+^3$  for any  $\mathbf{x}(0), \tilde{\mathbf{x}}(0) \in \mathbb{R}_+^2$  and for all  $t \geq 0$ , where  $\mathbf{P}^*$  is not an empty set. . . . 58

3.8 Trajectories from Brusselator (blue) space mapped by 3.39 to  $\mathbb{R}_+^3$  (red). 62

5.1  $\mathcal{N}$  CRN which induced the MAK-ODEs (5.8). . . . . 80

5.2  $\tilde{\mathcal{N}}$  CRN which induced the MAK-ODEs (5.11). . . . . 80

5.3 (a) Solid lines: solutions of (5.8) with different initial conditions. Set of kinetic constants as in Table 5.1. Black circle: stable steady state. White circle: unstable steady state. Dotted line: locus of equilibrium. (b) Equilibrium bifurcation diagram for  $x_3$  showing multiple steady states as  $k_1$  vary. Solid line: stable branch. Dotted line: unstable branch. . . . . 84

5.4 (a) Solid lines: solutions of (5.8) with different initial conditions. Set of kinetic constants as in Table 5.2. Black circle: stable steady state. White circle: unstable steady state. Dotted line: locus of equilibrium. (b) Equilibrium bifurcation diagram for  $x_3$  showing multiple steady states as  $k_1$  vary. Solid line: stable branch. Dotted line: unstable branch. . . . . 86



## List of Figures

---

5.5	Bifurcation scenario for degenerate steady state varying $k_1$ : vector field (5.8) goes from a stable steady state (Figs. 5.5a,b) to an unstable saddle (Figs. 5.5c,d) which undergoes a supercritical Hopf bifurcation (Figs. 5.5e,f). Time evolution of species $x_1$ (black line), $x_2$ (dashed line) and $x_3$ (dotted line). Black circle: stable steady state. White circle: unstable steady state. . . . .	87
5.6	Solid lines: solutions of (5.11) with different initial conditions. Set of kinetic constants as in Table 5.3. Black circle: stable steady state. White circle: unstable steady state. Dotted line: locus of equilibrium. . . . .	89
5.7	Continuation of $x_1$ using $k_6$ from the set $\mathbf{K}_2$ . Solid line stable equilibrium. Dashed line unstable equilibrium. LP=Limit Point. . . . .	91
5.8	Bifurcation diagram in the $(k_6, k_1)$ space from the set $\mathbf{K}_1$ . LP=Limit Point. BT=Bogdanov-Takens. ZH=Zero Hopf(Neutral saddle). CP=Cusp Point. . . . .	91
5.9	Upper panel: Bifurcation diagram in the $(k_6, k_1)$ space from the set $\mathbf{K}_2$ . Lower panel: augmented region to show the Limit Point Cycle (LPC).LP=Limit Point. BT=Bogdanov-Takens. ZH=Zero Hopf (Neutral saddle). CP=Cusp Point. . . . .	92
5.10	Two different oscillations projected in the $x_1 - x_2$ space from the oscillatory region at the left of the Cusp Point in Figure 5.9. Upper panel: $(k_6, k_1) = (8, 25)$ . Lower panel: $(k_6, k_1) = (3.39, 12.46)$ ; remaining kinetic constants as in $\mathbf{K}_2$ . . . . .	92
5.11	Bifurcation diagram for degenerate steady state varying $k_6$ from set $\mathbf{K}_3$ . H=Hopf. LP=Limit Point. . . . .	93
5.12	Bifurcation diagram for degenerate steady state in the $(k_6, k_1)$ space.NS=Neimark-Sacker, LPC=Limit Point of Cycles. . . . .	93

## List of Figures

---

5.13 Quasi-periodic oscillations in the $x_1 - x_2$ plane at the Neimark-Sacker point $(k_6, k_1) = (1.897181, 3.039192)$ . . . . .	94
--	----

# List of Tables

4.1	Kinetic rate constants reported in [1] for $GF_D$ vector field. All kinetic constants have $M(\text{Molar})/s(\text{seconds})$ units . . . . .	71
4.2	Parameter values for auxiliary equations in $GF_D$ vector field. $M = \text{Molar}$ , $s = \text{seconds}$ . . . . .	72
5.1	$\mathcal{N}$ steady states and their stability for kinetic constants $k_1 = 2.9872232$ , $k_2 = k_3 = k_7 = 1$ , $k_4 = 12.626548$ , $k_5 = 5.6433885$ , $k_6 = 0.85914091$ . . . . .	83
5.2	$\mathcal{N}$ steady states and their stability for kinetic constants $k_1 = 11.107337$ , $k_2 = k_7 = 1$ , $k_3 = 0.17891084$ , $k_4 = 5.7767046$ , $k_5 = 1.0096634$ , $k_6 = 3.194528$ . . . . .	83
5.3	$\tilde{\mathcal{N}}$ steady states and their stability for kinetic constants $\tilde{k}_1 = 15.696713$ , $\tilde{k}_2 = \tilde{k}_3 = \tilde{k}_6 = 1$ , $\tilde{k}_4 = 0.33799396$ , $\tilde{k}_5 = 4.8020616$ . . . . .	88

---

## *Notation*

$N$ : Stoichiometric matrix.

$\bar{\mathbb{R}}_+^n$ : The set of non-negative real numbers.

$\mathbb{R}_+^n$ : The set of strictly positive real numbers.

$\mathbf{x}$ : Vector of chemical species concentrations.

$X_i$ : Chemical specie.

$\mathbf{z}$ : Vector of transformed chemical species concentrations in a tangent space.

$\Phi$ : Diffeomorphism.

$\Phi^{-1}$ : Inverse of a diffeomorphism.

## *Abbreviations*

ADOT: Advanced Deficiency One Theory.

BCRN: Bio-Chemical Reaction Network.

CFSTR: Continuous Flow Stirred Tank Reactor.

CRN: Chemical Reaction Network.

CRNT: Chemical Reaction Network Theory.

DOT: Deficiency One Theorem.

DZT: Deficiency Zero Theorem.

MCCO: Mechanistic Classification of Chemical Oscillators.

SNA: Stoichiometric Network Analysis.

---

## *Resumen*

El dogma fundamental de la cinética química establece que puede existir más de una red de reacción química (RRQ) que explique los datos experimentales. Más aún, las RRQ validadas experimentalmente no necesariamente son del mismo tamaño, es decir, pueden diferir entre ellas en el número de especies y/o reacciones químicas. Sin embargo, las Ecuaciones Diferenciales Ordinarias (EDOs) que se derivan de las RRQ candidatas, son capaces de reproducir el comportamiento experimental para un conjunto apropiado de valores de parámetros, representados por las constantes cinéticas de reacción en la respectivas RRQ.

Un ejemplo del dogma antes mencionado en el campo de la cinética química no lineal, es la reacción química oscilatoria de Belousov-Zhabotinsky (BZ). Varias RRQ se han propuesto y validado para explicar el comportamiento oscilatorio y caótico que la reacción BZ es capaz de generar [3]. En particular, en este trabajo se discuten la RRQ denominada Oregonator, con tres especies químicas, y las RRQ reportadas en [1], que toman en cuenta nueve, siete y cuatro especies químicas, respectivamente, las cuales modelan la reacción de BZ. La dinámica de las especies químicas en el Oregonator, y las tres primeras RRQ en [1], están descritas por EDOs derivadas de la Ley de Acción de Masas (LAM); las EDOs asociadas a la cuarta RRQ en [1] no son del tipo LAM, sin embargo, ajustan muy bien las observaciones experimentales.

Lo anterior motiva las siguientes preguntas: ¿Por qué distintas RRQ de la reacción BZ son capaces de reproducir la misma realidad experimental, a pesar de las diferencias en el número de especies y reacciones químicas?. ¿En qué sentido las EDOs de dos o más RRQ que explican las mismas observaciones experimentales pueden ser

---

consideradas equivalentes?

Como primera aproximación para responder estas preguntas, se aplicaron elementos de teoría de grafos y Análisis Estequiométrico de la Red (ASR) [4], a las RRQ Oregonator y Brusselator, siendo esta última la primera RRQ que demostró la capacidad de EDOs-LAM de exhibir oscilaciones en las concentraciones de especies químicas, de manera análoga a las observadas en la reacción BZ. El uso de esta aproximación permitió hallar una transformación no invertible tal que el pseudo-grafo dirigido y pesado del Brusselator posea el mismo patrón de dirección y pesos que el del Oregonator, pero no lo opuesto. Esto es, el Brusselator es equivalente gráficamente al Oregonator bajo la acción de un mapa no invertible.

En la búsqueda de equivalencia entre el Brusselator, Oregonator y las RRQ en [1], se aplicaron otros criterios basados en teoría de grafos: (1) Teoría de Redes de Reacción Química (TRRQ) [5] y, (2) la Clasificación Mecánica de Osciladores Químicos (CMOQ) [2]. La aplicación de ambas teorías no permitió establecer conclusiones definitivas en relación a la posible equivalencia entre las RRQ mencionadas.

Por lo anterior, en esta tesis se propone el concepto de *equivalencia dinámica* entre EDOs no (necesariamente del tipo de LAM) inducidas por RRQ. La equivalencia dinámica se define como la composición de funciones difeomórficas construidas con las derivadas de Lie de una función observable, que asignan la evolución temporal de las concentraciones de especies químicas (espacio de estados) de una RRQ a otra, y viceversa. Este enfoque se aplica al Brusselator, el Oregonator y la cuarta RRQ reportada en [1].

Palabras clave: equivalencia dinámica, redes de reacción química, autocatálisis.

---

## *Abstract*

The fundamental dogma of chemical kinetics states that there might be more than one Chemical Reaction Network (CRN) that fits a given experimental reality. Moreover, the experimentally validated CRNs are not necessarily of the same size, that is, they might differ in the number of chemical species and reactions. Nevertheless, the Ordinary Differential Equations (ODEs) induced by the candidate CRNs, are able to reproduce the observed experimental behavior for a particular set of parameters, represented by reaction rate kinetic constants of the CRNs.

An example of the mentioned dogma in the field of nonlinear kinetics, is the oscillatory reaction of Belousov-Zhabotinsky (BZ). Several CRNs has been propounded and validated to explain the oscillatory and chaotic behavior in the BZ reaction [3]. In particular, in this work are discussed the CRN termed Oregonator, with three chemical species, and CRNs reported in [1], with nine, seven and four chemical species, respectively, all of them valid models for the BZ reaction. The dynamics of the Oregonator's chemical species, and the first three CRNs in [1], are governed by ODEs derived from Mass Action Kinetics (MAK); ODEs associated to the fourth CRN in [1] are not ODEs of MAK type, nevertheless, they fit very well the experimental observations.

The aforementioned facts motivates the following questions: Why different CRNs of the BZ reaction are able to account for the same experimental reality, despite their differences in the number of chemical species and reactions? In what sense the sets of ODEs from two or more CRNs explaining the same experimental reality can be considered equivalents?

As a first approximation to answer these questions, elements from graph theory and Stoichiometric Network Analysis (SNA) [4], were applied to the Oregonator and Brusselator, the latter being the first CRN whose MAK-ODEs exhibit oscillations

---

in the chemical species concentration space, analogous to those observed in the BZ reaction. Using this approach is possible to find a non-invertible map such that the directed and weighted Brusselator's pseudo-graph have the same pattern of direction and weights of the Oregonator's pseudo-graph, but not the opposite. That is, the Brusselator is equivalent from a graph viewpoint to the Oregonator under the action of a non-invertible map.

Searching equivalence among the Brusselator, Oregonator and CRNs reported in [1], other criteria based on graph theory were applied: (1) Chemical Reaction Network Theory (CRNT) [5] and, (2) Mechanistic Classification of Chemical Oscillators (MCCO) [2]. The application of both theories does not offer definitive conclusions concerning the possible equivalence among the mentioned CRNs.

In order to circumvent this issue, in this thesis we propose the concept of *dynamical equivalence* among ODEs (MAK type or not) induced by CRNs. Dynamical equivalence is defined as the composition of diffeomorphic functions, constructed using the Lie derivatives of an observable function, which map chemical species concentrations (state space) of one CRNs to a second CRN, and vice versa. This approach is applied to the Brusselator, the Oregonator and the fourth CRN in [1].

Keywords: dynamical equivalence, chemical reaction networks, autocatalysis.



# 1. Introduction

The fundamental dogma of chemical kinetics states that there might be more than one Chemical Reaction Network (CRN) that fits a given experimental reality. Those valid CRNs not necessarily share the same number of chemical species or reactions. Nevertheless, their Ordinary Differential Equations (ODEs) are able to reproduce the same observed experimental behavior. Furthermore, it might be the case that the set of ODEs induced by the validated CRNs are not of the same type, *e.g.* Mass Action Kinetics (MAK) type. Thus, it is possible to have ODEs derived from CRNs with different dimension whose solutions, *i.e.* the time evolution of chemical species concentrations, behaves in the same way as observed in experiments. Then, it is natural to think that, despite their differences in dimension, the validated CRNs have common features: they are equivalent in some sense.

This thesis focus on the study of *dynamical equivalence* in CRNs. In particular, it can be distinguished two possible scenarios: (1) the system of ODEs of two or more CRNs have the same dimension or, (2) the system of ODEs among the CRNs are of distinct dimension. In the first scenario, two CRNs are said to be dynamical equivalents if it is possible to map solutions (concentrations of chemical species) of one CRN into solutions of a second CRN, through the composition of two diffeomorphic maps. For the second scenario, the system with higher dimension can be “immersed” into the system of lower dimension, thus defining a projection after composition of their

respective diffeomorphic maps. Because both systems do not have the same dimension, they are termed *partially dynamical equivalents*. For both cases, diffeomorphic maps are constructed by means of recursive Lie derivatives [6, 7, 8] of a single observable function (single output in the control literature) along the vector field defined by the set of ODEs induced by the CRN.

The remaining of this chapter provides the motivation to study the equivalence among CRNs through a series of examples which illustrates the fundamental dogma in chemical kinetics. The literature review related with equivalence concepts in CRNs is presented as well. Finally, a description of this thesis is given along with the hypothesis, the general objective of this work and the applied methodology.

## 1.1 Motivating examples

The every day job of a chemist is to use different techniques to identify as much chemical species can provide him for a particular reaction. Then, based on experience, previous results reported in journals, and even by pure intuition, the chemist proceed to write down several candidate CRNs. We can think that a CRN is an algorithm of how the already identified chemical species combine with each other in order to produce the measured chemical products at the end of the reaction. Some CRNs will fit the data, some others not. The worst case scenario arises when none of the candidate CRNs fits the data. For those CRNs that do stand for the experimental observations, structural differences within the set of validated CRNs are possible, such as variations in the number of chemical species and reactions. This fact it is known as the *fundamental dogma of chemical kinetics* [3]: more than one CRN can explain the observed global reaction.

By means of three examples, it is clarified what do we mean by global reaction and how the corresponding ODEs are derived assuming MAK from the validated CRNs.

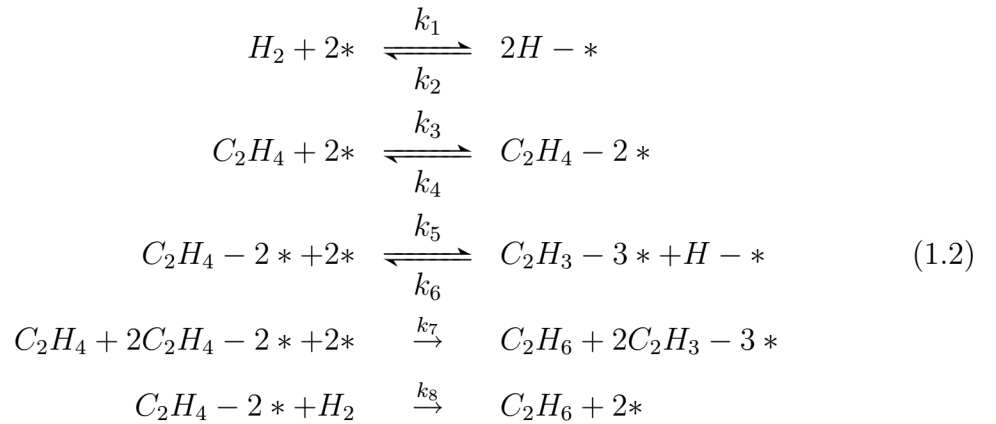
The first example comes from the ethylene hydrogenation on a rhodium catalytic surface [9] for which nine CRNs fit the experimental data. The second example shows several biochemical reaction networks (BCRN) which stands for the formation of products by means of a single substrate [10]. Third example is the *par excellence* in nonlinear kinetics, the Belusouv-Zhabotinsky (BZ) reaction [3].

### 1.1.1 A heterogeneous catalytic example

Suppose that chemical species ethylene and hydrogen,  $C_2H_4$ ,  $H_2$ , respectively, are fed at a constant rate into a well mixed Continuous Flow Stirred Tank Reactor (CFSTR), *i.e.* a chamber where is a sufficient amount of catalyst (rhodium) so that the main product at the end of the reactor is composed by  $C_2H_6$ , primarily;  $C_2H_4$  and  $H_2$  are carried out from the reactor in minor quantities. Also, let us assume that the reaction takes place at constant temperature. Then, the global reaction can be written as:

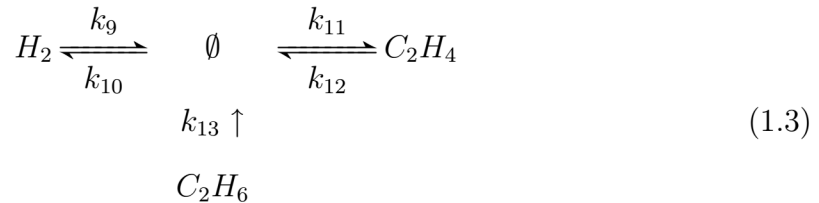


Let us consider the following CRN for this global reaction, which reflects what is supposed to be occurring inside the reactor:



where the symbol “\*” represents vacant catalytic sites on the surface’s catalyst. The adsorbed chemical species upon the catalytic surface are represented by “chemical

specie- $*$ ”, *e.g* the hydrogen  $2H - *$ . In order to model the inlet and outlet of chemical species to and from the CFSTR, we add the following pseudo-reactions:



The symbol “ $\rightleftharpoons$ ” in CRN (1.2), indicates a reversible reaction; it is a condensed way to express that both reactions,  $H_2 + 2* \rightarrow 2H - *$  and  $2H - * \rightarrow H_2 + 2* \rightarrow$ , are taking place at a rate encoded by the kinetic constants,  $k_1$  and  $k_2$ , respectively. Additionally, the pseudo-reaction,  $\emptyset \rightarrow H_2$ , stands for the entering of  $H_2$  into the reactor, with a fed rate of  $k_{10}$ . On the other hand, the reverse pseudo-reaction,  $H_2 \rightarrow \emptyset$ , serves to depict the leaving of  $H_2$  from the reactor with a rate  $k_9$ . Following this nomenclature, we have that  $C_2H_4$  enters and leaves the reactor meanwhile  $C_2H_6$  only leaves the reactor, both at their corresponding rates. Hence, the  $\emptyset$  symbol represents the surroundings or constant pool of chemical species [11].

As we can see, the CRN (1.2) tell us in a detailed fashion how chemical species  $C_2H_4$ ,  $H_2$  react each other to form  $C_2H_6$ , with the participation of intermediate species formed during the course of the reaction. For example, reactions:



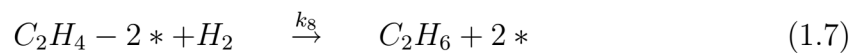
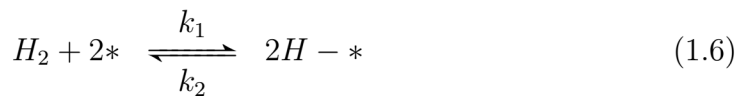
express that bimolecular hydrogen hit two vacant sites on the catalytic surface, giving as a consequence two hydrogen atoms adsorbed on both vacant sites in a reversible process. In the same way,  $C_2H_4$  hits the catalytic surface becoming adsorbed by two vacant sites,  $C_2H_4 - 2*$ . This adsorbed species reacts with two adjacent catalytic sites to produce more adsorbed species,  $C_2H_3 - 3*$  and  $H - *$ . Then, adsorbed species  $2C_2H_4 - 2*$  along with two catalytic sites  $2*$  reacts with  $C_2H_4$  to produce the

final product  $C_2H_6$ , accompanied by the adsorbed specie  $2C_2H_3 - 3*$ . Finally, the adsorbed specie  $C_2H_4 - 2*$  reacts with bimolecular hydrogen to produce  $C_2H_6$  and the two original catalytic sites,  $2*$ , showed at the beginning of the reaction. Thus, the number of catalytic sites must be conserved, *i.e.* the number of vacant sites plus the number of adsorbed chemical species do not vary as time goes by. Such a *conservation relation* can be written as:

$$x_2(t) + x_3(t) + 2x_5(t) + 3x_6(t) = \omega \in \mathbb{R}_+, \forall t \geq 0 \quad (1.5)$$

where  $x_i(t)$ ,  $i = 1, \dots, 7$ , represents the instant concentration (in appropriate units) of chemical species  $x_1(t) = H_2$ ,  $x_2(t) = *$ ,  $x_3(t) = H - *$ ,  $x_4(t) = C_2H_4$ ,  $x_5(t) = C_2H_4 - 2*$ ,  $x_6(t) = C_2H_3 - 3*$  and  $x_7(t) = C_2H_6$ .

It is pertinent to illustrate how the CRN (1.2) along with (1.3) gives rise to an associated set of MAK-ODEs. Accordingly, MAK states that reaction rates (at constant temperature) are proportional to products of reactants' concentrations. The form of the rate functions can be deduced from the reaction itself. To begin with, let us choose the chemical specie,  $H_2$ , which participates in reactions:



Consider reaction (1.7). The likelihood of the  $H_2$  collision with two catalytic sites “\*” is presumably reflected in the product  $x_1^1(t)x_2^2(t)$ , where the powers 1 and 2, at which concentrations are raised, are known as stoichiometric coefficients. Thus, the molar occurrence rate is taken to be  $k_1x_1(t)x_2^2(t)$ , where  $k_1$  is a rate constant for the reaction  $H_2 + 2* \rightarrow 2H - *$ . Similarly, the reverse reaction,  $2H - * \rightarrow H_2 + 2*$ , induce

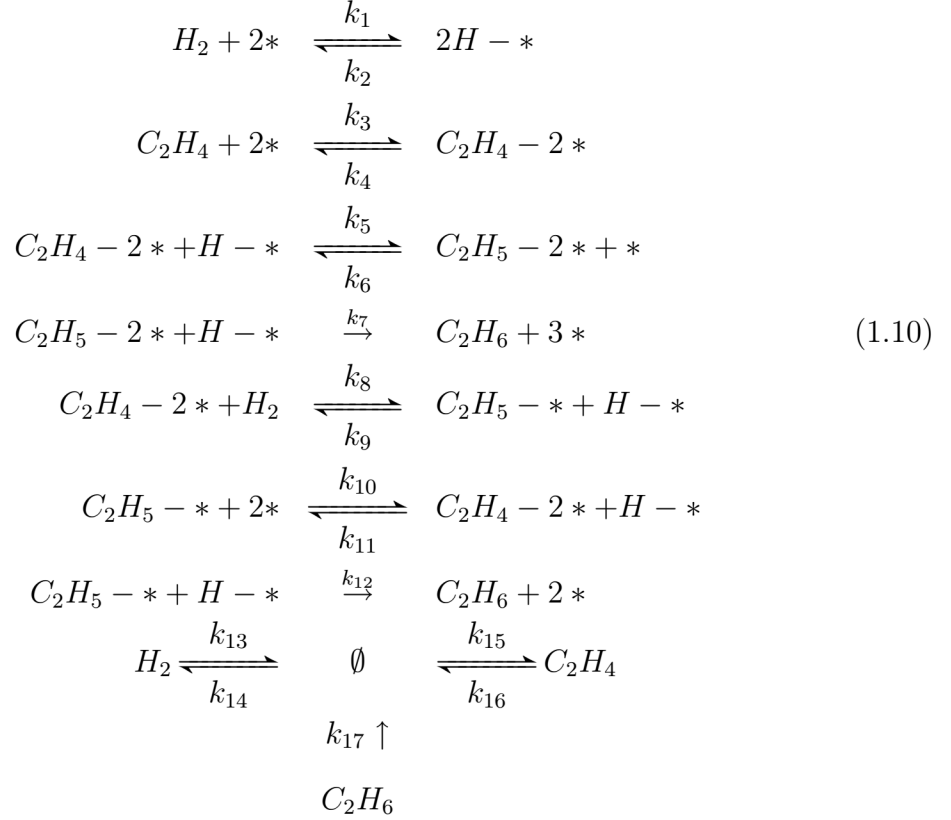
the reaction rate function  $k_2x_3^2(t)$ . Reaction  $C_2H_4 - 2* + H_2 \rightarrow C_2H_6 + 2*$  requires that the adsorbed specie  $C_2H_4$  be hit by one molecule of  $H_2$ , so the occurrence rate is taken to be  $k_8x_1(t)x_5(t)$ . To account for the concentration of  $H_2$  at the exit of the reactor, we have the reaction  $H_2 \rightarrow \emptyset$ , from which it is derived the rate  $k_9x_1(t)$ ; opposite reaction,  $\emptyset \rightarrow H_2$ , described the entering of  $H_2$  at a constants rate  $k_{10}$ . Now, we are in a position to formulate the MAK-ODE that govern the  $H_2$  concentration. It only remains to identify if we loose (-) or gain (+) molecules of  $H_2$  for every reaction at a rate indicated by the reaction: if  $H_2$  appears at the left of the chemical arrow, we loose molecules of  $H_2$ ; we gain molecules of  $H_2$  if it is located at the right of the chemical arrow.

From the convention adopted above, we write for  $H_2$  and the remaining species:

$$\begin{aligned}
\frac{dx_1(t)}{dt} &= \dot{x}_1(t) = -k_1x_1(t)x_2^2(t) + k_2x_3^2(t) - k_8x_1(t)x_5(t) - k_9x_1(t) + k_{10} \\
\dot{x}_2(t) &= -2k_1x_1x_2^2(t) + 2k_2x_3^2(t) - 2k_3x_2^2(t)x_4(t) + 2k_4x_5(t) - 2k_5x_2^2(t)x_5(t) \\
&\quad + 2k_6x_3(t)x_6(t) - 2k_7x_2^2(t)x_4(t)x_5^2(t) + 2k_8x_1(t)x_5(t) \\
\dot{x}_3(t) &= 2k_1x_1(t)x_2^2(t) - 2k_2x_3^2(t) + k_5x_2^2(t)x_5(t) - k_6x_3(t)x_6(t) \\
\dot{x}_4(t) &= -k_3x_2^2(t)x_4(t) + k_4x_5(t) - k_7x_2^2(t)x_4(t)x_5^2(t) + k_{11} - k_{12}x_4(t) \quad (1.9) \\
\dot{x}_5(t) &= k_3x_2^2(t)x_4(t) - k_4x_5(t) - k_5x_2^2(t)x_5 + k_6x_3(t)x_6(t) - 2k_7x_2^2(t)x_4(t)x_5^2 \\
&\quad - k_8x_1(t)x_5(t) \\
\dot{x}_6(t) &= k_5x_2^2(t)x_5(t) - k_6x_3(t)x_6(t) + 2k_7x_2^2(t)x_4(t)x_5^2(t) \\
\dot{x}_7(t) &= k_7x_2^2(t)x_4(t)x_5^2 + k_8x_1(t)x_5(t) - k_{13}x_7(t)
\end{aligned}$$

Then, the system of Equations (1.9), constitutes the full system of MAK-ODEs induced by CRN (1.2)-(1.3). Note that the existence of conservation relation (1.5) restricts the solutions of Equations (1.9) to evolve within the plane defined by Equation (1.5).

Now, let us consider an alternate CRN for the global reaction (1.1):



It is straightforward to check the participation of eight chemical species through seventeen reactions in CRN (1.10): it has an additional chemical species and four more reactions with respect to CRN (1.2). We identify the chemical species concentrations of CRN (1.10) by  $x_1(t) = H_2$ ,  $x_2(t) = *$ ,  $x_3(t) = H - *$ ,  $x_4(t) = C_2H_4$ ,  $x_5(t) = C_2H_4 - 2*$ ,  $x_6(t) = C_2H_5 - 2*$ ,  $x_7(t) = C_2H_6$ ,  $x_8(t) = C_2H_5 - *$ . The full set of

MAK-ODEs for CRN (1.10) is:

$$\begin{aligned}
\dot{x}_1(t) &= -k_1x_1(t)x_2^2(t) + k_2x_3^2(t) - k_8x_1(t)x_5(t) + k_9x_3(t)x_8(t) - k_{13}x_1(t) + k_{14} \\
\dot{x}_2(t) &= -2k_1x_1(t)x_2^2(t) + 2k_2x_3^2(t) - 2k_3x_2^2(t)x_4(t) + 2k_4x_5(t) + k_5x_3(t)x_5(t) \\
&\quad - k_6x_2(t)x_6(t) + 3k_7x_3(t)x_6(t) - 2k_{10}x_2^2(t)x_8(t) + 2k_{11}x_3(t)x_5(t) \\
&\quad + 2k_{12}x_3(t)x_8(t) \\
\dot{x}_3(t) &= 2k_1x_1(t)x_2^2(t) - 2k_2x_3^2(t) - k_5x_3(t)x_5(t) + k_6x_2(t)x_6(t) - k_7x_3(t)x_6(t) \\
&\quad + k_8x_1(t)x_5(t) - k_9x_3(t)x_8(t) + k_{10}x_2^2(t)x_8(t) - k_{11}x_3(t)x_5(t) \\
&\quad - k_{12}x_3(t)x_8(t) \\
\dot{x}_4(t) &= -k_3x_2^2(t)x_4(t) + k_4x_5(t) + k_{15} - k_{16}x_4(t) \\
\dot{x}_5(t) &= k_3x_2^2(t)x_4(t) - k_4x_5(t) - k_5x_3(t)x_5(t) + k_6x_2(t)x_6(t) - k_8x_1(t)x_5(t) \\
&\quad + k_9x_3(t)x_8(t) + k_{10}x_2^2(t)x_8(t) - k_{11}x_3(t)x_5(t) \\
\dot{x}_6(t) &= k_5x_3(t)x_5(t) - k_6x_2(t)x_6(t) - k_7x_3(t)x_6(t) \\
\dot{x}_7(t) &= k_7x_3(t)x_6(t) + k_{12}x_3(t)x_8(t) \\
\dot{x}_8(t) &= k_8x_1(t)x_5(t) - k_9x_3(t)x_8(t) - k_{10}x_2^2(t)x_8(t) + k_{11}x_3(t)x_5(t) + k_{12}x_3(t)x_8(t)
\end{aligned} \tag{1.11}$$

subject to the conservation relation, *i.e.* balance of surface catalytic sites:

$$x_2(t) + x_3(t) + 2x_5(t) + 2x_6(t) + x_8(t) = \omega \in \mathbb{R}_+, \forall t \geq 0 \tag{1.12}$$

It turns out that both sets of MAK-ODEs, Equations (1.9)-(1.11), are two of nine, among the eighty one proposed CRNs for global reaction (1.1), that can support the pair of stable steady states founded experimentally along with the conserved number of catalytic sites [9]. Note that CRNs (1.2) and (1.10) does not induce MAK-ODEs of the same dimension. Nevertheless, both CRNs and their corresponding MAK-ODEs are consistent with the available data collected from experiments [9]. In other words, there are kinetic constants that parametrize the set of MAK-ODEs (1.9) and



(1.11) such that both set of solutions converge to specific steady states in chemical species concentration spaces, not necessarily of the same dimension. Therefore, CRNs (1.2)-(1.3) and (1.10), along with their MAK-ODEs, are equivalent, as stated by the fundamental dogma in chemical kinetics.

It is noteworthy that examples of the fundamental dogma in chemical kinetics are not exclusive of the chemical engineering field. Biochemical systems are also a source of examples of the fundamental dogma. Furthermore, it might be CRNs standing for the same global reaction but with different properties, such as the capacity or not for bistability. This issue is illustrated for a set of putative Biochemical Reaction Networks (BCRNs).

### 1.1.2 A biochemical reaction network example

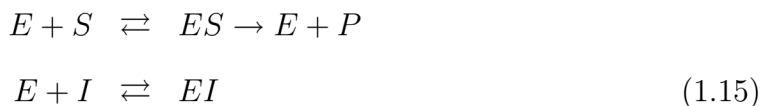
Metabolic pathways involved on the cell operation are also susceptible to be modeled by MAK, using the same concepts showed for the heterogeneous catalytic example. In this situation, the cell is modeled as a CFSTR. For the case of elementary enzyme catalysis involved on the transformation of a single substrate,  $S$ , (a molecule that is catalyzed by an enzyme,  $E$ ) into a product,  $P$ , we have four commonly accepted BCRNs [12] which account for the global reaction:



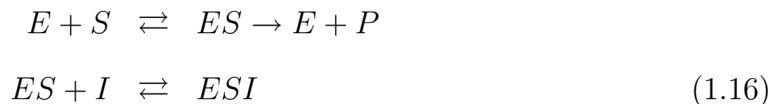
Michaelis-Menten kinetics:



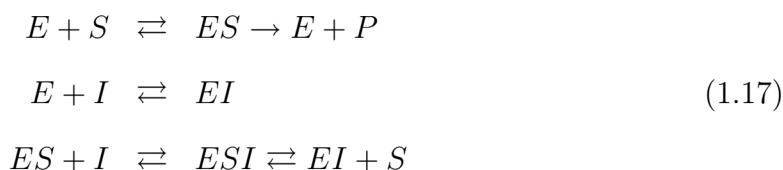
Competitive inhibition:



Uncompetitive inhibition:



Mixed inhibition:



where  $ES$  is the chemical complex enzyme-substrate,  $I$  stands for the inhibitor,  $EI$  and  $ESI$  are the chemical complexes of enzyme-inhibitor and enzyme-substrate-inhibitor, respectively;  $P$  is the final product of reaction. In addition, we assume that substrates and inhibitors are supplied at fixed rates into the CFSTR; the total concentration of enzyme is conserved (in the same fashion as catalytic sites) and the free enzyme remains entrapped within the CFSTR; substrates, inhibitors, and products are removed (or degraded) at rates proportional to their current concentrations. For the sake of brevity, the appropriate pseudo-reactions for inlet and outlet to and from the CFSTR of substrates, inhibitors and products, has been omitted.

By visual inspection it can be checked that BCRN (1.14) is a subnetwork of (1.15)-(1.17). Also, BCRN (1.15) is a subnetwork of (1.17), along with BCRN (1.16). Nevertheless, even though there exists structural similarities among them, only (1.17) has the property of bistability [10]. Thus, it might be the case that several CRNs stand for the same global reaction, but some of them can possess additional dynamical properties, such as bistability or oscillations. A biochemical example closely related to this issue is presented in Chapter 5, where two BCRN stands for a neurodegenerative disease, representing two possible routes of production of a pathological protein. However, both BCRNs displays different dynamical scenarios [13].

Another reaction which offers an ample variety of CRNs with different dimensions and distinct dynamical features among them [3, and references therein] is the BZ reaction. Due to its dynamical richness, there has been multiple efforts to condense in one CRN all the range of nonlinear behaviors the BZ reaction is capable of, sometimes leading to scientific controversy (see for example [14, 15]). Next section briefly reviews some CRNs designed for the BZ reaction, which allow us to make patent the issue of dynamical equivalence among CRNs.

### 1.1.3 *The Belusouv-Zhabotinsky reaction*

At the beginning of the 1950's, Russian chemist Boris Pavlovich Belusouv was developing an inorganic model of the Krebs cycle. This reaction is an universal part of the metabolism by which acetyl residues are oxidized to carbon dioxide at the mitochondria. He propose the metal ion cerium instead of the protein-bound metal ions common in the enzymes of living cells, this lead to a mixed solution of citric acid in water with acidified bromate as oxidant and yellow ceric ions as catalyst. The solution exhibited periodic states, it turned from colorless to yellow, and back again (see Figure 1.1). Oscillations were observable for as long as one hour, while effervescing carbon dioxide. By 1951, Belusuov sent photos of the course of the reaction along with a detailed formulation to several Russian journals. His work was rejected on the basis that his reaction violates the second law of thermodynamics. Four years later, in 1955, Ilya Prigogine stablished its theory on non-equilibrium thermodynamics give an explanation for how sustained oscillations might arise from chemical reactions. Meanwhile, Belousov published his results in the memories of a radiology congress, later published into English [3, and references therein].

In 1961, Anatole Zhabotinsky became aware of the Belousov's discovery and develop a better formulation of reaction to study the observed oscillations. Later on,

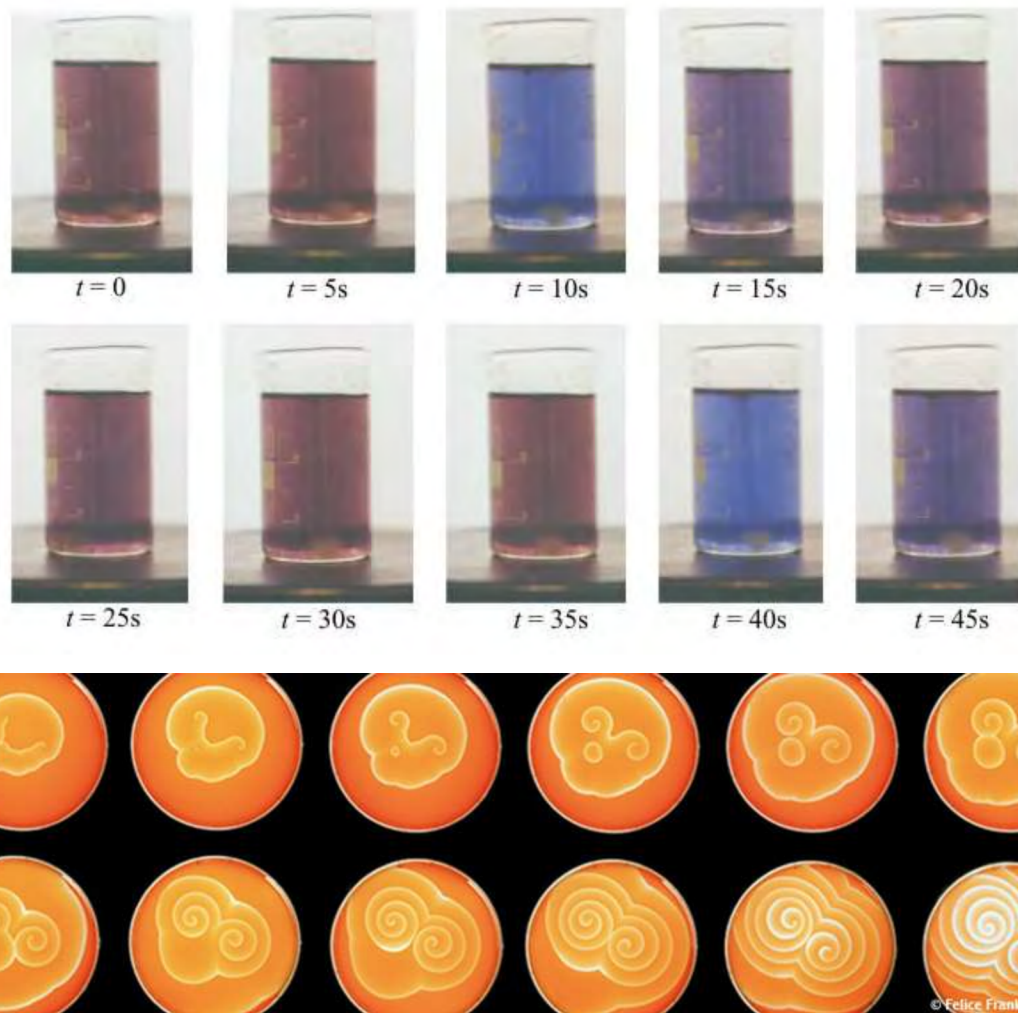


**Figure 1.1:** *Experimental dynamics of the BZ reaction. Upper panel: oscillations in color under batch and well stirred conditions. Lower panel: pattern formation in a Petri dish where the solution is not well stirred.*

in 1967, Prigogine and Lefever [16] published the Brusselator, a CRN modeled with Mass Action Kinetics (MAK) that exhibit sustained oscillations and pattern formation as in the BZ reaction. The next year, during a conference on Biochemical and Biological Oscillators held at Prague, the scientific community of Western countries took notice of the BZ reaction and the growing evidence that nonlinear phenomena can be exhibit by CRNs.

Field, Koros and Noyes (FKN) [17] from Oregon University, designed in 1972 the first CRN specifically to explain the BZ reaction experimental behavior. They provide a set of reaction rate kinetic constants based on thermodynamic and experiment collected data. The FKN-CRN contains fifteen chemical species and eleven reactions. Two years later, Field and Noyes [18] simplified the FKN-CRN, reducing it up to five reactions and three chemical species ( $\text{HBrO}_2$ ,  $\text{Br}^-$  and  $\text{Ce}^{+4}$ ), yet preserving the essential dynamics of the observed BZ reaction which has been coined as the Oregonator. Dynamic analysis of the Oregonator showed that it could reproduce and predict most of the observed behavior, *e.g.* oscillations and bistability, but could not display complex oscillations or chaos [19].

Janz, Vanecek and Field [19] expanded the Oregonator to modeled as a CFSTR; they find bursting phenomena similar to those observed in experiments at low flow rate. Turner *et. al.* [19] model all the reactions in the Oregonator as reversible ones under CFSTR conditions. Increasing the flow rates they find periodic and chaotic regions but not at the rates used for experiments. Showalter, Noyes and Bar-Eli (SNB) [19] expanded the Oregonator up to a seven variable CRN, allowing reversibility and replacing the autocatalytic reaction by two reactions that account for oxybromine chemistry. This expansion reproduced complex periodic waveforms at approximately the correct flow rates but not chaos.

Several CRNs of different chemistry and dimensions were proposed along the years to fit the new collected data concerning the detailed chemical processes in the BZ

reaction. Among others, Gyorgy and Field [1], based on a CRN with a eighty reactions accounting for the new detailed chemistry derived from experiments, devised a CRN with eleven variable chemical species and nineteen reactions (hereafter CRN  $GF_A$ ; see Figure 1.2) under a CFSTR operation. Surprisingly, CRN  $GF_A$  embodied and agreed with virtually all experimentally observed complex phenomena displayed by the BZ reaction at low flow rates [19].

TABLE I: Model A<sup>a</sup>

	rate constant	ref
A1. $\text{HOBr} + \text{Br}^- + \{\text{H}^+\} \rightarrow \text{Br}_2 + \{\text{H}_2\text{O}\}$	$6.0\text{E}+8 \text{ M}^{-1} \text{ s}^{-1}$	46
A2. $\text{Br}_2 + \{\text{H}_2\text{O}\} \rightarrow \text{HOBr} + \text{Br}^- + \{\text{H}^+\}$	$2.0 \text{ s}^{-1}$	46
A3. $\text{Br}^- + \text{HBrO}_2 + \{\text{H}^+\} \rightarrow 2\text{HOBr}$	$5.2\text{E}+5 \text{ M}^{-1} \text{ s}^{-1}$	25, 26
A4. $\text{Br}^- + \{\text{BrO}_3^-\} + \{2\text{H}^+\} \rightarrow \text{HOBr} + \text{HBrO}_2$	$0.01352 \text{ s}^{-1}$	25, 26
A5. $\text{HOBr} + \text{HBrO}_2 \rightarrow \text{Br}^- + \{\text{BrO}_3^-\} + \{2\text{H}^+\}$	$3.2 \text{ M}^{-1} \text{ s}^{-1}$	25
A6. $2\text{HBrO}_2 \rightarrow \{\text{BrO}_3^-\} + \text{HOBr} + \{\text{H}^+\}$	$3.0\text{E}+3 \text{ M}^{-1} \text{ s}^{-1}$	25
A7. $\{\text{BrO}_3^-\} + \text{HBrO}_2 + \{\text{H}^+\} \rightarrow 2\text{BrO}_2^* + \{\text{H}_2\text{O}\}$	$0.858 \text{ s}^{-1}$	25, 26
A8. $2\text{BrO}_2^* + \{\text{H}_2\text{O}\} \rightarrow \{\text{BrO}_3^-\} + \text{HBrO}_2 + \{\text{H}^+\}$	$4.2\text{E}+7 \text{ M}^{-1} \text{ s}^{-1}$	25
A9. $\text{Ce(III)} + \text{BrO}_2^* + \{\text{H}^+\} \rightarrow \text{HBrO}_2 + \text{Ce(IV)}$	$1.612\text{E}+4 \text{ M}^{-1} \text{ s}^{-1}$	25, 26
A10. $\text{HBrO}_2 + \text{Ce(IV)} \rightarrow \text{Ce(III)} + \text{BrO}_2^* + \{\text{H}^+\}$	$7.0\text{E}+3 \text{ M}^{-1} \text{ s}^{-1}$	25, 26
A11. $\text{MA} + \text{Br}_2 \rightarrow \text{BrMA} + \text{Br}^- + \{\text{H}^+\}$	$40.0 \text{ M}^{-1} \text{ s}^{-1}$	47
A12. $\text{MA} + \text{HOBr} \rightarrow \text{BrMA} + \{\text{H}_2\text{O}\}$	$8.2 \text{ M}^{-1} \text{ s}^{-1}$	48
A13. $\text{MA} + \text{Ce(IV)} \rightarrow \text{MA}^* + \text{Ce(III)} + \{\text{H}^+\}$	$0.3^c \text{ M}^{-1} \text{ s}^{-1}$	27
A14. $\text{BrMA} + \text{Ce(IV)} \rightarrow \text{Ce(III)} + \text{Br}^- + \{\text{products}\}$	$30.0^c \text{ M}^{-1} \text{ s}^{-1}$	27
A15. $\text{MA}^* + \text{BrMA} \rightarrow \text{MA} + \text{Br}^- + \{\text{products}\}$	$2.4\text{E}+4^c \text{ M}^{-1} \text{ s}^{-1}$	27
A16. $\text{MA}^* + \text{Br}_2 \rightarrow \text{BrMA} + \text{Br}^*$	$1.5\text{E}+8 \text{ M}^{-1} \text{ s}^{-1}$	26, 49
A17. $\text{MA}^* + \text{HOBr} \rightarrow \text{Br}^* + \{\text{products}\}$	$1.0\text{E}+7 \text{ M}^{-1} \text{ s}^{-1}$	26, 49
A18. $2\text{MA}^* \rightarrow \text{MA} + \{\text{products}\}$	$3.0\text{E}+9 \text{ M}^{-1} \text{ s}^{-1}$	27, 50
A19. $\text{Br}^* + \text{MA} \rightarrow \text{Br}^- + \text{MA}^* + \{\text{products}\}$	$1.0\text{E}+5 \text{ M}^{-1} \text{ s}^{-1}$	26

<sup>a</sup>The values  $[\text{H}_2\text{O}] = 55 \text{ M}$ ,  $[\text{BrO}_3^-] = 0.1 \text{ M}$ ,  $[\text{H}^+] = 0.26 \text{ M}$  are included in the appropriate rate constants. The mixed-feed concentrations are  $[\text{MA}]_{\text{in}} = 0.25 \text{ M}$ ,  $[\text{Ce(III)}]_{\text{in}} = 0.000833 \text{ M}$ . These are exactly the experimental conditions of refs 14–18.  $\text{E}+n \equiv \times 10^n$ . <sup>b</sup> $\text{MA} = \text{CH}_2(\text{COOH})_2$ ;  $\text{MA}^* = {}^*\text{CH}(\text{COOH})_2$ ;  $\text{BrMA} = \text{BrCH}(\text{COOH})_2$ . <sup>c</sup>Adjustable rate constant.

**Figure 1.2:**  $GF_A$  CRN, taken from [1]. Chemical species in curly braces are held constant during the course of reaction.

Further analysis of CRN  $GF_A$  lead to a set of reduced CRNs:  $GF_B$ , with nine variables and thirteen reactions (Figure 1.3, upper panel);  $GF_C$ , a seven variable CRN with eleven reactions (Figure 1.3, middle panel) and two four variable CRNs not following MAK,  $GF_D$  (Figure 1.3, lower panel). The first  $GF_D$  model is derived using quasi-steady-state assumption (QSSA), meanwhile the second is obtained by

TABLE II: Model B<sup>b</sup>

	rate constant
B1. $\text{HOBr} + \text{Br}^- + \{\text{H}^+\} \rightarrow \text{Br}_2 + \{\text{H}_2\text{O}\}$	$6.0\text{E}+8 \text{ M}^{-1} \text{ s}^{-1}$
B2. $\text{Br}^- + \text{HBrO}_2 + \{\text{H}^+\} \rightarrow 2\text{HOBr}$	$5.2\text{E}+5 \text{ M}^{-1} \text{ s}^{-1}$
B3. $\text{Br}^- + \{\text{BrO}_3^-\} + \{2\text{H}^+\} \rightarrow \text{HOBr} + \text{HBrO}_2$	$0.01352 \text{ s}^{-1}$
B4. $2\text{HBrO}_2 \rightarrow \{\text{BrO}_3^-\} + \text{HOBr} + \{\text{H}^+\}$	$3.0\text{E}+3 \text{ M}^{-1} \text{ s}^{-1}$
B5. $\{\text{BrO}_3^-\} + \text{HBrO}_2 + \{\text{H}^+\} \rightarrow 2\text{BrO}_2^* + \{\text{H}_2\text{O}\}$	$0.858 \text{ s}^{-1}$
B6. $2\text{BrO}_2^* + \{\text{H}_2\text{O}\} \rightarrow \{\text{BrO}_3^-\} + \text{HBrO}_2 + \{\text{H}^+\}$	$4.2\text{E}+7 \text{ M}^{-1} \text{ s}^{-1}$
B7. $\text{Ce(III)} + \text{BrO}_2^* + \{\text{H}^+\} \rightarrow \text{HBrO}_2 + \text{Ce(IV)}$	$1.612\text{E}+4 \text{ M}^{-1} \text{ s}^{-1}$
B8. $\text{HBrO}_2 + \text{Ce(IV)} \rightarrow \text{Ce(III)} + \text{BrO}_2^* + \{\text{H}^+\}$	$7.0\text{E}+3 \text{ M}^{-1} \text{ s}^{-1}$
B9. $\{\text{MA}\} + \text{Br}_2 \rightarrow \text{BrMA} + \text{Br}^- + \{\text{H}^+\}$	$40.0 \{\text{MA}\} \text{ s}^{-1}$
B10. $\{\text{MA}\} + \text{Ce(IV)} \rightarrow \text{MA}^* + \text{Ce(III)} + \{\text{H}^+\}$	$0.3^c \{\text{MA}\} \text{ s}^{-1}$
B11. $\text{BrMA} + \text{Ce(IV)} \rightarrow \text{Ce(III)} + \text{Br}^- +$ [products]	$30.0^c \text{ M}^{-1} \text{ s}^{-1}$
B12. $\text{MA}^* + \text{BrMA} \rightarrow \{\text{MA}\} + \text{Br}^- +$ [products]	$2.4\text{E}+4^c \text{ M}^{-1} \text{ s}^{-1}$
B13. $2\text{MA}^* \rightarrow \{\text{MA}\} +$ [products]	$3.0\text{E}+9 \text{ M}^{-1} \text{ s}^{-1}$

<sup>a</sup>A 9-variable model derived from model A.  $[\text{H}_2\text{O}] = 55 \text{ M}$ ,  $[\text{BrO}_3^-] = 0.1 \text{ M}$ ,  $[\text{H}^+] = 0.26 \text{ M}$  are included in the appropriate rate constants. <sup>b</sup> $\text{MA} \equiv \text{CH}_2(\text{COOH})_2$ ;  $\text{MA}^* \equiv {}^*\text{CH}(\text{COOH})_2$ ;  $\text{BrMA} \equiv \text{BrCH}(\text{COOH})_2$ . <sup>c</sup>Adjustable rate constant.

TABLE III: Model C<sup>a</sup>

	rate constant
C1. $\text{Br}^- + \text{HBrO}_2 + \{\text{H}^+\} \rightarrow 2\text{BrMA}$	$5.2\text{E}+5 \text{ M}^{-1} \text{ s}^{-1}$
C2. $\text{Br}^- + \{\text{BrO}_3^-\} + \{2\text{H}^+\} \rightarrow \text{BrMA} + \text{HBrO}_2$	$0.01352 \text{ s}^{-1}$
C3. $2\text{HBrO}_2 \rightarrow \{\text{BrO}_3^-\} + \text{BrMA} + \{\text{H}^+\}$	$3.0\text{E}+3 \text{ M}^{-1} \text{ s}^{-1}$
C4. $\{\text{BrO}_3^-\} + \text{HBrO}_2 + \{\text{H}^+\} \rightarrow 2\text{BrO}_2^* + \{\text{H}_2\text{O}\}$	$0.858 \text{ s}^{-1}$
C5. $2\text{BrO}_2^* + \{\text{H}_2\text{O}\} \rightarrow \{\text{BrO}_3^-\} + \text{HBrO}_2 + \{\text{H}^+\}$	$4.2\text{E}+7 \text{ M}^{-1} \text{ s}^{-1}$
C6. $\text{Ce(III)} + \text{BrO}_2^* + \{\text{H}^+\} \rightarrow \text{HBrO}_2 + \text{Ce(IV)}$	$1.612\text{E}+4 \text{ M}^{-1} \text{ s}^{-1}$
C7. $\text{HBrO}_2 + \text{Ce(IV)} \rightarrow \text{Ce(III)} + \text{BrO}_2^* + \{\text{H}^+\}$	$7.0\text{E}+3 \text{ M}^{-1} \text{ s}^{-1}$
C8. $\{\text{MA}\} + \text{Ce(IV)} \rightarrow \text{MA}^* + \text{Ce(III)} + \{\text{H}^+\}$	$0.3^c \{\text{MA}\} \text{ s}^{-1}$
C9. $\text{BrMA} + \text{Ce(IV)} \rightarrow \text{Ce(III)} + \text{Br}^- +$ [products]	$30.0^c \text{ M}^{-1} \text{ s}^{-1}$
C10. $\text{MA}^* + \text{BrMA} \rightarrow \{\text{MA}\} + \text{Br}^- +$ [products]	$2.4\text{E}+4^c \text{ M}^{-1} \text{ s}^{-1}$
C11. $2\text{MA}^* \rightarrow \{\text{MA}\} +$ [products]	$3.0\text{E}+0 \text{ M}^{-1} \text{ s}^{-1}$

<sup>a</sup>A 7-variable chaotic model derived from model B.  $[\text{H}_2\text{O}] = 55 \text{ M}$ ,  $[\text{BrO}_3^-] = 0.1 \text{ M}$ ,  $[\text{H}^+] = 0.26 \text{ M}$  are included in the appropriate rate constants. <sup>b</sup> $\text{MA} \equiv \text{CH}_2(\text{COOH})_2$ ;  $\text{MA}^* \equiv {}^*\text{CH}(\text{COOH})_2$ ;  $\text{BrMA} \equiv \text{BrCH}(\text{COOH})_2$ . <sup>c</sup>Adjustable rate constant.

TABLE IV: Model D<sup>a</sup>

	rate ( $r_i$ )
D1. $\text{Br}^- + \text{HBrO}_2 + \{\text{H}^+\} \rightarrow 2\text{BrMA}$	$r_1 = k_{D1}[\text{H}^+][\text{Br}^-][\text{HBrO}_2]$ $k_{D1} = 2.0\text{E}+6 \text{ M}^{-2} \text{ s}^{-1}$
D2. $\text{Br}^- + \{\text{BrO}_3^-\} + \{2\text{H}^+\} \rightarrow \text{BrMA} + \text{HBrO}_2$	$r_2 = k_{D2}[\text{BrO}_3^-][\text{H}^+]^2[\text{Br}^-]$ $k_{D2} = 2.0 \text{ M}^{-3} \text{ s}^{-1}$
D3. $2\text{HBrO}_2 \rightarrow \text{BrMA}$	$r_3 = k_{D3}[\text{HBrO}_2]^2$ $k_{D3} = 3.0\text{E}+3 \text{ M}^{-1} \text{ s}^{-1}$
D4. $0.5\text{HBrO}_2 + \{\text{BrO}_3^-\} + \{\text{H}^+\} \rightarrow \text{HBrO}_2 + \text{Ce(IV)}$	$r_4 = k_{D4}[\text{H}^+][\text{Ce}]_{\text{tot}} - [\text{Ce(IV)}][\text{BrO}_2^*]_{\text{tot}}$ $k_{D4} = 6.2\text{E}+4 \text{ M}^{-2} \text{ s}^{-1}$
D5. $\text{HBrO}_2 + \text{Ce(IV)} \rightarrow 0.5\text{HBrO}_2$	$r_5 = k_{D5}[\text{HBrO}_2][\text{Ce(IV)}]$ $k_{D5} = 7.0\text{E}+3 \text{ M}^{-1} \text{ s}^{-1}$
D6. $\text{Ce(IV)} + \{\text{MA}\} \rightarrow$	$r_6 = k_{D6}[\text{MA}][\text{Ce(IV)}]$ $k_{D6} = 0.3^c \text{ M}^{-1} \text{ s}^{-1}$
D7. $\text{BrMA} + \text{Ce(IV)} \rightarrow \text{Br}^-$	$r_7 = k_{D7}[\text{Ce(IV)}][\text{BrMA}]$ $k_{D7} = 30.0^c \text{ M}^{-1} \text{ s}^{-1}$
D8. $\text{BrMA} \rightarrow \text{Br}^-$	$r_8 = k_{D8}[\text{BrMA}][\text{MA}^*]_{\text{QSS}}$ $k_{D8} = 2.4\text{E}+4 \text{ M}^{-1} \text{ s}^{-1}$

<sup>a</sup>Chemical scheme of the two 4-variable models (depending on whether eq 3 or 4 is used for  $[\text{BrO}_2^*]_{\text{tot}}$ ) derived from model C. In this model  $\text{BrO}_3^-$ ,  $\text{H}^+$  and MA have fixed concentrations. The differential equations for these models are given in the text. <sup>b</sup> $\text{MA} \equiv \text{CH}_2(\text{COOH})_2$ ;  $\text{MA}^* \equiv {}^*\text{CH}(\text{COOH})_2$ ;  $\text{BrMA} \equiv \text{BrCH}(\text{COOH})_2$ .  $[\text{MA}^*]_{\text{QSS}}$  and  $[\text{BrO}_2^*]_{\text{tot}}$  are defined in the text. <sup>c</sup>Adjustable rate constant.

Figure 1.3:  $GF_B$  (upper panel),  $GF_C$  (middle panel) and  $GF_D$  (lower panel) CRNs were taken from [1]. Chemical species in curly braces are held constant during the course of reaction.

equilibrium assumptions (EQ). The latter model ( $GF_{Deq}$ ) match better the experiments for low flow rates than  $GF_{Dqssa}$ ; both show complex periodicities and chaos at high flow rates [1].

By no means CRNs reported by Gyorgy and Field [1] are unique, but are some of the most well documented in terms of reaction rates constants obtained from experiments. In this respect, we stress the fact that the *non MAK* model ( $GF_D$ ) fits very well the experiments, which in mathematical terms means that there are fractional powers in the ODES associated to the product of chemical species concentrations taking place within the CRN.

Taking into account the aforementioned examples as a motivation, in this thesis the concept of *dynamical equivalence* for CRNs is studied. The dynamical equivalence is obtained when the time evolution of chemical species concentrations are carried to a second space of chemical species concentrations from a second CRN, which might have a different dimension than the former CRN. The maps that carries solutions from one space into another are local diffeomorphisms, constructed using Lie derivatives [6, 7, 8].

## 1.2 State of knowledge

The topic of determining conditions under which CRNs with different reaction structure, *i.e.* different number of chemical species and reaction, exhibit the same qualitative dynamics (fundamental dogma of chemical kinetics), has gained attention recently [20, 21, 22, 23, 24, 25].

Structural indistinguishability stands for the problem of determining the uniqueness of the parameterisation or model structure, from input/output data [22, 23]. In a series of papers[22, 23, and references therein], the indistinguishability is tested for competing models structures (CRNs) for a given process with a given output.



Corollary 4 in [22] allows for testing structural indistinguishability between two candidate CRNs. As a case study, author's in [23], analyze the distinguishability of two CRNs standing for the single enzyme-single substrate reaction (Michaelins-Menten and Henry CRNs), for distinct output functions. The approach presented involves constructing, when possible, a smooth mapping between the trajectories of two candidate models. The smooth map is founded using Lie derivatives of the outputs after the (nonlinear) observability rank condition is fulfilled [6, 7]. This approach is focused on systems of ODEs derived from chemical kinetics in a broad sense, *i.e.* is not restricted to MAK-ODEs though they must have the same dimension.

Johnston and Siegel [24] consider MAK-ODEs induced by different CRNs with the same number of chemical species but not necessarily the same number of complexes and reactions. They call two MAK-ODEs *conjugate* systems if there exists a non-trivial linear mapping (not the identity map) which takes trajectories of one system into trajectories of the other. In particular, they focus on the subset of linearly conjugate systems. Author's in [24] do not require *a priori* knowledge of the second candidate CRN. Instead, they exploit the concept of *source complexes*, (*i.e.* the linear combination of chemical species at the left of the chemical arrow), defined in [20] in order to construct a target CRN which is a linear conjugate of the first (and known) CRN. Moreover, the target CRN has the property of being *weakly reversible*, *i.e.* there is a path connecting each complex (*i.e.* the linear combination of chemical species at the left and right of the chemical arrow) in the CRN, which has been proved to have locally stable dynamics (see [26] for details). Thus, the (possible more complex) CRN from which the target CRN is derived, also will posses locally stable dynamics.

Necessary and sufficient conditions have been provided in [20], such that two CRNs are capable of induce the same MAK-ODEs under an appropriate selection of kinetic constants. Authors in [20] named this feature *confoundability*, where the key point is that the vector space spanned by the linear combination of chemical species located

---

at the left hand of the chemical arrow in both CRNs is not empty ([20, see Theorem 4.4]). Also, MAK-ODEs are required to be of the same dimension.

In [21, 25], two (or more) CRNs are *dynamically equivalent* if they have the same MAK-ODEs, for a fixed set of complexes. Using a linear programming approach, author's in [21, 25] are able to find *sparse* and *dense* realizations of a given CRN [21, 25]. A *sparse realization* is a CRN with the minimal number of reactions that induce the same dynamics of the original one. On the contrary, a *dense realization* posses the maximal number of reactions that induce the same dynamics of the initial CRN. Moreover, dense realizations are unique and contain all the possible CRNs dynamical equivalent as a proper subgraph. In particular, the aim of the algorithm reported in [21] is to find realizations for which the MAK-ODEs exhibits locally stable dynamics. Thus, contrary to the work in [24], all the complexes can be used to construct the realizations, not just the source complexes (*i.e.* those at the left of the chemical arrow).

The approaches discussed above does not consider the scenario where two systems of ODEs are of distinct dimension, which do occurs in practice. Moreover, from a control system point of view, it is also required that the output between candidate systems be the same (cf. [22, 23]). It will be seen that the approach propounded in this thesis is less restrictive.

Next, a description of this thesis is given along with the chapters that conformed.

## 1.3 Description of the thesis

### 1.3.1 Hypothesis

The hypothesis of this thesis can be stated as:

“It is possible to express the time evolution of chemical species concentrations of one CRN as function of the time evolution of chemical species concentrations of a

second CRN, even when both sets of ODEs are not of the same dimension, by means of a change of coordinates.”

Specifically, it is proposed in this thesis to carry the solutions of one set of ODEs into a second set of solutions of another CRN via the mathematical composition of (local) diffeomorphic maps. We say that two CRNs are dynamical equivalents if the composition of diffeomorphic maps is possible and well defined within the domain of interest, *i.e* the semi-positive orthant. When one of the CRNs under consideration for dynamical equivalence is of distinct dimension and the composition is possible and well defined, then we say that the CRNs are partially dynamically equivalents. To the best of our knowledge, this situation has not been explored within the chemical kinetics literature. Thus, it is expected that results derived from the hypothesis contribute to a better understanding of the fundamental dogma in chemical kinetics for CRNs.

### 1.3.2 Objectives

The objective of this thesis is to analyze and propound methodologies to establish the equivalence between CRNs, with not necessarily the same dimension in the vector fields defined by the ODEs derived from the CRNs.

We can identify the following particular objectives: (1) set the mathematical conditions for the existence of dynamical equivalence for ODEs from CRNs with the same or distinct dimension. (2) Interpretation of the results in terms of chemical kinetics.

### 1.3.3 Methodology

In order to achieve the objective we propose the diffeomorphic maps be constructed using the recursive Lie derivatives of a single observable (output) function along the

vector field defined by the ODEs induced by the CRNs. We identify the singular points where diffeomorphic maps are not valid, along with those point in both parameter and state space where the mathematical composition of diffeomorphic maps carries solutions to the semi-positive orthant, the domain of phenomenological interest. Furthermore, we do not restrict the proposed approach to ask for the same observable function for the ODEs induced by the CRNs under consideration.

To illustrate our approach, we state preference for oscillatory CRNs such as Brusselator, Oregonator and the four dimensional CRN described in [1], which are closely related with the BZ reaction presented in the motivational examples section.

Chapter 2 is devoted to provide the mathematical framework on which CRNs are modeled along with its induced ODEs. A pair of graph theoretical formalisms oriented to classify and extract dynamical properties from CRNs structure alone, is also discussed. In addition, because its paramount role in the dynamical equivalence definition, construction of a change of coordinates (diffeomorphism) by means of recursive Lie derivatives is also explained.

A first attempt to approach the notion of dynamical equivalence between CRNs using graph theory and Lie derivatives is presented in Chapter 3. In particular, dynamical equivalence between two oscillatory CRNs of different dimension, 2 and 3, respectively, is studied.

Ideas presented in Chapter 3 are implemented in Chapter 4 to study the dynamical equivalence among several CRNs which stands for the BZ reaction. Particularly, the dynamical equivalence between Oregonator and a CRN that does not follows MAK but stands very well for the experimental evidence is presented.

Due to the extension from three to four years for PhD studies by CONACyT, as an aside, the dynamics of an autocatalytic CRN which models a neurodegenerative disease progression is investigated at Chapter 5. The deficiency formalism presented in Chapter 2 is exploited to identify sets of kinetic constants inducing complex behavior,

*e.g* bistability, sustained oscillations. Motivated by the existence of a steady state fulfilling one of the Shilnikov's conditions [27], a bifurcation analysis on the Prion system was performed, revealing the existence of degenerate steady states such as Bogdanov-Takens points.

Discussion of results are drawn in Chapter 6.

## 2. Mathematical Framework

The aim of this chapter is to provide the mathematical framework on which reaction systems are modeled. The dynamics of reaction systems are commonly described by ODEs derived from standard mass balance considerations. These dynamics result from the combination of a chemical reaction network (CRN), which encodes the reactions that are supposed to occur in the reactor, and reaction kinetics, e.g. positive scalar functions of a particular form. Additionally, the Chemical Reaction Network Theory (CRNT) formalism is presented, which allows to classify any CRN under the assumption of MAK with a nonnegative index, called the *deficiency* ( $\delta \geq 0$ ), computed from the network structure alone [5]. The CRNT is useful to determine whether or not a CRN endowed with MAK can or cannot support multiple (positive) steady states [5, 28]. In the same vein, Stoichiometric Network Analysis (SNA) is a graph theoretical formalism which enable to decompose the entire CRN into subnetworks in order to identify those subnetworks responsible for bistability or oscillations [4]. Mechanistic Classification of Chemical Oscillators (MCCO) developed in [2] relies heavily upon the SNA.

### 2.1 *Chemical reaction networks*

A CRN is a detailed description of the pathway leading from the reactants to the products, including as complete a characterization as possible of the composition and

other properties of reaction intermediates [29]. Formally:

**Definition 2.1.1** ([30]). *A chemical reaction network consists of three finite sets:*

1. *a set  $\mathcal{S}$  of distinct species of the network;*
2. *a set  $\mathcal{C} \subset \bar{\mathbb{R}}_+^{\mathcal{S}}$  of distinct complexes of the network;*
3. *a set  $\mathcal{R} \subset \mathcal{C} \times \mathcal{C}$  of distinct reactions, with the following properties:*
  - (a)  *$(u, u) \notin \mathcal{R}$  for any  $u \in \mathcal{R}$ .*
  - (b) *for each  $u \in \mathcal{C}$  there exists  $u' \in \mathcal{C}$  such that  $(u, u') \in \mathcal{R}$  or such that  $(u', u) \in \mathcal{R}$ .*

The set of *complexes* are linear combinations of chemical species which appear at the left and right of the chemical arrow. We note that the word “complex” is often taken to mean, within the (bio)chemistry literature, a macromolecular assembly. Because the term “complex” has a longstanding tradition in the CRNT literature, we thought it best to retain its usage.

For illustrative purposes, let us consider the full Brusselator CRN [3].



where the first reaction express that one molecule of  $X_3$  gives one molecule of  $X_1$ . Second reaction tell us that two molecules of  $X_1$  combines with one molecule of  $X_2$  in order to get three molecules of  $X_1$ : there is a net gain of one molecule for specie  $X_1$ . This type of reaction is called *autocatalytic*, because a species catalyse its own production. The remaining reactions can be read in the same manner. In

terms of sets, we have that  $\mathcal{S} = \{X_1, \dots, X_6\}$ , with  $s = 6$ . The set of complexes  $\mathcal{C} = \{X_3, X_1, 2X_1 + X_2, 3X_1, X_4 + X_1, X_2 + X_5, X_6\}$  and  $c = 7$ . Note that complex  $\{X_1\}$  appears as product (right side of reaction arrow) and as a reactive (left side of reaction arrow), but it is counted once; this rule applies for every complex in the CRN. The set of reactions is then  $\mathcal{R} = \{X_3 \rightarrow X_1, 2X_1 + X_2 \rightarrow 3X_1, X_4 + X_1 \rightarrow X_2 + X_5, X_1 \rightarrow X_6\}$ , where  $r = 4$ . The associated graph of the full Brusselator CRN is depicted in Figure 2.1.

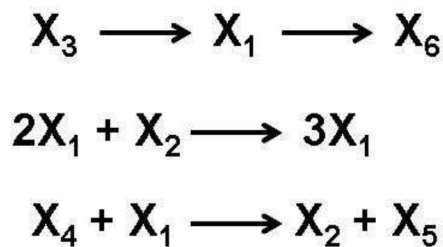


**Figure 2.1:** CRN associated to the full Brusselator.

Note that the set of complexes are the vertices of the associated graph of the CRN. Henceforth, the complexes of a CRN are the vertices of the associated graph of the CRN. Following the convention stated in [30], they must be displayed once.

Thus, we can generalize a CRN as:

$$\sum_{i=1}^s a_{ji} X_i \rightarrow \sum_{i=1}^s b_{ji} X_i, \quad j = 1, \dots, r \quad (2.5)$$

where  $a_{ji}$  and  $b_{ji}$  are nonnegative integers, called stoichiometric coefficients, arranged in their associated matrices  $A, B \in \mathbb{Z}^{r \times s}$ . The *stoichiometric* matrix  $N \in \mathbb{Z}^{s \times r}$  is then defined as:

$$N = (B - A)^{tr} \quad (2.6)$$

where  $tr$  denotes the usual matrix transpose operation. For the full Brusselator we



have:  $A, B \in \mathbb{Z}^{4 \times 6}$

$$A = \begin{bmatrix} 0 & 0 & 1 & 0 & 0 & 0 \\ 2 & 1 & 0 & 0 & 0 & 0 \\ 1 & 0 & 0 & 1 & 0 & 0 \\ 1 & 0 & 0 & 0 & 0 & 0 \end{bmatrix}, \quad B = \begin{bmatrix} 1 & 0 & 0 & 0 & 0 & 0 \\ 3 & 0 & 0 & 0 & 0 & 0 \\ 0 & 1 & 0 & 0 & 1 & 0 \\ 0 & 0 & 0 & 0 & 0 & 1 \end{bmatrix} \quad (2.7)$$

to finally obtain  $N \in \mathbb{Z}^{6 \times 4}$ :

$$N = \begin{bmatrix} 1 & 1 & -1 & -1 \\ 0 & -1 & 1 & 0 \\ -1 & 0 & 0 & 0 \\ 0 & 0 & -1 & 0 \\ 0 & 0 & 1 & 0 \\ 0 & 0 & 0 & 1 \end{bmatrix} \quad (2.8)$$

In general,  $N$  does not have maximal row rank. For  $d = \text{rank}(N)$ , there exist  $s - d$  conservation relations:

$$W^{tr} \cdot x = \omega \quad (2.9)$$

with  $W^{tr} \cdot N = 0$  for a  $W \in \mathbb{R}^{s \times (s-d)}$ , where  $\omega \in \mathbb{R}_+$ . It can be seen that  $d = 4$  for matrix (2.8), thus there are  $6 - 4 = 2$  conservation relations in the chemical species concentration space. These can be computed to be:

$$x_1 + x_2 + x_3 + x_6 = \omega_1, \quad \forall t \geq 0 \quad (2.10)$$

$$x_4 + x_5 = \omega_2, \quad \forall t \geq 0 \quad (2.11)$$

Thus, conservation relations can be used to reduce the number of MAK-ODEs induced by a CRN; in this particular case, by two.

## 2.2 Reaction kinetics

The rate of reactant consumption and product formation in the reactor is expressed by the reaction kinetics. Each reaction in the CRN has associated a reaction rate, basically a nonnegative time varying function:

$$v_j(\mathbf{k}, \mathbf{x}(t)) = k_j \phi_j(x(t)), \quad j = 1, \dots, r \quad (2.12)$$

where  $k_j$  is called the *rate constant*. Hereafter, we assume that  $k_j$  belongs to the positive orthant  $\mathbb{R}_+^r, \forall t \geq 0$ . The form of the scalar function  $\phi_j$ , is readily obtained from the CRN invoking MAK, which states that the rate of reaction is proportional (reaction rate constant) to the product of the concentrations of the reactants raised by their stoichiometric coefficients as reactants. Mathematically:

$$\phi_j(\mathbf{x}(t)) = \prod_{i=1}^s x_i^{a_{ji}}(t), \quad j = 1, \dots, r \quad (2.13)$$

where  $\mathbf{x}(t) = (x_1(t), \dots, x_s(t))^{tr}$  is the vector of time varying *chemical species concentrations*, belonging to the nonnegative orthant,  $\bar{\mathbb{R}}_+^s = \mathbb{R}_+^s \cup \{0\}$ . Thus, as soon as one of the reactants becomes exhausted or is not present at the beginning of the reaction, then  $\phi_j(\mathbf{x}(t)) = 0$  for some  $x_i(t)$ . We shall assume that reactants are always present in the reaction. Also, for the sake of brevity the explicit dependence on time of  $x_i(t)$  will be omitted hereafter. In particular, the vector of MAK reaction rates for the full Brusselator CRN reads as follows:

$$v(\mathbf{k}, \mathbf{x}) = (k_1 x_3, k_2 x_1^2 x_2, k_3 x_1 x_4, k_4 x_1)^T \quad (2.14)$$

Now, we have all the elements to derive the associated set of MAK-ODEs for a given CRN.

### 2.3 Differential equations associated to CRNs

The dynamics of a CRN within an isothermal well stirred closed chemical reactor, in liquid solution such that not appreciable variation within the reactor volume exists as reaction progress, are described by the following set of ODEs:

$$\frac{d\mathbf{x}}{dt} = \dot{\mathbf{x}} = N \cdot v(\mathbf{x}, \mathbf{k}) = \mathbf{f}(\mathbf{x}, \mathbf{k}), \quad \mathbf{x}(0) \geq 0 \quad (2.15)$$

If  $v(\mathbf{k}, \mathbf{x})$  is derived from MAK, then we say that Equation (2.15) are the MAK-ODEs induced by a CRN. For instance, let us assume an excess amount of reactants  $X_3, X_4$  in the full Brusselator CRN are initially present inside the reactor, at constant temperature and with no interchange of mass, that is, none chemical species enters or leaves the reactor as time goes by. Then, assuming MAK and following Equation (2.15), the dynamics of the chemical species within the closed reactor are modeled by:

$$\dot{x}_1 = k_1 x_3 + k_2 x_1^2 x_2 - k_3 x_1 x_4 - k_4 x_1, \quad x_1(0) > 0 \quad (2.16)$$

$$\dot{x}_2 = -k_2 x_1 x_2^2 + k_3 x_1 x_4, \quad x_2(0) > 0 \quad (2.17)$$

$$\dot{x}_3 = -k_1 x_3, \quad x_3(0) \geq 0 \quad (2.18)$$

$$\dot{x}_4 = -k_3 x_1 x_4, \quad x_4(0) \geq 0 \quad (2.19)$$

$$\dot{x}_5 = k_3 x_1 x_4, \quad x_5(0) \geq 0 \quad (2.20)$$

$$\dot{x}_6 = k_4 x_1, \quad x_6(0) \geq 0 \quad (2.21)$$

In order to account for an open operation of the reactor, *i.e* a CFSTR operation, we define the *zero complex*,  $\emptyset$ , which stands for the interchange of mass into and from the reactor and does not have any participation in the dynamics:  $\emptyset$  is not a chemical specie with an associated row in matrices  $A$  or  $B$ : is the zero vector in  $\mathbb{R}^s$ ; this simply stresses the fact that a chemical specie is entering or leaving the reactor. If a chemical(s) specie(s) enters the reactor, then it is necessary to add to the CRN

the following *pseudo-reaction(s)*,  $\emptyset \rightarrow X_i$ . Here  $X_i$  is a product, thus should be counted in the  $B$  matrix. Using MAK the feed rate has the form  $Fx_i^{in}$ , where  $F$  is the feed rate velocity and  $x_i^{in}$  the concentration of  $X_i$  in the feed stream. Both are considered as time invariant, thus they can be expressed as a kinetic constant, say  $k_j^f = F \cdot x_i^{in}$ . On the other hand, to model the withdrawal of a chemical specie(s) from the reactor we add the following pseudo-reaction(s)  $X_i \rightarrow \emptyset$ , where  $X_i$  is a reactant whose stoichiometric coefficient need to be considered in matrix  $A$ . Following MAK, we have the reaction rate  $k_j^*x_i(t)$ , where  $k_j$  can be considered as the rate of depletion of  $X_i$  from the reactor. Note that  $X_i$  might not enter and leave the reactor at the same rate, that is,  $F \neq k_j^*$ .

Using again the full Brusselator CRN, let us consider that  $X_1$  enters and leaves the reactor at different rates. Then, the following reactions need to be added to the full Brusselator CRN,  $\emptyset \rightleftharpoons X_1$ , where the forward reaction (entering) induce the MAK rate  $Fx_1^{in}$  and for the reverse reaction (depletion) we have  $k^*x_1$ . Thus, the new dynamics of  $X_1$  reads:

$$\dot{x}_1 = k_1x_3 + k_2x_1x_2^2 - k_3x_1x_4 - k_4x_1 + Fx_1^{in} - k^*x_1, \quad x_1(0) > 0 \quad (2.22)$$

Nevertheless, the zero complex can also appear when modeling a CRN when certain chemical species are considered constant. For example, we shall suppose for the full Brusselator that species  $X_3, X_4$  and  $X_5, X_6$  are added to or removed from the reactor in such a manner within the reactor fixed at values  $x_3^*, x_4^*, x_5^*, x_6^*$ , respectively. Then, for some reasonable time scale, the CRN of real interest will be:



where chemical species  $X_3, X_4, X_5$  and  $X_6$  has been stripped away from the original

CRN. The resulting (full row rank) stoichiometric matrix and MAK rate vector are:

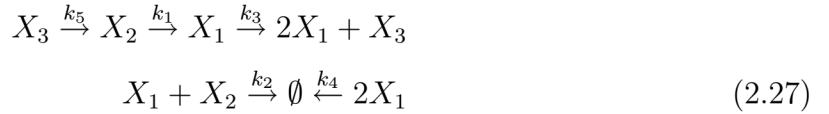
$$N = \begin{bmatrix} 1 & 1 & -1 & -1 \\ 0 & -1 & 1 & 0 \end{bmatrix}, \quad v(\mathbf{x}, \mathbf{k}) = (k_1, k_2 x_1^2 x_2, k_3 x_1, k_4 x_1)^T \quad (2.24)$$

where  $k_1 = k'_1 x_3^*$ ,  $k_3 = k'_3 x_4^*$ , because  $\dot{x}_3 = \dot{x}_4 = 0$  along with  $\dot{x}_5 = \dot{x}_6 = 0$ . Then, the resulting MAK-ODEs induced by the reduced Brusselator CRN are:

$$\dot{x}_1 = k_1 + k_2 x_1^2 x_2 - k_3 x_1 - k_4 x_1, \quad x_1(0) \geq 0 \quad (2.25)$$

$$\dot{x}_2 = -k_2 x_1^2 x_2 + k_3 x_1, \quad x_2(0) \geq 0 \quad (2.26)$$

It is convenient for the rest of this thesis to present the Oregonator CRN and their associated MAK-ODEs. Following the same procedure as in the Brusselator of stripping away those time invariant chemical species, we get the CRN [18]:



with stoichiometric matrix and vector of reaction rates

$$N = \begin{bmatrix} 1 & -1 & 1 & -2 & 0 \\ -1 & -1 & 0 & 0 & 1 \\ 0 & 0 & 1 & 0 & -1 \end{bmatrix}, \quad v(\mathbf{x}, \mathbf{k}) = (k_1 x_2, k_2 x_1 x_2, k_3 x_1, k_4 x_1^2, k_5 x_3)^T \quad (2.28)$$

to finally obtain the MAK-ODEs corresponding to Oregonator CRN:

$$\begin{aligned} \dot{x}_1 &= k_1 x_2 - k_2 x_1 x_2 + k_3 x_1 - 2k_4 x_1^2 \\ \dot{x}_2 &= -k_1 x_2 - k_2 x_1 x_2 + k_5 x_3 \\ \dot{x}_3 &= k_3 x_1 - k_5 x_3 \end{aligned} \quad (2.29)$$

Next, we briefly review a mathematical formalism oriented to elucidate whether or not MAK-ODEs can support multiple (positive) steady states, from the CRN's structure.

## 2.4 Chemical reaction network theory

The CNRT is a formalism based on a non-negative integer called *deficiency*,  $\delta \geq 0$ , of a CRN [30, 28]. This integer relates the structure of the CRN with the existence or not of (multiple) equilibria for the corresponding system of MAK-ODEs. The dynamical information the deficiency provides is embraced by the Deficiency Zero Theorem (DZT), and the Deficiency One Theorem (DOT) along with the Advanced Deficiency One Theory (ADOT). Before review them, some terminology inherent to the CRNT formalism is presented.

The *complexes* of a CRN are the linear combinations of chemical species that appear before and after the reaction arrow [5]. Complexes are restricted to appear just once in the graphical representation of the CRN under study, including the zero complex,  $\emptyset$ . Thus, from a graph theoretical point of view, complexes are the vertex of the graph associated to the CRN. Additionally, a CRN it can be composed by more than one subnetwork, that is, it might be sub-graphs whose union yield the whole CRN. Such pieces are termed *linkage classes*. Formally, a linkage class is a group of complexes that are connected by reaction arrows, *i.e.* the number of separate “pieces” of which the network is composed. If all reactions within the CRN are reversible, *i.e.* all complexes are linked by  $\rightleftharpoons$ , then it is said that the CRN is *reversible* [5]. Nevertheless, a CRN is *weakly reversible* if, whenever there is a directed (reaction) arrow path leading from complex, say  $C$  to complex  $C'$ , there is also a directed arrow path leading from  $C'$  back to  $C$ . Thus, all reversible CRNs are weakly CRNs, but not the converse [5]. Alternatively, a CRN is weakly reversible if each reaction arrow is contained within a directed arrow cycle.

The mathematical definition of the deficiency is:

$$\delta = |\mathcal{C}| - |\mathcal{L}| - \text{rank}(N) \quad (2.30)$$

where  $|\mathcal{C}|$  is the number of complexes (including the zero complex,  $\emptyset$ ) and  $|\mathcal{L}|$  the

number of *linkage classes*.

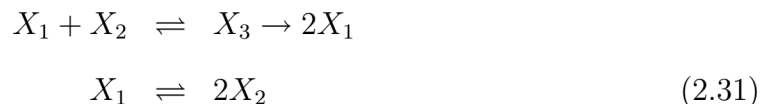
Now, we have the sufficient terminology to state the DZT (further details can be found at [5]).

**Theorem 2.4.1.** *For any reaction network of deficiency zero, the following statements hold true:*

1. *If the network is not weakly reversible, then for arbitrary kinetics (not necessarily mass action), the differential equations for the corresponding reaction system cannot admit a positive steady state (i.e. a steady state in  $\mathbb{R}_+^s$ ).*
2. *If the network is not weakly reversible, then for arbitrary kinetics (not necessarily mass action), the differential equations for the corresponding reaction system cannot admit a cyclic composition trajectory along which all species concentrations are positive.*
3. *If the network is weakly reversible, then for mass action kinetics (but regardless of the positive values the rate constants take), the resulting differential equations have the following properties:*

*There exists within each positive stoichiometric compatibility class precisely one steady state; that steady state is asymptotically stable; there is no nontrivial cyclic composition trajectory along which all species concentrations are positive.*

For example, let us consider the following CRN:



We have that the set of complexes is  $\mathcal{C} = \{X_1 + X_2, X_3, 2X_1, X_1, 2X_2\}$ , thus  $|\mathcal{C}| = 5$ . In the same way, we can identify the set of linkage classes:  $\mathcal{L} = \{\{X_1 + X_2 \rightleftharpoons$

$X_3 \rightarrow 2X_1$ ,  $\{X_1 \rightleftharpoons 2X_2\}$ . Therefore,  $|\mathcal{L}| = 2$ . It is straightforward to check that  $\text{rank}(N) = 3$ , where  $N \in \mathbb{R}^{3 \times 5}$ . In addition, the CRN is not weakly reversible; then  $\delta = 5 - 2 - 3 = 0$ . Thus, condition (1) and (2) of the DZT hold.

The DOT provides less powerful results than similar to the DZT: is restricted to CRN whose dynamics are governed by MAK and gives no stability information [5]. Nevertheless, the DOT has been extended to embrace CRNs with deficiency higher than one: the ADOT [31]. The DOT has been implemented in a freely available Windows program [28]. To get a full description of the DOT, see [31].

The dynamical information the DOT along with its enhancement, the ADOT, can be summarized as follows:

- If  $\delta = 1$  and the network satisfies some additional conditions, DOT can decide whether the CRN can or cannot admit multiple steady states by solving systems of equalities and inequalities which are guaranteed to be linear [28, 30, 31, 32].
- If  $\delta > 1$ , the ADOT along with its algorithm [28, 32, 31] might have to consider nonlinear inequalities to decided about multistationarity of the CRN.

It is beyond the scope of this thesis to provide a thoroughly description of DOT and the ADOT; the interested reader is referred to [31] for details. We turn now our attention to a second graph theoretical approach.

## *2.5 Stoichiometric network analysis and the mechanistic classification of chemical oscillators*

The key feature of SNA theory is to analyze the dynamics of the system in the reaction rate space, rather than in the species concentration space (see Figure 2.2). This approach enables to draw some conclusions about the CRN dynamics without



specifying the concentration values or kinetic parameters evaluated at the steady state. That is, for a chosen set of parameters  $\mathbf{k} \in \mathbb{R}_+^r$ , any steady state of the system must satisfies the condition:

$$N \cdot v(\mathbf{x}, \mathbf{k}) = 0 \quad (2.32)$$

where all the stationary reaction rates belongs to the intersection of the  $\ker(N)$  with  $\mathbb{R}_+^r$ , forming a convex polyhedral cone,  $K_{v(x,k)}$  [4], as depicted in Figure 2.2. The unique and minimal set of generating vectors spanning  $K_{v(x,k)}$  are called *extreme currents*, arranged in the matrix  $E \in \bar{\mathbb{R}}_+^{r \times f}$ , where  $f \geq \dim(\ker(N))$  [4]. The extreme currents presented in this thesis were computed with the program routine FluxAnalyzer [33].

$$K_{v(x,k)} = \{v(\mathbf{x}, \mathbf{k}) \in \bar{\mathbb{R}}_+^r \mid N \cdot v(\mathbf{x}, \mathbf{k}) = 0, v(x, k) \geq 0\} \quad (2.33)$$

$$= \{\ker(N) \cap \bar{\mathbb{R}}_+^r\} \quad (2.34)$$

$$= \left\{ \sum_{p=1}^f j_p E_p > 0, \forall p \right\} \quad (2.35)$$

The non-negative entries of the extreme currents denote subnetworks for which a steady state exists [4]. The parameters  $j > 0$ , are called *convex parameters* and quantify the influence of an extreme current on full network dynamics. The reaction rates can be expressed as a linear combination of convex parameters as follows:

$$v(j) = \sum_{p=1}^f j_p E_p \quad (2.36)$$

The jacobian matrix, after a suitable map transformation [4], and the use of Equation (3.9), can be expressed as:

$$Jac(v) = N \text{diag}(v) \kappa^{tr} \text{diag}(h_i) \quad (2.37)$$

$$\Rightarrow Jac(j) = N \text{diag}\left(\sum_{p=1}^f j_p E_p\right) \kappa^{tr} \text{diag}(h_i) \quad (2.38)$$

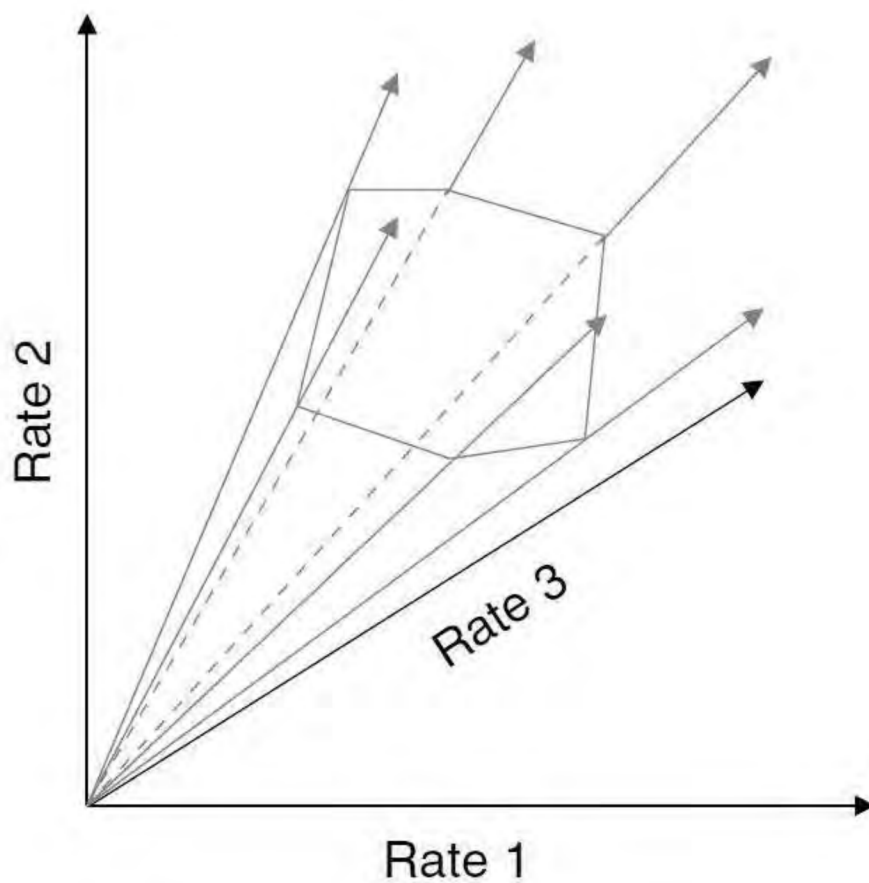


**Figure 2.2:** *The convex cone formed by reaction rates in a CRN.*

where  $h_i = x_{i,ss}^{-1}, i = 1, \dots, s$  is the inverse steady state concentrations and  $\kappa \in \mathbb{R}^{s \times r}$  is the *kinetic matrix* where the *kinetic exponents* of the  $i$ -th chemical specie in the  $j$ -th reaction are arranged [4, 2].

SNA can be used to identify those extreme currents cycles leading to instability. A classification of chemical oscillators based on certain characteristics of these cycles has been reported to be fruitful [2, 4]. To perform the MCCO is necessary to draw the entire *network diagram*,  $D_N$ , where the chemical species are connected by arrows denoting reactions. The total number of feathers of an arrow equals the stoichiometric number of that specie as reactant and the total number of barbs equals the stoichiometric number of a specie as product in the corresponding reaction. Using those subnetworks defined by the extreme currents, a *current diagram*  $D_C$ , is drawn in the same fashion. This  $D_C$  requires that the sum over all feathers equals the sum over all barbs for every species in the diagram (see Figure 2.3).

The current cycles are classified depending upon if the kinetic order (number of feathers) of the exit reaction ( $\kappa_{exit}$ ) from the cycle is lower than, equal to, or higher than the kinetic order of the cycle ( $\kappa_{cycle}$ ). Figure 2.3 graphically summarize these concepts.

- if  $\kappa_{exit} > \kappa_{cycle}$  the current is a *weak current cycle*, which is always stable.
- if  $\kappa_{exit} = \kappa_{cycle}$  the current cycle is termed *critical current cycle* (CCC), which can lead to instability (and possibly to oscillations) depending in other features of the network.
- if  $\kappa_{exit} < \kappa_{cycle}$  the network has a *strong cycle* (SC) and therefore a source of instability.

Based on this classification is possible to categorize oscillatory reactions into two majors classes [2]:

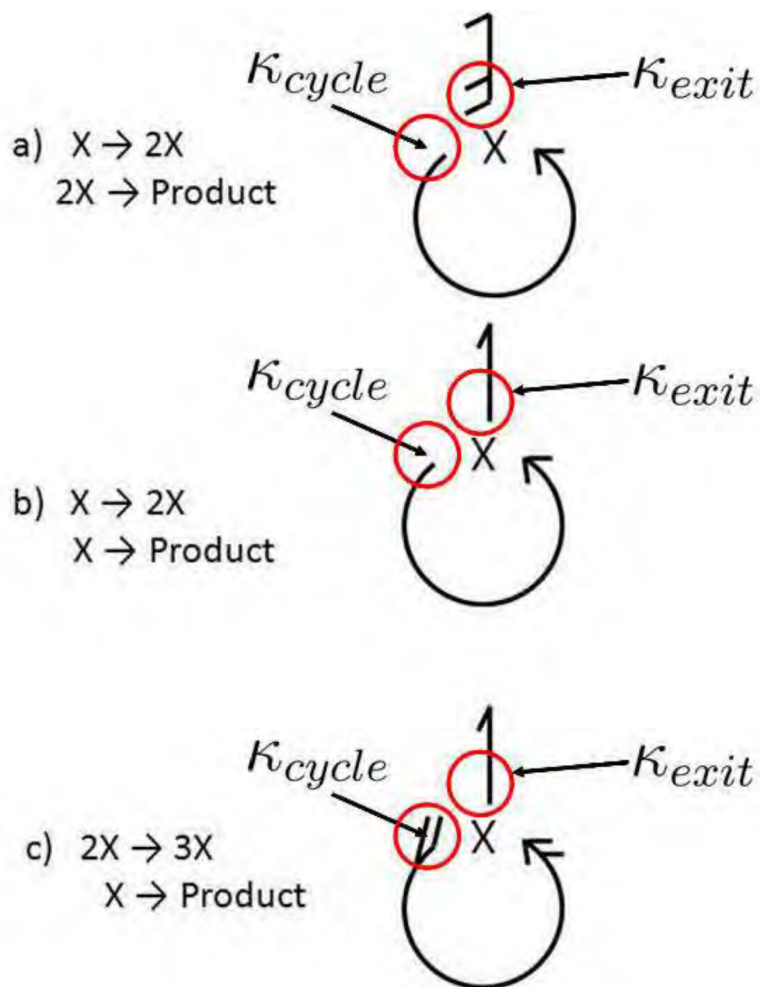


**Figure 2.3:** Simple current cycles adapted from [2]. (a) weak (2,1;  $\kappa_{exit} = 2, \kappa_{cycle} = 1$ ); (b) critical (1,1); and (c) strong (1,2).

- Category 1. Networks containing a CCC and a destabilizing exit reaction.
- Category 2. Networks whose instability arises from a SC

Up to now, the graph theoretical approaches are valid tools under steady state conditions. Next section presents a dynamical approach based on a change of coordinates using Lie derivatives.

## 2.6 Change of coordinates via Lie derivatives

Modern nonlinear control theory makes extensive use of geometrical methods to feedback linearize nonlinear systems as opposed to the standard Taylor approximation approach by means of a change of coordinates defined by a *diffeomorphism* [6, 7, 8]. Such a change of coordinates allows to write the nonlinear system as a linearized one upon which is easier to perform control tasks locally [6, 7, 8]. Then, the concept of diffeomorphism can be considered as a generalization of the concept of change of coordinates. In this sense, we can define it as:

**Definition 2.6.1.** *A function  $\Phi : \mathbb{R}^n \rightarrow \mathbb{R}^n$ , defined in a region  $\Omega$ , is called a diffeomorphism if it is smooth, and if its inverse  $\Phi^{-1}$  exists and is smooth.*

If the region  $\Omega$  is the whole space  $\mathbb{R}^n$ , then  $\Phi(x)$  is a *global* diffeomorphism; otherwise, it is said to be a *local* diffeomorphism, *i.e.* the transformation is defined in a finite neighborhood of a given point. Thus, given a nonlinear function  $\Phi(x)$ , it is possible to verify whether it is a local or global diffeomorphism using the following lemma [8]:

**Lemma 2.6.2.** *Let  $\Phi(x)$  be a smooth function defined in a region  $\Omega$  in  $\mathbb{R}^n$ . If the Jacobian matrix  $\frac{\partial \Phi(\mathbf{x})}{\partial \mathbf{x}}$  is nonsingular at a point  $\mathbf{x} = \mathbf{x}_0$  of  $\Omega$ , then  $\Phi(\mathbf{x})$  defines a local diffeomorphism in a subregion of  $\Omega$ .*

There are several ways to construct diffeomorphisms, ranging from pure intuition to differential embeddings, among others [34, 35, 36]. Within the control literature, the construction of diffeomorphisms it is straightforward by means of recursive Lie derivatives of a scalar function, *i.e.* an observable function [6, 7, 8].

Formally, we can write the set of MAK-ODEs as  $\dot{\mathbf{x}} = \mathbf{f}(\mathbf{x}, \mathbf{k})$ , where  $\mathbf{f}$  is the vector field that maps points from some open set  $\mathcal{D} \subset \mathbb{R}^n$  to a tangent space. Consider the existence of a smooth output function  $y = h(\mathbf{x})$ , where  $h : \mathbb{R}^n \rightarrow \mathbb{R}$ . In particular, for chemical reactions, any measurable chemical specie(s) concentration(s) or a (non)linear combination of them will be valid as an output function. A coordinate transformation (diffeomorphism)  $\mathbf{z} = \Phi(\mathbf{x})$  around  $\mathbf{x}_0$  can be constructed via Lie derivatives as follows [6, 7, 8]:

$$\mathbf{z} = \Phi(\mathbf{x}) = (h(\mathbf{x}), L_f h(\mathbf{x}), \dots, L_f^{s-1} h(\mathbf{x}))^{tr} \quad (2.39)$$

where  $s$  is the dimension of the chemical species concentration vector,  $\mathbf{x} = (x_1, \dots, x_s)$ . The Lie derivative of the output or observable function  $y = h(\mathbf{x})$  along the vector field,  $\mathbf{f}(\mathbf{x}, \mathbf{k})$ , is defined as:

$$L_f h(\mathbf{x}) = \sum_{i=1}^s f_i(\mathbf{x}, \mathbf{k}) \frac{\partial h(\mathbf{x})}{\partial x_i} \quad (2.40)$$

The new system of ODEs as a function of  $z$ 's is obtained using  $\mathbf{x} = \Phi^{-1}(\mathbf{z})$ :

$$\dot{\mathbf{z}} = \frac{\partial \Phi(\mathbf{x})}{\partial \mathbf{x}} \dot{\mathbf{x}} = \frac{\partial \Phi(\mathbf{x})}{\partial \mathbf{x}} \cdot \mathbf{f}(\mathbf{x}, \mathbf{k}) \quad (2.41)$$

which yields to:

$$\begin{aligned} \dot{z}_1 &= z_2 \\ \dot{z}_2 &= z_3 \\ &\vdots \\ \dot{z}_{s-1} &= z_s \\ \dot{z}_s &= w(z_1, \dots, z_s) \end{aligned} \quad (2.42)$$

The “staircase” form of Equation (2.47) is known in the control literature as the Brunovsky canonical and controllable form [6, 7]. Nevertheless, along this thesis, we do not consider explicitly a control input, *i.e.* a second vector field (typically denoted as  $g(\mathbf{x})$ ), added to the ODEs induced by the CRNs. Because we do not take into account for the construction of  $\Phi(\mathbf{x})$  the role of  $g(\mathbf{x})$  upon the CRN dynamics, the concept of *relative degree*, *i.e.* the number of Lie derivatives that the output function need to be computed along the vector field such that control input appears explicitly [6, 7], is not explored.

Now, let us illustrate the procedure of change of coordinates using Lie derivatives for the Brusselator (2.25) with  $y = h(\mathbf{x}) = x_1$  as the observable function. Following Equations (2.39) and (2.40), we have:

$$\begin{aligned} \mathbf{z} &= \Phi(\mathbf{x}) = (h(\mathbf{x}), L_f h(\mathbf{x}))^{tr} \\ z_1(\mathbf{x}) &= h(\mathbf{x}) = x_1 \end{aligned} \tag{2.43}$$

$$z_2(\mathbf{x}) = L_f h(\mathbf{x}) = k_1 + k_2 x_1^2 x_2 - (k_3 + k_4) x_1 \tag{2.44}$$

with an inverse, *i.e.*  $\mathbf{x} = \Phi^{-1}(\mathbf{z})$  as:

$$x_1 = z_1 \tag{2.45}$$

$$x_2 = \frac{z_2 + (k_2 + k_3)z_1 - k_1}{k_2 z_1^2} \tag{2.46}$$

It not difficult to check from Equation (2.43) that  $\det\left(\frac{\partial\Phi(\mathbf{x})}{\partial\mathbf{x}}\right) = k_2 x_1^2 \neq 0$ . Therefore, the diffeomorphism  $\Phi$  is a local one whenever  $x_1(t) > 0, \forall t \geq 0$ ; kinetic constants are assumed to be positive, unless stated otherwise. Using Equation (2.45) we can write the Brusselator’s MAK-ODEs (2.25) in terms of variables  $z$ ’s instead of chemical

concentrations,  $x'$ s:

$$\dot{\mathbf{z}} = \frac{\partial \Phi(\mathbf{x})}{\partial \mathbf{x}} \cdot \mathbf{f}(\mathbf{x}, \mathbf{k}) \quad (2.47)$$

$$\dot{z}_1 = z_2 \quad (2.48)$$

$$\dot{z}_2 = -k_2(k_2 + k_3)z_1^3 + (k_1 - z_2)k_2z_1^2 + (k_2 + k_3)z_1 + \frac{2z_2(z_2 - z_1)}{z_1} \quad (2.49)$$

As we can see, diffeomorphisms allows to map solutions, *i.e.* trajectories of a set of MAK-ODEs into an equivalent space formed by recursive derivatives. This is shown in Figure 2.4 for the reduced Brusselator.

## 2.7 Concluding comments

The mathematical framework for the modeling of CRNs has been established. In particular, the ODEs from the MAK assumption were derived for an isothermal, closed and open, chemical reactor. It was illustrated for the Brusselator and Oregonator CRNs that, stripping away those chemical species considered as time invariant, the resulting CRN might induce MAK-ODEs associated to open reactor conditions. Graph formalism such as the CRNT and MCCO were introduced as useful tools to classify CRNs. However, these formalisms assume steady state conditions. The construction of a diffeomorphism (change of coordinates) using recursive Lie derivatives of an observable function along the ODEs derived from a particular CRN, is not restricted to a steady state assumption as illustrated for the Brusselator CRN in its oscillatory regime.

The mathematical framework presented in this chapter are revisited and investigated in chapter 3 for oscillatory CRNs of the same and distinct dimension.



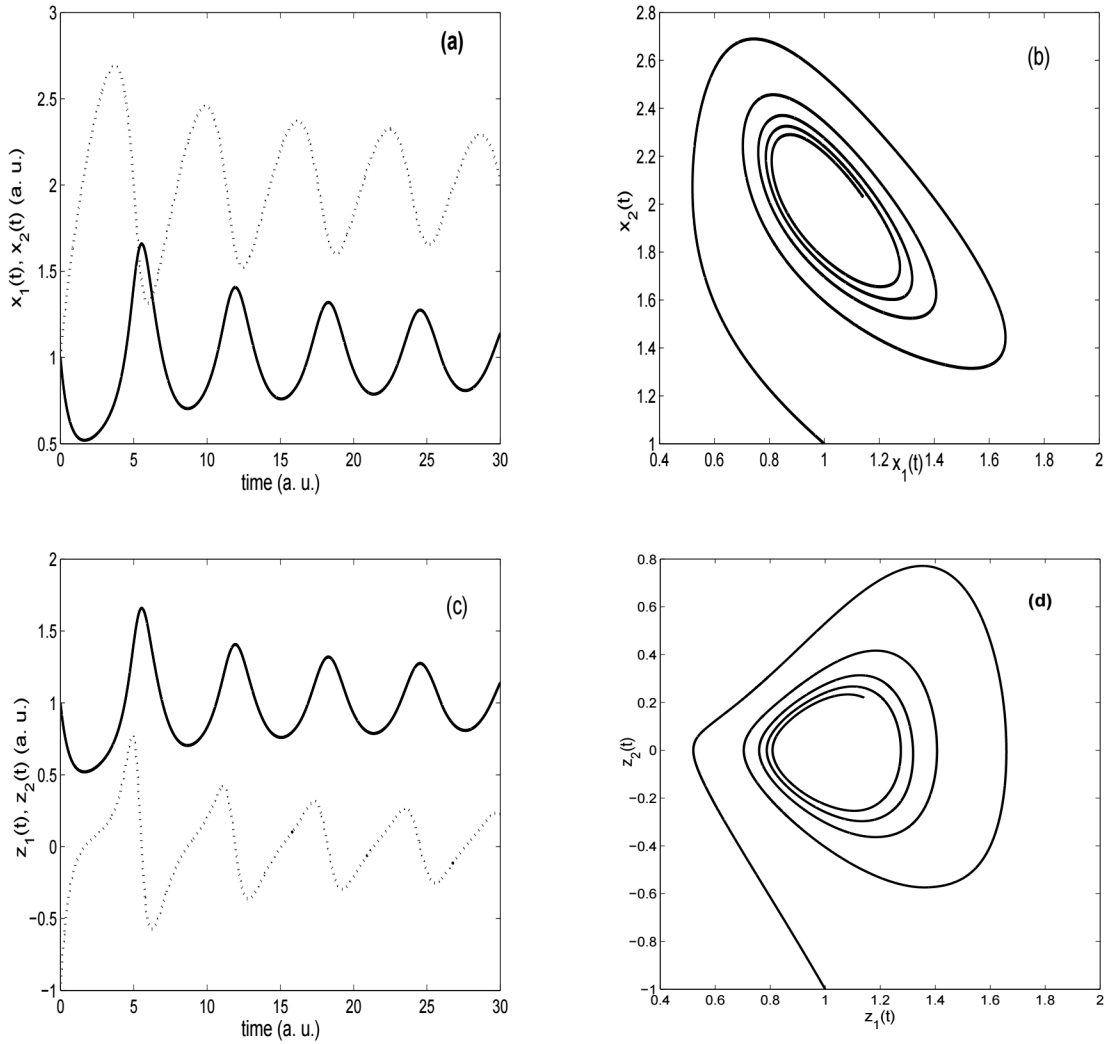


**Figure 2.4:** Oscillatory dynamics of the reduced Brusselator for both chemical and transformed spaces. Kinetic constants  $k_1 = k_2 = k_4 = 1, k_3 = 2$ . Initial conditions  $\mathbf{x}(0) = (1, 1)$ . (a) Time evolution of  $x_1$  (solid line) and  $x_2$  (dotted line); (b) Chemical species concentration state space; (c) Time evolution of  $x_1$  (solid line) and  $x_2$  (dotted line) after change of coordinates, i.e.  $z_1$  and  $z_2$  as in Equation (2.45); (d) Dynamics in transformed state space.

# 3. Towards a Dynamical Equivalence Between Distinct Oscillatory CRNs

This chapter presents an implementation of both graph approaches reviewed in chapter 1 and the Lie derivative approach, *i.e.* a change of coordinates, towards a dynamical equivalent between two oscillatory CRNs of different dimension (two and three, respectively). The CRNs used as core examples are the Brusselator and the Oregonator. The former the first designed reaction network oriented to explain, mathematically, the sustained oscillations and pattern formation observed in the BZ reaction [3]; the latter, the first chemically respectable reaction network for the BZ [3].

## 3.1 *Graph approaches*

### 3.1.1 *Chemical reaction network theory*

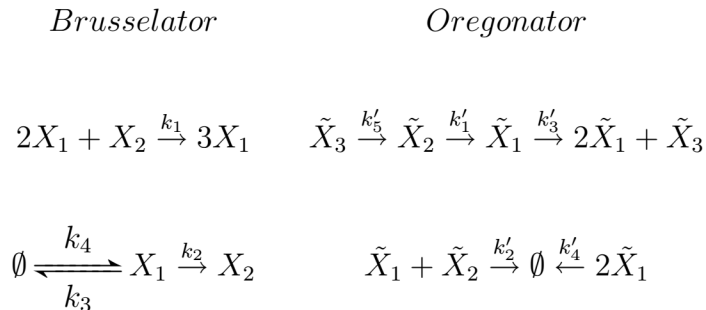
The CNRT is a formalism based on a non-negative integer called *deficiency*,  $\delta$ , of a CRN [30, 28]. This integer relates the structure of the network with the existence or not of (multiple) equilibria for the corresponding system of ODEs as in (2.32). Let

us recall the mathematical definition of the deficiency given in chapter 2:

$$\delta = |\mathcal{C}| - |\mathcal{L}| - \text{rank}(N) \quad (3.1)$$

where  $|\mathcal{C}|$  is the number of complexes (including the zero complex,  $\emptyset$ ) and  $|\mathcal{L}|$  the number of *linkage classes*.

We might ask if for two or more oscillatory CRN that stands for the same reaction, does the deficiency must be the same? Let us find out for the Brusselator and Oregonator, depicted below:



We shall denote as  $\tilde{X}_i$ ,  $i = 1, 2, 3$  the species for the Oregonator; lower case letters are reserved for chemical species concentrations. In order to compute their deficiencies, we need the dimension of their stoichiometric spaces, thus for the networks above we have:

$$N = \begin{bmatrix} 1 & -1 & -1 & 1 \\ -1 & 1 & 0 & 0 \end{bmatrix} \quad (3.2)$$

$$\tilde{N} = \begin{bmatrix} 1 & -1 & 1 & -2 & 0 \\ -1 & -1 & 0 & 0 & 1 \\ 0 & 0 & 1 & 0 & -1 \end{bmatrix} \quad (3.3)$$

None of them is rank deficiency, thus no conservation relations exists.

Recall that complexes of a CRN are the objects that appear before and after the reaction arrows, and each one of them must appear only once in the network. The set

of complexes for the Brusselator CRN are:  $\{\emptyset, X_1, X_2, 2X_1+X_2, 3X_1\}$ , thus  $|\mathcal{C}| = 5$ . Brusselator is composed by two linkage classes, the sets of complexes  $L_1 = \{2X_1 + X_2, 3X_1\}$  and  $L_2 = \{\emptyset, X_1, X_2\}$ , thus  $|\mathcal{L}| = 2$ . In addition,  $\text{rank}(N) = 2$ . Therefore,  $\delta = 5 - 2 - 2 = 1$ . The DOT implemented in [28] returns: the network cannot admit multiple positive steady states or a degenerate positive steady state (a non-hyperbolic steady state) no matter what positive values the kinetic constants might have. The DOT remains silent about the stability of the system. It is straightforward to check the uniqueness of a steady state in the Brusselator CRN, and its loss of stability so that trajectories reach a stable limit cycle, *i.e.* sustained oscillations [37]. Note that multistationarity does not preclude the possibility for oscillations to appear [38].

For the Oregonator CRN the set of complexes reads:  $\{\emptyset, \tilde{X}_1, \tilde{X}_2, \tilde{X}_3, 2\tilde{X}_1, 2\tilde{X}_1 + \tilde{X}_3, \tilde{X}_1 + \tilde{X}_2\}$ , therefore  $|\tilde{\mathcal{C}}| = 7$ . It can be seen that Oregonator CRN is composed by two linkage classes, thus  $|\tilde{\mathcal{L}}| = 2$ . Accordingly,  $\text{rank}(\tilde{N}) = 3$ . Computing the deficiency for the Oregonator we have:  $\tilde{\delta} = 7 - 2 - 3 = 2$ . Moreover, using the CRNT Toolbox [28] to apply the ADT, it is concluded that taken with mass action kinetics, the network cannot admit multiple steady states or a degenerate steady state no matter what (positive) values the rate constants might have.

Thus, we have shown that, despite their distinct deficiencies, both Brusselator and Oregonator share the following dynamical properties: (1) non-existence of multiple positive steady states and, (2) capacity for sustained oscillations. Therefore, if one has interest to classify (in this case) oscillatory CRNs such a classification cannot be based on the deficiency concept solely. On the other hand, it can be proved that a CRN must have  $\delta \geq 1$  in order to support bistability or oscillations [30, 32]. Moreover, if two or more CRNs support the same experimental data, deficiencies among them need not to be equal, as shown in [31, 11, 9]. In this sense, the concept of deficiency is not suitable as an equivalence property at the steady state for Brusselator and Oregonator CRN.

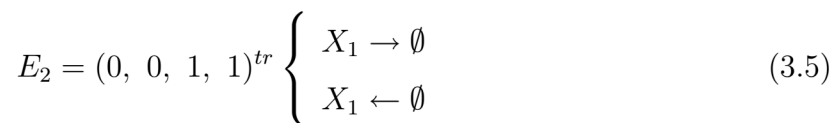
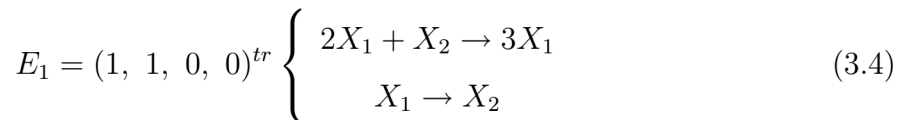
In order to circumvent this issue, a complementary graphical approach, strongly oriented for chemical oscillators, is implemented in the next section.

### 3.1.2 Mechanistic classification of chemical oscillators.

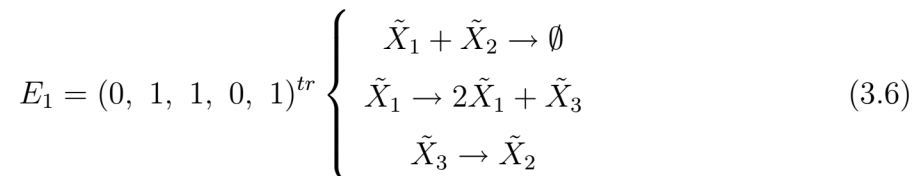
It was stated in Section 2.5 that SNA can be used to identify those extreme currents cycles leading to instability. A classification of chemical oscillators based on certain characteristics of these cycles has been reported to be fruitful [2, 4].

In order to perform the Mechanistic Classification of Chemical Oscillators (MCCO) it is necessary to extract, from the stoichiometric matrix, the *extreme currents* vectors. Such vectors lie in the intersection of the null space of the stoichiometric matrix,  $N$ , and the non-negative orthant,  $\mathbb{R}_+^r$ ; this intersection defines sub-networks that may cause instabilities which ultimately lead to sustained oscillations or more complex behavior [2, 4].

Using those subnetworks defined by the extreme currents, a *extreme current diagram*,  $D_E$ , is drawn. This  $D_E$  requires that the sum over all feathers equals the sum over all barbs for every species in the diagram. From (3.2), we have the extreme currents for the Brusselator:



meanwhile for the Oregonator, the extreme currents computed from (3.3) are:



$$E_2 = (1, 0, 1, 1, 1)^{tr} \left\{ \begin{array}{l} \tilde{X}_2 \rightarrow \tilde{X}_1 \\ \tilde{X}_1 \rightarrow 2\tilde{X}_1 + \tilde{X}_3 \\ 2\tilde{X}_1 \rightarrow \emptyset \\ \tilde{X}_3 \rightarrow \tilde{X}_2 \end{array} \right. \quad (3.7)$$

The extreme currents (3.4) and (3.6), which lead to oscillations for both Brusselator and Oregonator, respectively, are depicted in Figures 3.1 and 3.2.

(a) Brusselator

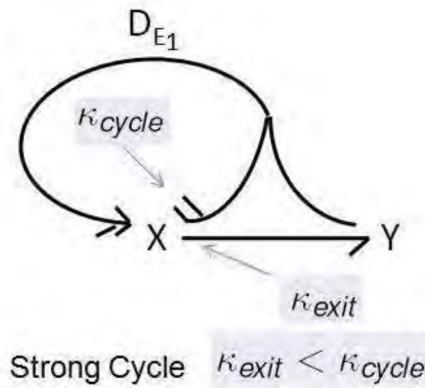


**Figure 3.1:** Brusselator extreme current diagram, where  $X = X_1$ ,  $Y = X_2$ . Adapted from [2].

Following nomenclature in [2], and comparison of Figures 3.1-3.2 with Figure 2.3, it can be seen that Brusselator CRN belongs to Category 2 due to the presence of a strong cycle [2]. On the other hand, because the Oregonator CRN contains a CCC and  $Y = \tilde{X}_2$  is generated in a chain reaction via at least one intermediate,  $Z = \tilde{X}_3$ , this oscillator belongs to a subdivision of Category 1, the so-called 1B [2]. As we can see the MCCO approach also shows that both, Brusselator and Oregonator, have unrelated mechanistic structure at steady state.

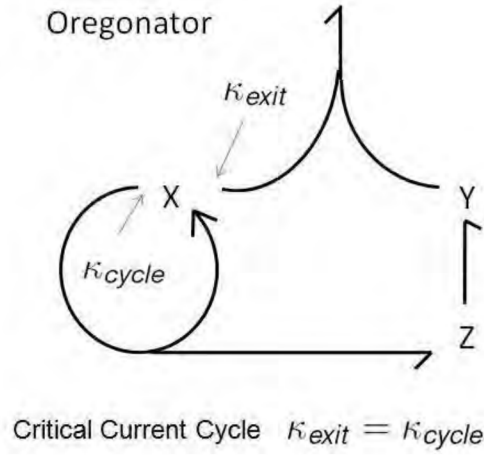


**Figure 3.2:** Oregonator extreme current diagram where  $X = \tilde{X}$ ,  $Y = \tilde{X}_2$ ,  $Z = \tilde{X}_3$ . Adapted from [2].

Nevertheless, recall that extreme currents vectors span the steady state space by means of the convex cone:

$$\begin{aligned}
 K_{v(x,k)} &= \{v(\mathbf{x}, \mathbf{k}) \in \bar{\mathbb{R}}_+^r \mid N \cdot v(\mathbf{x}, \mathbf{k}) = 0, v(x, k) \geq 0\} \\
 &= \{\ker(N) \cap \bar{\mathbb{R}}_+^r\} \\
 &= \left\{ \sum_{p=1}^f j_p E_p > 0, \forall p \right\}
 \end{aligned} \tag{3.8}$$

where the parameters  $j > 0$ , are called *convex parameters* and quantify the influence of an extreme current on the full network dynamics. Note that the steady state space of both Brusselator and Oregonator is spanned by two extreme current vectors. Thus, both CRNs define a line segment in a four and five dimensional space, respectively. That is, their jacobian matrices will be weighted by two convex parameters and their linear combinations. As shown in Section 2.5, reaction rates can be expressed as a

linear combination of convex parameters as follows:

$$v(j) = \sum_{p=1}^f j_p E_p \quad (3.9)$$

and the jacobian matrix, after a suitable map transformation [4] with the use of Equation 3.9, can be expressed as:

$$\begin{aligned} Jac(v) &= N \text{diag}(v) \kappa^{tr} \text{diag}(h_i) \\ \Rightarrow Jac(j) &= N \text{diag}\left(\sum_{p=1}^f j_p E_p\right) \kappa^{tr} \text{diag}(h_i) \end{aligned} \quad (3.10)$$

where  $h_i = x_{i,ss}^{-1}$ ,  $i = 1, \dots, s$  is the inverse of steady state concentrations and  $\kappa \in \mathbb{R}^{s \times r}$  is the *kinetic matrix* where the *kinetic exponents* of the  $i$ -th chemical specie in the  $j$ -th reaction are arranged [4, 2].

For the Brusselator, the kinetic matrix is:

$$\kappa = \begin{bmatrix} 2 & 1 & 1 & 0 \\ 1 & 0 & 0 & 0 \end{bmatrix} \quad (3.11)$$

meanwhile for the Oregonator:

$$\kappa = \begin{bmatrix} 0 & 1 & 1 & 2 & 0 \\ 1 & 1 & 0 & 0 & 0 \\ 0 & 0 & 0 & 0 & 1 \end{bmatrix} \quad (3.12)$$

Then, using (3.10), (3.4) and (3.11) without the  $\text{diag}(h_1, h_2)$  term, the jacobian for the Brusselator in convex coordinates is:

$$Jac|_{Brus} = \begin{bmatrix} j_1 - j_2 & j_1 \\ -j_1 & -j_1 \end{bmatrix} \quad (3.13)$$

In the same way, using (3.10), (3.6) and (3.12), Oregonator's jacobian can be written as:



$$Jac|_{Oreg} = \begin{bmatrix} -3\tilde{j}_2 & \tilde{j}_2 - \tilde{j}_1 & 0 \\ -\tilde{j}_1 & -\tilde{j}_1 - \tilde{j}_2 & \tilde{j}_1 + \tilde{j}_2 \\ \tilde{j}_1 + \tilde{j}_2 & 0 & -\tilde{j}_1 - \tilde{j}_2 \end{bmatrix} \quad (3.14)$$

In terms of graph theory, the jacobian defines a *directed graph*,  $\mathcal{G}_D$ , because is not a symmetric matrix in general. How the arcs are oriented is encoded in the adjacency (=jacobian) matrix. For instance, let  $v_1, v_2, \dots, v_\nu$  be the vertices of a directed graph  $\mathcal{G}_D$ . Then, the *adjacency matrix* of  $\mathcal{G}_D$  is the  $\nu \times \nu$  matrix  $\mathbf{A}=[a_{ji}]$  in which  $a_{ji}$  is the number of arcs of  $\mathcal{G}_D$  with tail  $v_j$  and head  $v_i$ . With each arc of  $\mathcal{G}_D$  let there be associated a real number  $w$ , called its *weight*, *i.e.* the entries of the jacobian matrix. Additionally, within the context of CRNs, a *pseudograph* is a graph that have self-loops and multi-arcs (or multi-edges) [39].

Recalling graph definitions above and defining chemical species as vertices, the Brusselator's pseudograph is depicted in Figure 3.3, and Oregonator's pseudograph in Figure 3.4.

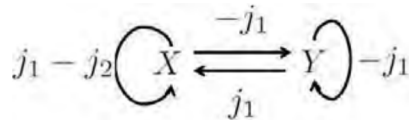


**Figure 3.3:** *Weighted directed pseudograph for Brusselator.  $X = X_1, Y = X_2$*

It can be seen that the structure of the Brusselator's graph is embedded in the Oregonator's graph (see interaction between species  $\{X, Y\}$  and  $\{\tilde{X}, \tilde{Y}\}$ ), *i. e.* both graphs share this particular interaction or motif. Nevertheless, this interaction does not suffices to declare both Brusselator and Oregonator as equivalent chemical oscillators because their source of instabilities is different. Moreover, one can find a transformation from the Oregonator's space defined by its jacobian into the Brus-

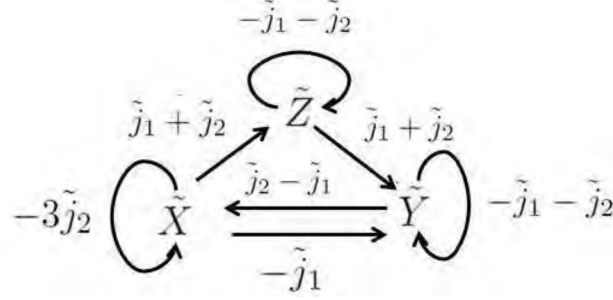


**Figure 3.4:** *Weighted directed pseudograph for Oregonator.  $X = \tilde{X}$ ,  $Y = \tilde{X}_2$ ,  $Z = \tilde{X}_3$*

selector’s jacobian space, *i.e.* a transformation that changes the linear combination of weights to obtain the same linear combination of weights as in the Brusselator’s jacobian. Mathematically, the idea can be written as:

$$Jac_{Oreg}^* = T \cdot Jac_{Oreg} \quad (3.15)$$

$$Jac_{Oreg}^* \cdot Jac_{Oreg}^{-1} = T \quad (3.16)$$

$$T = \begin{bmatrix} \frac{\tilde{j}_2^2 - \tilde{j}_1^2 - \tilde{j}_1 \tilde{j}_2}{2\tilde{j}_2(\tilde{j}_2 - 2\tilde{j}_1)} & \frac{\tilde{j}_2^2 - 5\tilde{j}_1 \tilde{j}_2 + \tilde{j}_1^2}{2\tilde{j}_2(\tilde{j}_2 - 2\tilde{j}_1)} & \frac{\tilde{j}_2^2 - 5\tilde{j}_1 \tilde{j}_2 + \tilde{j}_1^2}{2\tilde{j}_2(\tilde{j}_2 - 2\tilde{j}_1)} \\ \frac{\tilde{j}_1(\tilde{j}_1 + 2\tilde{j}_2)}{2\tilde{j}_2(\tilde{j}_2 - 2\tilde{j}_1)} & \frac{\tilde{j}_1(4\tilde{j}_2 - \tilde{j}_1)}{2\tilde{j}_2(\tilde{j}_2 - 2\tilde{j}_1)} & \frac{\tilde{j}_1(4\tilde{j}_2 - \tilde{j}_1)}{2\tilde{j}_2(\tilde{j}_2 - 2\tilde{j}_1)} \\ 0 & 0 & 0 \end{bmatrix} \quad (3.17)$$

Where “\*” serves to identify the target Oregonator’s jacobian with the same linear combination of convex parameters,  $\tilde{j}'$ s, as in the Brusselator’s jacobian. We note that  $Jac_{Oreg}^*$  is a square matrix with the third row and column with zeroes; otherwise, it could not be interpreted as an adjacency matrix of the new pseudo-graph with the same entries as in the Brusselator. Furthermore,  $T$  has nonlinear entries, which are difficult to interpret within the context of the MCCO approach and the SNA.

On the other hand, if we want to follow the same idea to find a transformation from the Brusselator’s jacobian to Oregonator’s jacobian entries, is not possible to

invert the augmented (from two to three) Brusselator jacobian because the row and column of zeroes. In this sense, next section shows an alternative approach where the inversion of continuous and differentiable maps is assured for some neighborhood in state space thus allowing to express one CRN's state space as function of a second CRN's state space.

### 3.2 Change of coordinates using Lie derivatives

This section presents a coordinate transformation defined by the composition of diffeomorphic maps as a *dynamical equivalence* criteria between two vector fields induced by different oscillatory CRN. The diffeomorphic maps are constructed by means of Lie derivatives which creates a tangent space to the vector fields. These maps, through their inverses, makes possible to express the concentrations of chemical species of both CRN as a function of the other, point by point in time. We call these composition of maps the *dynamical equivalence*. The dynamical equivalence concept is illustrated by means of an example between Brusselator and the Minimal MAK System with Limit Cycle (MMAKS-LC) CRN, both with the same dimension of states (chemical species concentrations) but different number of reactions and observable functions. In particular, for these systems the dynamical equivalence approach yield to a quite interested phenomena, coined in [40] as *chirality* in a synchronization framework: trajectories of one system are the mirror reflection of the other one. Afterwards, the dynamical equivalence for CRN of distinct state dimension is investigated using the Brusselator and Oregonator CRNs.

Let us consider two (non)linear systems from vector fields induced by CRNs given by  $\mathbf{x} = \mathbf{f}(\mathbf{x}, \mathbf{k})$ ,  $y = h(\mathbf{x})$  and  $\tilde{\mathbf{x}} = \tilde{\mathbf{f}}(\tilde{\mathbf{x}}, \mathbf{k}')$ ,  $\tilde{y} = \tilde{h}(\tilde{\mathbf{x}})$ . For these systems the state variables are  $\mathbf{x} \in \bar{\mathbb{R}}_+^s$  and  $\tilde{\mathbf{x}} \in \bar{\mathbb{R}}_+^{s'}$ , with smooth vector fields  $\mathbf{f} : \bar{\mathbb{R}}_+^s \times \mathbb{R}_+^r \rightarrow \mathbb{R}^s$ ,  $\tilde{\mathbf{f}} : \mathbb{R}^{s'} \times \mathbb{R}_+^{r'} \rightarrow \mathbb{R}^{s'}$ . Associated to each system there is a smooth scalar output

function  $h : \mathbb{R}^s \rightarrow \mathbb{R}$  and  $\tilde{h} : \mathbb{R}^{s'} \rightarrow \mathbb{R}$ . Then, it is possible to construct a change of coordinates,  $z = \Phi(x)$ , for each system using their trajectories and the associated tangent spaces by means of Lie derivatives, as shown in Section 2.6.

$$\mathbf{z} = \Phi(\mathbf{x}) = \begin{bmatrix} h(\mathbf{x}) \\ L_f h(\mathbf{x}) \\ \vdots \\ L_f^{s-1} h(\mathbf{x}) \end{bmatrix} \quad (3.18)$$

where  $s$  is the number of elements forming the vector  $\mathbf{x} = (x_1, \dots, x_s)$ , of chemical species concentrations. Note that if  $\mathbf{x}_{ss}$  is a steady state for  $\mathbf{f}(\mathbf{x}_{ss}, \mathbf{k}) = 0$  and if also  $h(\mathbf{x}_{ss}) = 0$ , then  $\mathbf{z}_{ss} = \Phi(\mathbf{x}_{ss}) = 0$ . That is, the steady state is also preserved under the action of  $\Phi$ . Condition  $h(\mathbf{x}_{ss}) = 0$  can be always be satisfied by a suitable origin translation of the output space.

We are interested in finding a transformation  $H : \mathbb{R}^s \rightarrow \mathbb{R}^{s'}$  which map the tangents spaces of one system into the state space of another system. This is defined as dynamical equivalence. Formally:

**Definition 3.2.1.** *Two vector fields,  $\mathbf{f}(\mathbf{x}, \mathbf{k})$ ,  $\mathbf{x} \in \mathbb{R}_{\geq 0}^s$ ,  $\mathbf{k} \in \mathbb{R}_{> 0}^r$  and  $\tilde{\mathbf{f}}(\tilde{\mathbf{x}}, \mathbf{k}')$ ,  $\tilde{\mathbf{x}} \in \mathbb{R}_{\geq 0}^{s'}$ ,  $\mathbf{k}' \in \mathbb{R}_{> 0}^{r'}$ , for  $\mathbf{x}_0 \in \mathbb{R}_{\geq 0}^s$  and  $\tilde{\mathbf{x}}_0 \in \mathbb{R}_{\geq 0}^{s'}$ , with  $s, r$  non necessarily equal to  $s', r'$ , induced by CRNs are dynamically equivalent if there exist  $\mathbf{x}, \tilde{\mathbf{x}} \in \mathbb{R}_{\geq 0}^s$  and  $\mathbf{k} \in \mathbb{R}_{> 0}^r$ ,  $\mathbf{k}' \in \mathbb{R}_{> 0}^{r'}$  such that  $\mathbf{x}(t) = \Phi^{-1} \circ \tilde{\Phi}(\tilde{\mathbf{x}}(t))$ ,  $\Phi^{-1} \circ \tilde{\Phi} : \mathbb{R}^s \rightarrow \mathbb{R}_{\geq 0}^s$ , or  $\tilde{\mathbf{x}}(t) = \tilde{\Phi}^{-1} \circ \Phi(\mathbf{x}(t))$ ,  $\tilde{\Phi}^{-1} \circ \Phi : \mathbb{R}^s \rightarrow \mathbb{R}_{\geq 0}^s$ , for all  $t \geq 0$ , with  $\Phi, \tilde{\Phi}$  being diffeomorphic maps. In addition,*

- *if  $s = s'$  then  $\mathbf{f}$  and  $\tilde{\mathbf{f}}$  are completely dynamically equivalent and*
- *if  $s \neq s'$  then  $\mathbf{f}$  and  $\tilde{\mathbf{f}}$  are partially dynamically equivalent.*

Next, the concept of dynamical equivalence for two socillatory CRNs of same dimension is illustrated.

### 3.2.1 Illustrative example

The example explores the use of two different observable functions. The first one serves as an illustration of the ideas above discussed. The second one stress the fact that there are observable functions that can lead to an simpler mathematical expression that enables a better picture for the dynamic equivalence.

Let us consider the following two vector fields induced by different CRNs. The first vector field comes from the Brusselator [37]:

$$\begin{aligned}\dot{x}_1 &= k_1 x_1^2 x_2 - k_2 x_1 - k_3 x_1 + k_4 \\ \dot{x}_2 &= -k_1 x_1^2 x_2 + k_2 x_1\end{aligned}\tag{3.19}$$

where  $\mathbf{x} = (x_1, x_2)^{tr} \in \mathbb{R}_+^2$ . The second vector field is induced by the Minimal MAK System With Limit Cycle (MMAKSWLC) [41]:

$$\begin{aligned}\dot{\tilde{x}}_1 &= k'_1 - k'_2 \tilde{x}_1 \tilde{x}_2^2 \\ \dot{\tilde{x}}_2 &= k'_2 \tilde{x}_1 \tilde{x}_2^2 - k'_3 \tilde{x}_2\end{aligned}\tag{3.20}$$

where  $\tilde{\mathbf{x}} = (\tilde{x}_1, \tilde{x}_2)^{tr} \in \mathbb{R}_+^2$ .

(a) Let us take  $y = h(\mathbf{x}) = x_1$ ,  $\tilde{y} = h(\tilde{\mathbf{x}}) = \tilde{x}_2$  as observable functions for Equations (3.19) and (3.20), respectively. We compute the Lie derivatives as in Equation (3.18) to construct  $\Phi(\mathbf{x}) = (h(x), L_f h(x))^{tr}$  which is well defined on  $\mathcal{D} = \{(x_1, x_2) \in \mathbb{R}^2 | x_1 > 0\}$ . On the other hand  $\tilde{\Phi}(\tilde{\mathbf{x}}) = (h(\tilde{x}), L_{\tilde{f}} h(\tilde{x}))^{tr}$ , which is valid at the domain  $\tilde{\mathcal{D}} = \{(\tilde{x}_1, \tilde{x}_2) \in \mathbb{R}^2 | \tilde{x}_2 > 0\}$ .

$$\mathbf{z} = \Phi(\mathbf{x}) = \begin{pmatrix} x_1 \\ k_1 x_1^2 x_2 - k_2 x_1 - k_3 x_1 + k_4 \end{pmatrix} \text{ and}\tag{3.21}$$

$$\tilde{\mathbf{z}} = \tilde{\Phi}(\tilde{\mathbf{x}}) = \begin{pmatrix} \tilde{x}_2 \\ k'_2 \tilde{x}_1 \tilde{x}_2^2 - k'_3 \tilde{x}_2 \end{pmatrix}\tag{3.22}$$

whose inverses reads as follows:

$$\mathbf{x} = \Phi^{-1}(\mathbf{z}) = \begin{pmatrix} z_1 \\ \frac{z_2 + (k_2 + k_3)z_1 - k_4}{k_1 z_1^2} \end{pmatrix} \quad (3.23)$$

$$\tilde{\mathbf{x}} = \tilde{\Phi}^{-1}(\tilde{\mathbf{z}}) = \begin{pmatrix} \frac{k'_3 \tilde{z}_1 + \tilde{z}_2}{k'_2 \tilde{z}_1^2} \\ \tilde{z}_1 \end{pmatrix} \quad (3.24)$$

Then, solving the equivalence  $\mathbf{z} \equiv \tilde{\mathbf{z}} \Rightarrow \Phi(\mathbf{x}) \equiv \tilde{\Phi}(\tilde{\mathbf{x}})$ , it is possible to compose the maps in order to get:

$$\mathbf{x} = \Phi^{-1} \circ \tilde{\Phi}(\tilde{\mathbf{x}}) = \begin{pmatrix} \tilde{x}_2 \\ \frac{k'_2 \tilde{x}_1 \tilde{x}_2^2 + (k_2 + k_3 - k'_3) \tilde{x}_2 - k_4}{k_1 \tilde{x}_2^2} \end{pmatrix} \quad \text{and} \quad (3.25)$$

$$\tilde{\mathbf{x}} = \tilde{\Phi}^{-1} \circ \Phi(\mathbf{x}) = \begin{pmatrix} \frac{k_1 x_1^2 x_2 + (k'_3 - k_2 - k_3) x_1 + k_4}{k'_2 x_1^2} \\ x_1 \end{pmatrix} \quad (3.26)$$

from where  $\Phi(\mathbf{x}) \equiv \tilde{\Phi}(\tilde{\mathbf{x}}) \Rightarrow \mathbf{x} = \Phi^{-1}(\tilde{\mathbf{z}})$  and  $\tilde{\mathbf{x}} = \tilde{\Phi}^{-1}(\mathbf{z})$ . Figure 3.5 illustrates graphically how the compositions are observed in the chemical species concentration space.

- (b) Now, let us take a linear combination of states, *i.e.*,  $y = h(\mathbf{x}) = x_1 + x_2$  and  $\tilde{y} = h(\tilde{\mathbf{x}}) = \tilde{x}_1 + \tilde{x}_2$ , as observable for Equations (3.19) and (3.20), respectively. Following above ideas, we compute the Lie derivatives to obtain:

$$\mathbf{z} = \Phi(\mathbf{x}) = \begin{pmatrix} x_1 + x_2 \\ -k_3 x_1 + k_4 \end{pmatrix} \quad \text{and} \quad (3.27)$$

$$\tilde{\mathbf{z}} = \tilde{\Phi}(\tilde{\mathbf{x}}) = \begin{pmatrix} \tilde{x}_1 + \tilde{x}_2 \\ k'_1 - k'_3 \tilde{x}_2 \end{pmatrix} \quad (3.28)$$

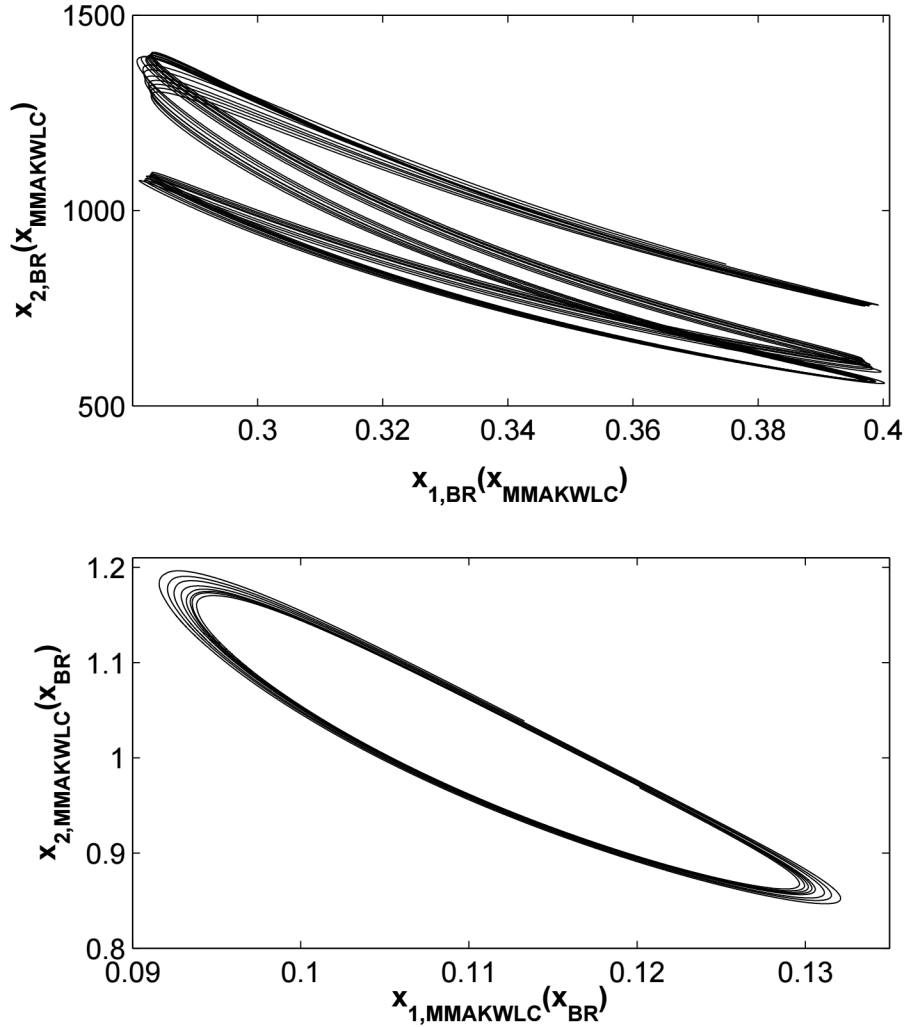


**Figure 3.5:** Composition of diffeomorphic functions for Brusselator and MMAKWLC CRNs, using as observable functions  $y = h(\mathbf{x}) = x_1$  and  $\tilde{y} = \tilde{h}(\tilde{\mathbf{x}}) = \tilde{x}_2$ . Upper panel: Brusselator's states as function of MMAKWLC's states. Lower panel: MMAKWLC's states as function of Brusselator's states. Initial conditions and kinetic parameters for the Brusselator:  $\mathbf{x}_{BR}(0) = (2, 2)$ ,  $k_1 = 1, k_2 = 2, k_3 = 1, k_4 = 1$ . Initial conditions and kinetic parameters for the MMAKWLC:  $\mathbf{x}_{MMAKWLC}(0) = (2, 2)$ ,  $k'_1 = 1, k'_2 = 27, k'_3 = 3$ .

with inverses given by:

$$\mathbf{x} = \Phi^{-1}(\mathbf{z}) = \begin{pmatrix} \frac{k_4 - z_2}{k_3} \\ z_1 + \frac{z_2 - k_4}{k_3} \end{pmatrix} \quad \text{and} \quad (3.29)$$

$$\tilde{\mathbf{x}} = \tilde{\Phi}^{-1}(\tilde{\mathbf{z}}) = \begin{pmatrix} \tilde{z}_1 + \frac{\tilde{z}_2 - k'_1}{k'_3} \\ \frac{k'_1 - \tilde{z}_2}{k'_3} \end{pmatrix} \quad (3.30)$$

For this particular choice of  $h(\mathbf{x})$ , we have for both systems that  $\mathcal{D} = \tilde{\mathcal{D}} = \bar{\mathbb{R}}_+^2$ , because the determinant of the Jacobian is independent of the states  $\mathbf{x}, \tilde{\mathbf{x}}$ ; that is,  $\det(\partial\Phi(\mathbf{x})/\partial\mathbf{x}) = k_3$ , and  $-k'_3$ , respectively. Again, by solving the equivalence  $\mathbf{z} \equiv \tilde{\mathbf{z}} \Rightarrow \Phi(\mathbf{x}) \equiv \tilde{\Phi}(\tilde{\mathbf{x}})$ , the composition of the maps yields:

$$\mathbf{x} = \Phi^{-1} \circ \tilde{\Phi}(\tilde{\mathbf{x}}) = \begin{pmatrix} \frac{k'_3}{k_3} \tilde{x}_2 - \frac{k'_1 - k_4}{k_3} \\ \tilde{x}_1 + \left(1 - \frac{k'_3}{k_3}\right) \tilde{x}_2 + \frac{k'_1 - k_4}{k_3} \end{pmatrix} \quad \text{and} \quad (3.31)$$

$$\tilde{\mathbf{x}} = \tilde{\Phi}^{-1} \circ \Phi(\mathbf{x}) = \begin{pmatrix} x_2 + \left(1 - \frac{k_3}{k'_3}\right) x_1 + \frac{k_4 - k'_1}{k'_3} \\ \frac{k_3}{k'_3} x_1 + \frac{k'_1 - k_4}{k'_3} \end{pmatrix} \quad (3.32)$$

to conclude that  $\Phi(\mathbf{x}) \equiv \tilde{\Phi}(\tilde{\mathbf{x}}) \Rightarrow \mathbf{x} = \Phi^{-1}(\tilde{\mathbf{z}})$  and  $\tilde{\mathbf{x}} = \tilde{\Phi}^{-1}(\mathbf{z})$ . These composition of maps are depicted in Figure 3.6.

Note that the dynamical equivalence between vector field (3.19) and (3.20) is general and can adopt distinct forms depending on: (1) the chosen observable and (2) parameter space. In particular, for the case (2), a mirror reflection of the state phase of both oscillators is found for the pair  $(k_3, k_4) = (k'_3, k'_1) \in \mathbf{P}^* = \mathbb{R}_+^4 \cap \mathbb{R}_+^3$ , where  $\mathbf{P}^*$  is not an empty set. If such parameter relation holds, we have that state variables of Equation (3.19) and Equation (3.20) become  $x_1 = \tilde{x}_2, x_2 = \tilde{x}_1$ . Figure 3.7 shows that the mirror reflection holds on for  $\mathbf{x}, \tilde{\mathbf{x}}$ , satisfying (3.19) and (3.20), for a  $\mathbf{x}(0), \tilde{\mathbf{x}}(0) \in \mathbb{R}_+^2$  and for all  $t \geq 0$ . A notable



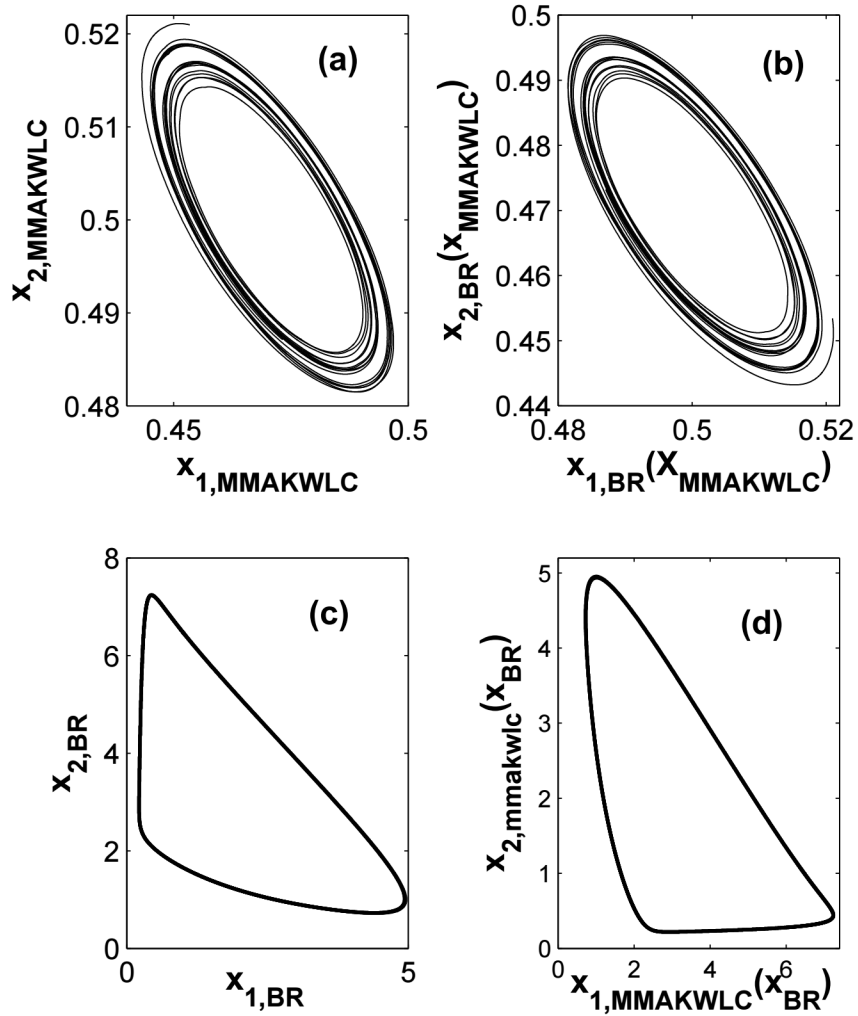


**Figure 3.6:** Composition of diffeomorphic functions for Brusselator and MMAKWLC CRNs, using as observable functions  $y = h(\mathbf{x}) = x_1 + x_2$  and  $\tilde{y} = \tilde{h}(\tilde{\mathbf{x}}) = \tilde{x}_1 + \tilde{x}_2$ . (a) MMAKWLC state phase. (b) Brusselator's states as function of MMAKWLC's states. (c) Brusselator state phase. (d) MMAKWLC's states as function of Brusselator's states. Initial conditions and kinetic parameters for the Brusselator:  $\mathbf{x}_{\text{BR}}(0) = (2, 2)$ ,  $k_1 = 1, k_2 = 3.2, k_3 = 2, k_4 = 1$ . Initial conditions and kinetic parameters for the MMAKWLC:  $\mathbf{x}_{\text{MMAKWLC}}(0) = (2, 2)$ ,  $k'_1 = 1, k'_2 = 8.5, k'_3 = 2$ .

fact is that the Lie algebra of derivations, from a observable along a vector field induced by a CRN, allows one to reproduce the time-evolution in this fashion, which depicts *chirality* onto the dynamics of both chemical reaction networks. Chirality phenomenon in dynamical systems has been previously reported in the reduced order chaos synchronization between Chua and Duffin oscillators [40]. Contrary to the work in [40], chirality in these CRNs was not achieved by a control command, both systems are of the same dimension and the mirror reflection of the dynamics can be superimposed.

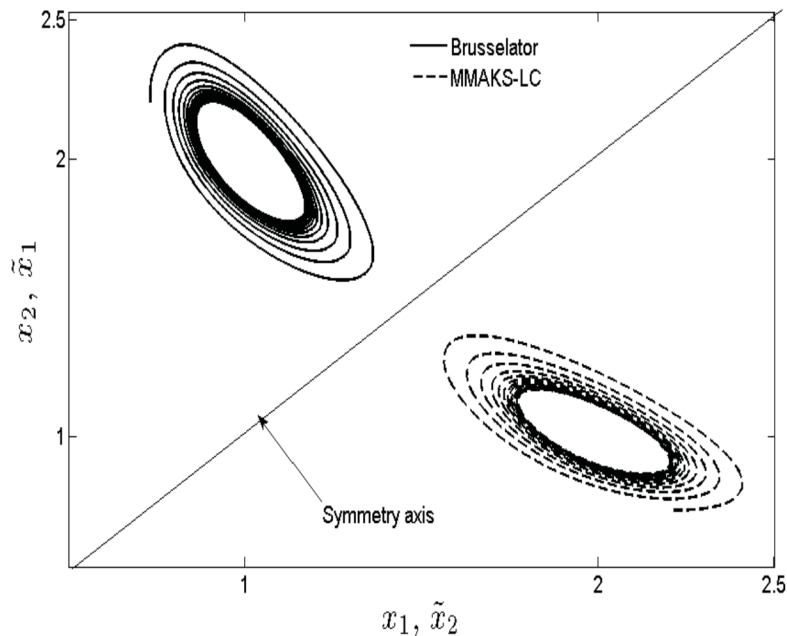


**Figure 3.7:** *Dynamical chirality phenomenon between Brusselator and the MMAKS-SWLC is found for  $(k_3, k_4) = (k'_3, k'_1) \in \mathbf{P}^* = \mathbb{R}_+^4 \cap \mathbb{R}_+^3$  for any  $\mathbf{x}(0), \tilde{\mathbf{x}}(0) \in \mathbb{R}_+^2$  and for all  $t \geq 0$ , where  $\mathbf{P}^*$  is not an empty set.*

So far, we have analyzed systems of the same dimension. Next, we turn our attention to the situation when both systems have distinct dimension and observable

functions using the Brusselator and Oregonator as case study. Because both CRNs have a common historical root, *i.e.* the BZ reaction, have different sources of instability (cf. Section 3.1.2) and they are of distinct dimension, they offer a good opportunity to study how can be related dynamically.

### 3.2.2 Brusselator and Oregonator dynamical equivalence.

The Oregonator CRN stands for the dynamical behavior of the chemical species  $\text{HBrO}_2$ ,  $\text{Br}^-$  and  $\text{Ce}^{+4}$  in the BZ reaction. Let us denote by  $\tilde{x}_1 = \text{HBrO}_2$ ,  $\tilde{x}_2 = \text{Br}^-$  and  $\tilde{x}_3 = \text{Ce}^{+4}$ , their chemical concentrations, respectively. Let us recall the MAK-ODEs associated to this CRN:

$$\begin{aligned}\dot{\tilde{x}}_1 &= k'_1\tilde{x}_2 - k'_2\tilde{x}_1\tilde{x}_2 + k'_3\tilde{x}_1 - 2k'_4\tilde{x}_1^2 \\ \dot{\tilde{x}}_2 &= -k'_1\tilde{x}_2 - k'_2\tilde{x}_1\tilde{x}_2 + k'_5\tilde{x}_3 \\ \dot{\tilde{x}}_3 &= k'_3\tilde{x}_1 - k'_5\tilde{x}_3\end{aligned}\tag{3.33}$$

Choosing  $\tilde{y} = h(\tilde{x}) = \tilde{x}_3$  as an output function we have that:

$$\tilde{\mathbf{z}}_{OR} = \tilde{\Phi}(\tilde{\mathbf{x}}_{OR}) = (h(\tilde{x}), L_f h(\tilde{x}), L_f^2 h(\tilde{x}))^{tr}$$

where:

$$\begin{aligned}h(\tilde{x}) &= \tilde{x}_3 \\ L_f h(\tilde{x}) &= k'_3\tilde{x}_1 - k'_5\tilde{x}_3 \\ L_f^2 h(\tilde{x}) &= k'_3((k'_1 - k'_2\tilde{x}_1)\tilde{x}_2 + (k'_3 - 2k'_4\tilde{x}_1)\tilde{x}_1) \\ &\quad - k'_5(k'_3\tilde{x}_1 - k'_5\tilde{x}_3)\end{aligned}\tag{3.34}$$

which is well defined for the set  $\mathcal{D}_{OR} := \{(\tilde{x}_1, \tilde{x}_2, \tilde{x}_3) \in \mathbb{R}^3 \mid \tilde{x}_1 \neq \frac{k'_1}{k'_2}, (\tilde{x}_2, \tilde{x}_3) \geq 0\}$ , thus  $\tilde{\Phi}_{OR} : \mathcal{D}_{OR} \rightarrow \bar{\mathbb{R}}_+ \times \mathbb{R} \times \mathbb{R}$ . The associate inverse map  $\tilde{\Phi}^{-1}(\tilde{\mathbf{z}}_{OR}) =$

$(\tilde{\phi}_1^{-1}, \tilde{\phi}_2^{-1}, \tilde{\phi}_3^{-1})^{tr}$  reads as follows:

$$\tilde{x}_1 = \tilde{\phi}_1^{-1}(\tilde{\mathbf{z}}) = \frac{\tilde{z}_2 + k'_5 \tilde{z}_1}{k'_3} \quad (3.35)$$

$$\tilde{x}_2 = \tilde{\phi}_2^{-1}(\tilde{\mathbf{z}}) = \frac{\tilde{z}_3 - k'_3(k'_3 - 2k'_4\mu)\mu + k'_5(k'_3\mu - k'_5\tilde{z}_1)}{k'_3(k'_1 - k'_2\mu)} \quad (3.36)$$

$$\tilde{x}_3 = \tilde{\phi}_3^{-1}(\tilde{\mathbf{z}}) = \tilde{z}_1 \quad (3.37)$$

where  $\mu(\tilde{z}) = \frac{k'_5\tilde{z}_1 + \tilde{z}_2}{k'_3}$ , such that  $\tilde{z}_2 + k'_5\tilde{z}_1 \neq \frac{k'_1 k'_3}{k'_2}$ , to avoid singularity for  $\tilde{\phi}_2^{-1}$ . In order to get the chemical species concentrations of the Brusselator as function of the Oregonator's concentrations, we define the following composition  $\mathbf{x}_{BR}^* = \Phi_{BR}^{-1}(\tilde{\Phi}_{OR}(\tilde{\mathbf{x}}_{OR}))$ :

$$\mathbf{x}_{BR}^* = \begin{pmatrix} \tilde{x}_3 \\ \frac{k'_3\tilde{x}_1 + (k_2 + k_3 - k'_5)\tilde{x}_3 - k_4}{k_1\tilde{x}_3^2} \end{pmatrix} \quad (3.38)$$

where “\*” stands for the composed states. The Oregonator's concentrations as function of Brusselator's are defined according to:  $\tilde{\mathbf{x}}_{OR}^* = \tilde{\Phi}_{OR}^{-1}(\Phi_{BR}(\mathbf{x}_{BR}))$ :

$$\tilde{\mathbf{x}}_{OR}^* = \begin{pmatrix} \frac{k_1 x_1^2 x_2 + (k'_5 - k_2 - k_3)x_1 + k_4}{k'_3} \\ \frac{\tilde{z}_3 - k'_3(k'_3 - 2k_4\epsilon)\epsilon + k'_5(k'_3 x_1 - k'_5\epsilon)}{k'_3(k'_1 - k'_2 x_1)} \\ x_1 \end{pmatrix} \quad (3.39)$$

where  $\epsilon(x_{BR}) = \frac{k_1 x_1^2 x_2 + (k'_5 - k_2 - k_3)x_1}{k'_3}$ . Note that  $\tilde{x}_{2,OR}^*$  depends also on  $\tilde{z}_3$ , which can be considered as zero because the Brusselator is a two dimensional system.

Of particular interest are the compositions defined in Equation (3.38)-(3.39). Through these compositions it is possible to map trajectories from the Brusselator's concentration space to Oregonator's concentration space, and vice versa. That is,  $\Phi_{BR}^{-1} \circ \tilde{\Phi}_{OR} : \mathcal{D}_{OR} \rightarrow \mathcal{D}_{BR}$  and  $\tilde{\Phi}_{OR}^{-1} \circ \Phi_{BR} : \mathcal{D}_{BR} \rightarrow \mathcal{D}_{OR}$ . Looking at Equations (3.38)-(3.39), we have that  $x_{1,BR}^* = \tilde{x}_3$  and  $\tilde{x}_{3,OR}^* = x_{1,BR}$ . Although the remainder chemical concentrations are mapped by rational expressions to other scales of magnitudes,  $x_{1,BR}$ ,  $\tilde{x}_{3,OR}$  are mapped by the identity map (free of parameters), thus we

can state that Brusselator and Oregonator are *partially dynamical equivalent* under this particular choice of  $(h(x), h(\tilde{x}))$ .

The regions of phenomenological interest for chemical species concentrations to be mapped are  $\mathcal{D}_{BR} \subset \mathbb{R}_+^2$ ,  $\mathcal{D}_{OR} \subset \mathbb{R}_+^3$ . To assure that trajectories from either subsets do not cross to the negative orthant, is not trivial because the composition maps depend on kinetic constants from both, Brusselator and Oregonator CRNs. Nevertheless, despite its apparent complexity, for the composition map  $\tilde{\Phi}_{OR}^{-1} \circ \Phi_{BR}$ , a set of kinetic constants and initial conditions, are readily find it as follows. From Equation (3.39) we have  $\tilde{x}_{1,OR}^* = \frac{k_1 x_1^2 x_2 + (k'_5 - k_2 - k_3)x_1}{k'_3}$ , and we want that  $\tilde{x}_{1,OR}^* > 0$ , thus:

$$\begin{aligned} k_1 x_1^2 x_2 + (k'_5 - k_2 - k_3)x_1 &> 0 \\ (k_1 x_1 x_2 + k'_5 - k_2 - k_3)x_1 &> 0 \\ k_1 x_1 x_2 + (k'_5 - k_2 - k_3) &> 0 \end{aligned}$$

and we arrive at the condition:

$$x_{1,BR} > \left( \frac{k_3 + k_2 - k'_5}{k_1} \right) \left( \frac{1}{x_{2,BR}} \right) \quad (3.40)$$

Again, from Equation (3.39),  $\tilde{x}_{2,OR}^* > 0$  is equivalent (after  $\epsilon$  factorization) to  $2k'_3 k_4 \epsilon^2 - (k'_3{}^2 + k'_5{}^2)\epsilon + k'_3 k'_5 x_1 > 0$ . Doing the proper algebraic manipulations to solve for  $x_1$ , we arrive to the following inequality:

$$x_{1,BR} > \left( \frac{\epsilon}{k'_5} \right) \left( k'_3 + \frac{k'_5{}^2}{k'_3} - 2k_4 \epsilon \right) \quad (3.41)$$

which implies that:

$$\epsilon < \left( \frac{1}{2k_4} \right) \left( k'_3 + \frac{k'_5{}^2}{k'_3} \right) \quad (3.42)$$

Notice that  $\epsilon = \tilde{x}_{1,OR}^* > 0$ , if Equation (3.40) holds.

The Brusselator undergoes a Hopf bifurcation for kinetics constants  $k_1 = k_3 = k_4 = 1$  and  $k_2 = 2$  [37]. From [18], we set  $k'_3 = 8 \times 10^3$ ,  $k'_5 = 1$ . Then, Equations

(3.40)-(3.42) holds for initial conditions  $\mathbf{x}_{BR}(0, 0) = (1, 3)$ . This particular sets of parameters and initial conditions lead to  $\epsilon < 4000$ . On the other hand, condition  $\tilde{x}_{3,OR}^* > 0$  is trivially satisfied. Figure (3.8) shows that  $\tilde{\Phi}_{OR}^{-1} \circ \Phi_{BR}$  preserves the qualitative behavior of Brusselator's states in the Oregonator's state space.

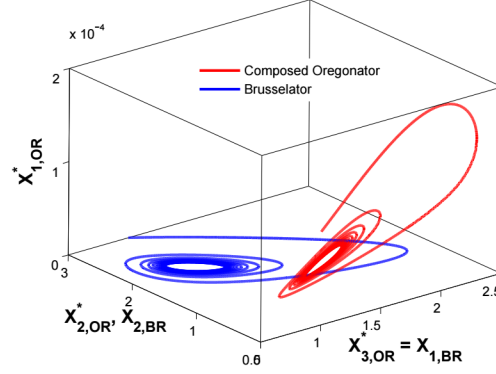


**Figure 3.8:** Trajectories from Brusselator (blue) space mapped by 3.39 to  $\mathbb{R}_+^3$  (red).

Conditions that the map  $\Phi_{BR}^{-1} \circ \tilde{\Phi}_{OR}$  must satisfies in order to stay in the positive orthant can be derived in the same manner; for instance,  $x_{1,BR}^* > 0$  is trivially satisfied. Condition  $x_{2,BR}^* > 0$  is equivalent to  $k'_3 \tilde{x}_1 + (k_2 + k_3 - k'_5) \tilde{x}_3 - k_4 > 0$ , which can be written as:

$$\tilde{x}_{1,OR} + \left( \frac{k_2 + k_3 - k'_5}{k'_3} \right) \tilde{x}_{3,OR} > \frac{k_4}{k'_3} \quad (3.43)$$

From this inequality is possible to prove the existence of kinetic constants such that (3.43) holds, if  $k_2 + k_3 > k'_5$ . Furthermore, upper and lower limits for  $\tilde{x}_{1,OR}$ ,  $\tilde{x}_{3,OR}$  can be derived from:

$$\tilde{x}_{1,OR} > \frac{k_4}{k'_3} - \left( \frac{k_2 + k_3 - k'_5}{k'_3} \right) \tilde{x}_{3,OR} \quad (3.44)$$

which implies that  $\tilde{x}_{3,OR} < \frac{k_4}{k_2 + k_3 - k'_5}$ . On the other hand, assuming  $\tilde{x}_{3,OR} = 0$ , implies  $\tilde{x}_{1,OR} > \frac{k_4}{k'_3}$ . Using the above numerical values for kinetics constants, we have  $\tilde{x}_{1,OR} > 2.5 \times 10^{-3}$  and  $\tilde{x}_{3,OR} < 0.5$ . The problem is that, for this set of parameters,  $\tilde{x}_{1,OR} \rightarrow$

$1 \times 10^{-11}$  as  $t \rightarrow \infty$ , which is quite below condition  $\tilde{x}_{1,OR} > 2.5 \times 10^{-3}$ . In this sense, it is required to explore the parameters space in order to fulfill the above conditions. It might be possible that, for those parameters, the Oregonator's MAK-ODEs do not display oscillations or any nonlinear phenomena at all.

### 3.3 Concluding remarks

The chemical species concentrations of two different oscillatory CRNs, not necessarily of the same dimension, can be expressed as function of the other, and vice versa, through composition of diffeomorphic maps. These maps were constructed via Lie derivatives of a suitable observable (a measure chemical specie) along the vector fields induced by the set of MAK-ODEs. For a set of kinetic constants and a suitable initial condition states, was possible to map trajectories from Brusselator's space onto Oregonator's space, preserving the qualitative dynamical nature displayed by the Brusselator. The opposite case, *i.e.* mapping Oregonator's trajectories onto Brusselator's was partially achieved for  $x_{1,BR}^*$ , thus both chemical oscillators can be regarded as *partially dynamic equivalent* for these chemical species. Conditions in parameters space that guarantee  $x_{2,BR}^* > 0$  cannot be fulfilled for typical values of both Brusselator and Oregonator CRNs. In this sense, a broad parametric search need to be performed.

It was shown that there exist observable functions that lead, for some region of parameter space, to algebraic expressions where dynamical equivalence can adopt the form of free parameter equalities. For the case of Brusselator and MMAKWLC CRN an antisymmetric dynamical equivalence was found, resembling a chirality phenomena.

# 4. Dynamical Equivalence in The Belousov-Zhabotinsky Reaction

This chapter presents the deficiency and stoichiometric network analysis of a family of deterministic chaotic CRNs, hereafter Gyorgy-Field (GF) CRNs, for the BZ reaction under CFSTR operation [1]. For the study of dynamical equivalence purposes, the Oregonator is compared with a four dimensional non-MAK CRN member of the Gyorgy-Field family of CRNs, derived from quasi-steady state assumption, which fits very well the experimental data [1].

## *4.1 Deficiency and stoichiometric analysis*

We present in Chapter 1 as motivational example the BZ reaction along with a family of CRNs, dubbed as GF CRNs, that fit very well the experimental observations. Also, it was mentioned that the Oregonator was the first low dimensional CRN that was able to reproduce some dynamical features of the BZ reaction. Here we are interested to study to what extent the  $GF_D$ , for example, is similar to the Oregonator CRN. In what follows, we perform a deficiency and stoichiometric analysis for the GF CRNs, as done for the Brusselator and Oregonator in Chapter 3, seeking elements of equivalence. Afterwards, we focus our attention for dynamical equivalence between  $GF_D$  and the Oregonator.



Recalling the mathematical definition of deficiency (cf. Section 2.4):

$$\delta = |\mathcal{C}| - |\mathcal{L}| - \text{rank}(N) \quad (4.1)$$

where  $|\mathcal{C}|$  is the number of complexes (including the zero complex,  $\emptyset$ ) and  $|\mathcal{L}|$  the number of *linkage classes*.

For the GF CRNs under CFSTR operation, chemical species  $MA$  and  $Ce^{+3}$  are fed into the reactor; all chemical species are removed at the same rate. Then, we have the following deficiencies associated to GF CRNs:

- GF<sub>A</sub>:  $|\mathcal{C}| = 35, |\mathcal{L}| = 9, \text{rank}(N) = 11$ , thus  $\delta_{GF_A} = 15$ .
- GF<sub>B</sub>:  $|\mathcal{C}| = 24, |\mathcal{L}| = 4, \text{rank}(N) = 9$ , thus  $\delta_{GF_B} = 11$ .
- GF<sub>C</sub>:  $|\mathcal{C}| = 20, |\mathcal{L}| = 4, \text{rank}(N) = 7$ , thus  $\delta_{GF_C} = 9$ .

Analysis of the CRNs [31, 28] states that taken with mass action kinetics, the network *may* have the capacity for multiple steady states. The computational implementation of the ADOT [28] was unable to construct any examples because of non-linearity; such examples may still exist. Because GF<sub>D</sub> are not of MAK type, they are not suitable for deficiency analysis. None of the GF CRNs share the same deficiency, *i.e.* is not an invariant among GF CRNs. We also note that either the Oregonator's deficiency ( $\delta_{oreg} = 2$ ) match with GF deficiencies under CFSTR operation.

The implementation of the second approach, *i.e.* MCCCCO, classify the Oregonator as an oscillator 1B, which means that the current cycle defined by one (of two) subnetworks forms a *critical current cycle* (CCC) [2, 3]. The CCC can produce instability, and hence the possibility of oscillation, depending on other features of the network. Other "parent" CRNs of the Oregonator, such as the FKN CRN also belongs to category 1B [2]. That is, at least within the family of CRNs from which the Oregonator results, the nature of the instability is preserved.

On the other hand, we may ask if GF CRNs also belong to 1B class chemical oscillators. In order to answer this question is necessary to compute and analyze all the possible subnetworks(currents) obtained from the augmented stoichiometric networks to account for the in-and-out of chemical species under a CSTR operation. A major drawback of SNA when used for CFSTR models is that the number of possible subnetworks exceeds by far the dimension of the null space of the stoichiometric matrix (cf. [4]). GF CRNs are not the exception: the SNA revealed that  $GF_A$  has 323 subnetworks,  $GF_B$  65, and  $GF_C$  36. Again,  $GF_D$  is not susceptible of being analyzed with SNA because is not a MAK CRN.

For simplicity in the analysis, we can seek those subnetworks that might induce instabilities within the  $GF_C$  CRN with the help of CRNT. It turns out that the CCC of the Oregonator has an infinite number of steady states. This kind of CRN has been termed as “pathological” [30]. Using this approach, we were able to identify at least 5 pathological subnetworks but their dynamical analysis was inconclusive seeking chaotic regions in parameter space. Note that it may exist combination of subnetworks and suitable parameter values for which chaos can be found. Moreover, it might be possible that such subnetworks be ubiquitous within GF CRNs.

## 4.2 Dynamical equivalence analysis

At the light of the results provided by CNRT and MCCO approaches, we turn our attention to an alternative approach. We have chosen to borrow from geometric control theory a procedure for the construction of diffeomorphic maps,  $\Phi$ , (a differentiable homeomorphism along with its inverse) using Lie derivatives of the output function along the ODEs induced by the CRNs [6, 7]. This approach has been used in a synchronization context [40], where an external signal (control input) steers trajectories of a slave system into the master’s trajectories, in order to asymptotically reduce the

error among states. We use the idea of composition of maps as in the synchronization framework but for *uncontrolled* systems, *i.e.* ODEs induced by CRNs. Thus, if such a composition is feasible, *i.e.* mapping composed trajectories into the nonnegative (positive) orthant  $\bar{\mathbb{R}}_+^s$  ( $\mathbb{R}_+^s$ ), then both CRNs will be *dynamically equivalent* in terms of their trajectories along time. This approach is consistent with indistinguishability [22, 23]. In contrast to the approaches in [20] and [21], the one proposed here is not restricted to find the identity map as a diffeomorphism; we are not seeking for maps that, after composition, leads to the *same* MAK-ODEs but constructing a generalization exploiting the state space. We note that our proposed approach is not restricted to MAK-ODEs either.

In this section, the concept of dynamical equivalence via Lie algebra of derivations is applied to two CRNs standing for the BZ reaction: the Oregonator and  $GF_D[1]$ . Before proceed, let us recall the definition of dynamical equivalence:

**Definition 4.2.1.** *Two vector fields,  $\mathbf{f}(\mathbf{x}, \mathbf{k}), \mathbf{x} \in \mathbb{R}_{\geq 0}^s, \mathbf{k} \in \mathbb{R}_{> 0}^r$  and  $\tilde{\mathbf{f}}(\tilde{\mathbf{x}}, \mathbf{k}'), \tilde{\mathbf{x}} \in \mathbb{R}_{\geq 0}^{s'}, \mathbf{k}' \in \mathbb{R}_{> 0}^{r'}$ , for  $\mathbf{x}_0 \in \mathbb{R}_{\geq 0}^s$  and  $\tilde{\mathbf{x}}_0 \in \mathbb{R}_{\geq 0}^{s'}$ , with  $s, r$  non necessarily equal to  $s', r'$ , induced by CRNs are dynamically equivalent if there exist  $\mathbf{x}, \tilde{\mathbf{x}} \in \mathbb{R}_{\geq 0}^s$  and  $\mathbf{k} \in \mathbb{R}_{> 0}^r, \mathbf{k}' \in \mathbb{R}_{> 0}^{r'}$  such that  $\mathbf{x}(t) = \Phi^{-1} \circ \tilde{\Phi}(\tilde{\mathbf{x}}(t))$ ,  $\Phi^{-1} \circ \tilde{\Phi} : \mathbb{R}^s \rightarrow \mathbb{R}_{\geq 0}^s$ , or  $\tilde{\mathbf{x}}(t) = \tilde{\Phi}^{-1} \circ \Phi(\mathbf{x}(t))$ ,  $\tilde{\Phi}^{-1} \circ \Phi : \mathbb{R}^s \rightarrow \mathbb{R}_{\geq 0}^s$ , for all  $t \geq 0$ , with  $\Phi, \tilde{\Phi}$  being diffeomorphic maps. In addition,*

- *if  $s = s'$  then  $\mathbf{f}$  and  $\tilde{\mathbf{f}}$  are completely dynamically equivalent and*
- *if  $s \neq s'$  then  $\mathbf{f}$  and  $\tilde{\mathbf{f}}$  are partially dynamically equivalent.*

Let us begin with the Oregonator. The Oregonator stands for the dynamical behavior of  $x_1 = HBrO_2$ ,  $x_2 = Br^-$  and  $x_3 = Ce^{+4}$ . Their associated MAK-ODEs are:

$$\begin{aligned}
 \dot{x}_1 &= k_1 x_2 - k_2 x_1 x_2 + k_3 x_1 - 2k_4 x_1^2 \\
 \dot{x}_2 &= -k_1 x_2 - k_2 x_1 x_2 + k_5 x_3 \\
 \dot{x}_3 &= k_3 x_1 - k_5 x_3
 \end{aligned} \tag{4.2}$$

In particular, we set  $y = h(x) = x_3$  to construct the diffeomorphic map 4.3. Computing the Lie derivatives of  $y$  along (4.2) we have  $\mathbf{z}_{OR} \triangleq \Phi(\mathbf{x}_{OR}) = (h(x), L_f h(x), L_f^2 h(x))^T$ , where:

$$\Phi(\mathbf{x}_{OR}) = \begin{pmatrix} x_3 \\ k_3 x_1 - k_5 x_3 \\ k_3((k_1 - k_2 x_1)x_2 + (k_3 - 2k_4 x_1)x_1) - k_5(k_3 x_1 - k_5 x_3) \end{pmatrix} \tag{4.3}$$

which span the three dimensional space whenever  $\Phi$  takes values from the set  $\mathcal{D}_{OR} := \{(x_1, x_2, x_3) \in \mathbb{R}^3 \mid x_1 \neq \frac{k_1}{k_2}, (x_2, x_3) \geq 0\}$ ; thus  $\Phi_{OR} : \mathcal{D}_{OR} \rightarrow \mathbb{R}_{>0} \times \mathbb{R}^2$ . The associate inverse map reads as follows:

$$\Phi^{-1}(\mathbf{z}_{OR}) = \begin{pmatrix} \frac{z_2 + k_5 z_1}{k_3} \\ \frac{z_3 - k_3(k_3 - 2k_4 \mu)\mu + k_5(k_3 \mu - k_5 z_1)}{k_3(k_1 - k_2 \mu)} \\ z_1 \end{pmatrix} \tag{4.4}$$

where  $\mu(z) = \frac{k_5 z_1 + z_2}{k_3}$ . Note that, if  $x_1 \neq \frac{k_1}{k_2} \Rightarrow z_2 + k_5 z_1 \neq \frac{k_1 k_3}{k_2}$ , which is sufficient to avoid lost of dimension for the space spanned by (4.4).

The vector field of  $\text{GF}_D$  reads:

$$\begin{aligned}
 \dot{\tilde{x}}_1 &= -\tilde{k}_1 \tilde{x}_1 \tilde{x}_2 + \tilde{k}_2 \tilde{x}_2 - 2\tilde{k}_3 \tilde{x}_1^2 + 0.5\tilde{k}_4 (Cet - \tilde{x}_3)[BrO_2]_{eq} - 0.5\tilde{k}_5 \tilde{x}_1 \tilde{x}_3 \\
 \dot{\tilde{x}}_2 &= -\tilde{k}_1 \tilde{x}_1 \tilde{x}_2 - \tilde{k}_2 \tilde{x}_2 + \tilde{k}_7 \tilde{x}_3 \tilde{x}_4 + \tilde{k}_8 \tilde{x}_4 [MA]_{qss} \\
 \dot{\tilde{x}}_3 &= \tilde{k}_4 (Cet - \tilde{x}_3)[BrO_2]_{eq} - \tilde{k}_5 \tilde{x}_1 \tilde{x}_3 - \tilde{k}_6 \tilde{x}_3 - \tilde{k}_7 \tilde{x}_3 \tilde{x}_4 \\
 \dot{\tilde{x}}_4 &= 2\tilde{k}_1 \tilde{x}_1 \tilde{x}_2 + \tilde{k}_2 \tilde{x}_2 + \tilde{k}_3 \tilde{x}_1^2 - \tilde{k}_7 \tilde{x}_3 \tilde{x}_4 - \tilde{k}_8 \tilde{x}_4 [MA]_{qss}
 \end{aligned} \tag{4.5}$$

where  $[BrO_2\cdot]_{eq}$ ,  $[MA\cdot]_{qss}$  are evaluated using the auxiliary expressions derived from equilibrium and quasi-steady-state assumptions [1]:

$$[BrO_2\cdot]_{eq} = \sqrt{\frac{k_{c4}[BrO_3^-][H^+]\tilde{x}_1}{k_{c5}[H_2O]}} \quad (4.6)$$

$$[MA\cdot]_{qss} = \frac{k_{c10}\tilde{x}_4 + \sqrt{(k_{c10}\tilde{x}_4)^2 + 8k_{c8}k_{c11}[MA]\tilde{x}_3}}{4k_{c11}} \quad (4.7)$$

As in the Oregonator, we set  $\tilde{y} = h(\tilde{x}) = \tilde{x}_3$  for  $GF_D$  model. Computing the Lie derivatives of  $\tilde{y}$  along (4.5), we have:

$$\tilde{\mathbf{z}}_{GF_D} \triangleq \tilde{\Phi}(\tilde{\mathbf{x}}) = (h(\tilde{\mathbf{x}}), L_f h(\tilde{\mathbf{x}}), L_f^2 h(\tilde{\mathbf{x}}), L_f^3 h(\tilde{\mathbf{x}}))^T, \quad (4.8)$$

where:

$$h(\tilde{x}) = \tilde{x}_3 \quad (4.9)$$

$$L_f h(\tilde{x}) = \tilde{k}_4(Cet - \tilde{x}_3)[BrO_2\cdot]_{eq} - \tilde{k}_5\tilde{x}_1\tilde{x}_3 - \tilde{k}_6\tilde{x}_3 - \tilde{k}_7\tilde{x}_3\tilde{x}_4 \quad (4.10)$$

$$L_f^2 h(\tilde{x}) = -\left(\tilde{k}_5\dot{\tilde{x}}_1 + \tilde{k}_7\dot{\tilde{x}}_4\right)\tilde{x}_3 - (q + \tilde{k}_5\tilde{x}_1 + \tilde{k}_7\tilde{x}_4)L_f h(\tilde{x}) \quad (4.11)$$

$$\begin{aligned} L_f^3 h(\tilde{x}) = & \left( (\tilde{k}_5 - 2\tilde{k}_7)\tilde{k}_1\tilde{x}_2 + (\tilde{k}_5^2 - 2\tilde{k}_3(\tilde{k}_7 + 2\tilde{k}_5))\tilde{x}_1 + \right. \\ & \tilde{k}_5(\tilde{k}_7\tilde{x}_4 + q - 0.5\tilde{k}_5\tilde{x}_3))\tilde{x}_3 - \tilde{k}_5 L_f h(\tilde{x})\dot{\tilde{x}}_1 + \\ & \left( (\tilde{k}_5 - 2\tilde{k}_7)\tilde{k}_1\tilde{x}_1 - \tilde{k}_2(\tilde{k}_5 + \tilde{k}_7) \right)\tilde{x}_3\dot{\tilde{x}}_2 + \\ & \left( 0.5\tilde{k}_5(\tilde{k}_4[BrO_2\cdot]_{eq} - \tilde{k}_5\tilde{x}_1) + \tilde{k}_7^2\tilde{x}_4 \right)\tilde{x}_3 + \\ & (q + \tilde{k}_5\tilde{x}_1 + \tilde{k}_7\tilde{x}_4)^2 - (\tilde{k}_5\dot{\tilde{x}}_1 + \tilde{k}_7\dot{\tilde{x}}_4)L_f h(x) + \\ & (\tilde{k}_7\tilde{x}_3(\tilde{k}_7(\tilde{x}_3 + \tilde{x}_4) + \tilde{k}_5\tilde{x}_1 + (\tilde{k}_8[MA\cdot]_{qss} + q)) - \\ & \tilde{k}_7 L_f h(x))\dot{\tilde{x}}_4 \end{aligned} \quad (4.12)$$

with  $q = \tilde{k}_6 + \tilde{k}_4[BrO_2\cdot]_{eq}$ . Furthermore, the maps  $\tilde{\Phi}, \tilde{\Phi}^{-1}$  span the four dimensional space provided that  $\det(\partial\tilde{\Phi}(\tilde{\mathbf{x}})/\partial\tilde{\mathbf{x}}) \neq 0$ , *i.e.* be nonsingular for some neighborhood  $\tilde{\mathcal{U}}_{GF_D} \subset \mathbb{R}^4$  ([7]). Thus, in order to find *sufficient* regions of singularity of

$\tilde{\Phi}(\tilde{\mathbf{x}})$  we need to solve:

$$\det \left( \frac{\partial \tilde{\Phi}(\tilde{\mathbf{x}})}{\partial \tilde{\mathbf{x}}} \right) = \frac{\partial \tilde{z}_2}{\partial \tilde{x}_1} \left[ \left( \frac{\partial \tilde{z}_3}{\partial \tilde{x}_2} \right) \left( \frac{\partial \tilde{z}_4}{\partial \tilde{x}_4} \right) - \left( \frac{\partial \tilde{z}_3}{\partial \tilde{x}_4} \right) \left( \frac{\partial \tilde{z}_4}{\partial \tilde{x}_2} \right) \right] + \frac{\partial \tilde{z}_2}{\partial \tilde{x}_4} \left[ \left( \frac{\partial \tilde{z}_3}{\partial \tilde{x}_1} \right) \left( \frac{\partial \tilde{z}_4}{\partial \tilde{x}_2} \right) - \left( \frac{\partial \tilde{z}_3}{\partial \tilde{x}_2} \right) \left( \frac{\partial \tilde{z}_4}{\partial \tilde{x}_1} \right) \right] = 0 \quad (4.13)$$

Tables 4.1-4.2 resumed the sets of kinetics rate constants for Equations (4.5) and (4.6), taken from those reported in [1].

Thus, a set of conditions for the solution of (4.13) becomes:

1.  $(\partial \tilde{z}_2 / \partial \tilde{x}_1) = 0$  and  $(\partial \tilde{z}_2 / \partial \tilde{x}_4) = 0$ . Thus, in general, either  $\tilde{z}_2 = \pi$ , where  $\pi \in \mathbb{R}$ , or  $\tilde{z}_2 = f(\tilde{x}_2, \tilde{x}_3)$ , exclusively. In particular, we have that  $(\partial \tilde{z}_2 / \partial \tilde{x}_1) = -\tilde{k}_5 \tilde{x}_3$  and  $(\partial \tilde{z}_2 / \partial \tilde{x}_4) = -\tilde{k}_7 \tilde{x}_3$ . Thus, because  $(\tilde{k}_5, \tilde{k}_7) \in \mathbb{R}_{>0}^2$ ,  $\tilde{x}_3^* = 0$  is the only possible solution. The map  $\Phi(\tilde{\mathbf{x}})$  preserves dimension provided that  $\tilde{x}_3^*(t_0) > 0$ ,  $\forall t \in [t_0, t_{end}]$ .
2.  $(\partial \tilde{z}_3 / \partial \tilde{x}_2) = (\partial \tilde{z}_4 / \partial \tilde{x}_2) = 0$ . This implies that either  $\tilde{z}_3 = \pi_1$  and  $\tilde{z}_4 = \pi_2$ , with  $(\pi_1, \pi_2) \in \mathbb{R}^2$ ; or  $\tilde{z}_3 = \tilde{z}_4 = f(\tilde{x}_1, \tilde{x}_3, \tilde{x}_4)$ , exclusively. In particular, solving the above homogeneous equations we have:

$$\tilde{x}_1^* = \frac{\tilde{k}_2 (\tilde{k}_5 + \tilde{k}_7)}{\tilde{k}_1 (\tilde{k}_5 - 2\tilde{k}_7)} = 1.2719 \times 10^{-4} \quad (4.14)$$

$$\tilde{x}_2^* = \frac{G(\tilde{x}_3, \mathbf{k}, [BrO_2]_{eq}, [MA]_{qss})}{\tilde{k}_1^2 \tilde{k}_2 \tilde{k}_7 (\tilde{k}_5 - 2\tilde{k}_7)^2} \quad (4.15)$$

**Table 4.1:** Kinetic rate constants reported in [1] for  $GF_D$  vector field. All kinetic constants have  $M$  (Molar)/s (seconds) units

Parameter	Value
$\tilde{k}_1$	$2.564 \times 10^6$
$\tilde{k}_2$	0.29583
$\tilde{k}_3$	3000
$\tilde{k}_4$	79484
$\tilde{k}_5$	7000
$\tilde{k}_6$	0.95
$\tilde{k}_7$	0.5
$\tilde{k}_8$	2400

**Table 4.2:** Parameter values for auxiliary equations in  $GF_D$  vector field.  $M =$  Molar,  $s =$  seconds.

Parameter	Value
$k_{c4}$	33 ( $M^2s$ )
$k_{c5}$	$7.63 \times 10^{-5}$ ( $M^2s$ )
$k_{c8}$	0.3 ( $Ms$ )
$k_{c10}$	$2.4 \times 10^4$ ( $Ms$ )
$k_{c11}$	$3 \times 10^9$ ( $Ms$ )
$[BrO_3^-]$	0.09 ( $M$ )
$[H^+]$	1.282 ( $M$ )
$[H_2O]$	55 ( $M$ )
$[MA]$	0.475 ( $M$ )
<i>Cet</i> (total cerium)	$1.6 \times 10^{-3}$ ( $M$ )



provided that  $\tilde{k}_5/\tilde{k}_7 \neq 2$ . Where

$$\begin{aligned}
 G(\tilde{x}_3, \mathbf{k}, \dots) = & -24\tilde{k}_5^2\tilde{k}_3\tilde{k}_2^2\tilde{k}_7 - \tilde{k}_5^3\tilde{k}_1^2\tilde{k}_4[\text{BrO}_2\cdot]_{eq}\tilde{x}_3 + 20\tilde{k}_7^3\tilde{k}_3\tilde{k}_2^2 \\
 & - \tilde{k}_5^4\tilde{k}_2\tilde{k}_1\tilde{x}_3 - 4\tilde{k}_5^3\tilde{k}_3\tilde{k}_2^2 + 12\tilde{k}_5^2\tilde{k}_2\tilde{k}_1\tilde{k}_7^2\tilde{x}_3 \\
 & + \tilde{k}_5^3\tilde{k}_1^2\tilde{k}_4[\text{BrO}_2\cdot]_{eq}\text{Cet} - 6\tilde{k}_5^2\tilde{k}_1^2\tilde{k}_4\tilde{k}_7[\text{BrO}_2\cdot]_{eq}\text{Cet} \\
 & + 12\tilde{k}_5\tilde{k}_1^2\tilde{k}_4\tilde{k}_7^2[\text{BrO}_2\cdot]_{eq}\text{Cet} - 16\tilde{k}_7^3\tilde{k}_2\tilde{k}_1\tilde{k}_5\tilde{x}_3 \\
 & + 6\tilde{k}_1\tilde{k}_2\tilde{k}_5^2\tilde{k}_7\tilde{k}_8[\text{MA}]_{qss} - 12\tilde{k}_1\tilde{k}_2\tilde{k}_5\tilde{k}_7^2\tilde{k}_8[\text{MA}]_{qss} \\
 & + 6\tilde{k}_1^2\tilde{k}_4\tilde{k}_5^2\tilde{k}_7[\text{BrO}_2\cdot]_{eq}\tilde{x}_3 - 12\tilde{k}_5\tilde{k}_1^2\tilde{k}_4\tilde{k}_7^2[\text{BrO}_2\cdot]_{eq}\tilde{x}_3 \\
 & - 8\tilde{k}_7^3\tilde{k}_1^2\tilde{k}_4[\text{BrO}_2\cdot]_{eq}\text{Cet} + 8\tilde{k}_7^3\tilde{k}_1^2\tilde{k}_4[\text{BrO}_2\cdot]_{eq}\tilde{x}_3 \quad (4.16)
 \end{aligned}$$

From the sufficient conditions in items 1 and 2, we can define a neighborhood,  $\tilde{\mathcal{D}}_{GF_D}$ , for which the map  $\tilde{\Phi}$  preserves dimension,  $\tilde{\mathcal{D}}_{GF_D} = \{(\tilde{x}_1, \tilde{x}_3) \in \mathbb{R}^2 \mid \tilde{x}_1 \neq \tilde{x}_1^*, \tilde{x}_3 > 0\}$ . Thus,  $\tilde{\Phi} : \tilde{\mathcal{D}}_{GF_D} \rightarrow \mathbb{R}_{>0} \times \mathbb{R}^3$ .

We have shown the domains where diffeomorphic maps preserves dimension. Thus, in principle, we have that  $\mathbf{z}_{OR} \equiv \tilde{\mathbf{z}}_{GF_D} \Rightarrow \Phi(\mathbf{x}_{OR}) = \tilde{\Phi}(\tilde{\mathbf{x}}_{GF_D})$ . Since  $\Phi^{-1}$  exists, we can compose the maps as  $\mathbf{x}_{OR} = \Phi^{-1} \circ \tilde{\Phi}(\tilde{\mathbf{x}}_{GF_D}) = \Phi^{-1}(\tilde{\mathbf{z}}_{GF_D})$ . Correspondingly, we have in the opposite direction:  $\tilde{\mathbf{x}}_{GF_D} = \tilde{\Phi}^{-1} \circ \Phi(\mathbf{x}_{OR}) = \tilde{\Phi}^{-1}(\mathbf{z}_{OR})$ . Given the highly involved algebraic expressions after composition, it is difficult to derive conclusions concerning the dynamical equivalence of both CRNs.

### 4.3 Concluding remarks

Perhaps the major drawback of the compositions of maps to express the states of one CRN as function of a second CRN are the highly involved algebraic expressions. Not to mention that such composition of maps, in general, may lead to equations which maps to the non-positive orthant. Nevertheless, the construction of  $\Phi$  and its composition with another map using (not the same) observable functions along

vector fields induced by MAK or not, it is an advantage. This fact could be useful for those experimental situations where is not possible to measure the same observable for two (or more) given candidate CRNs. It is an open question which kind (linear vs non-linear) of observable function would lead to a simpler composition of maps, clarifying the parameter space where dynamical equivalence looks more evident from an algebraic point of view.

# 5. An autocatalytic CRN for Prion replication

The results we shall present in this chapter were possible due to the extension of PhD programs from three to four years by CONACyT. This Chapter exploits the CRNT formalism to study potential dynamical scenarios of a neurodegenerative disease caused by a misfolding protein: the Prion. The replication of Prions occurs in an autocatalytic process, which is modeled within the context of CRNs for two possible routes of Prion appearance. Both autocatalytic CRNs are deficiency one networks and the implementation of the Deficiency One Theory (DOT) provided three sets of kinetic constants from which bistability and sustained oscillations are supported. Furthermore, there is a steady state for which one of the Shilnikov's condition for homoclinic chaos hold. This facts motivated a further numerical bifurcation analysis in order to find a homoclinic orbit to support the existence of chaos.

## 5.1 *Proteins might attack*

Prion diseases are infectious neurodegenerative diseases occurring in humans and animals with a lethal outcome (*e.g.* Creutzfeld-Jakob and Gerstmann-Straussler-Scheinker diseases in humans). The key issue of prion diseases is at the misfolding of the prion cellular protein,  $PrP^C$ , into its pathogen form,  $PrP^{Sc}$  [42, 43]. The

detailed molecular process that change the structure of  $PrP^C$  into a rich and lethal  $\beta$ -sheet structure,  $PrP^{Sc}$ , and later replication, is not yet fully understood [44]. What is known is that the presence of  $PrP^C$  is absolutely required for disease progression [42, 43]. The characteristic event in prion diseases is the aggregation of  $PrP^{Sc}$  into large amyloid plaques and fibrous structures associated with neurodegeneration; *i.e.*, at sufficiently high concentration of  $PrP^{Sc}$ , it self-aggregates irreversibly [43]. Replication takes place by inducing the same transition in other pre-existing  $PrP^C$  molecules through an autocatalytic reaction scheme. By autocatalysis, the protein can self-replicate avoiding the usual process involving polynucleotides, be they RNA or DNA. Actually, the fact that  $PrP^{Sc}$  imparts its conformational information on  $PrP^C$  constitutes a new dogma in molecular biology [43]. Another unique feature of prion diseases is about their tri-modal epidemiological manifestations [44], which can be:

1. Sporadic: spontaneous misfolding of  $PrP^C$  into  $PrP^{Sc}$ .
2. Infectious: conversion of  $PrP^C$  to  $PrP^{Sc}$  takes place by a pre-existing seed of  $PrP^{Sc}$ .
3. Genetic: changes in the letters within the amino acid sequence that code for the  $PrP^C$  leads to the production of a mutant version of  $PrP^C$  that acquires the  $PrP^{Sc}$  properties.

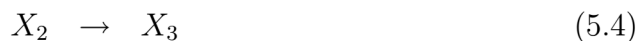
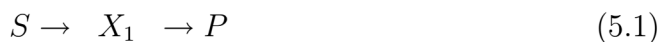
Efforts to derive a model of  $PrP^{Sc}$  replication can be found in literature [42, 43, 45, 46, and references therein]. Among them, an autocatalytic mechanism of four species and five reactions that accounts for both sporadic and infectious manifestation was published in [47]. The mechanism exhibits multiple steady states: one unstable and two stable ones. In particular, for the concentration of  $PrP^{Sc}$ , one stable steady state does not support the prion disease progression; the second one

evolves into the outbreak of the disease. This reaction mechanism is able to switch between the steady states depending upon external factors such as possible changes in metabolic processes (sporadic manifestation) or the external addition of  $PrP^{Sc}$  (infectious manifestation). Kinetic constants encode these external disturbances that influence the dynamical behavior of the system. Although this mechanism mimics the progression of prion diseases [47], some assumptions are invalid at the light of experimental evidence probably unknown at the time of publication. For instance, the reversibility of the autocatalytic replication of the  $PrP^{Sc}$ . Once the  $PrP^C$  change its natural conformation by the interaction with  $PrP^{Sc}$  molecules, the latter holds up because it is thermodynamically stable [48]. Furthermore, assumptions in [47] lead to a polynomial differential equation that is not a valid MAK-ODE [49]. Thus, there are non-negative initial conditions leading to negative concentrations, *i.e.* the sets  $\bar{\mathbb{R}}_+^n$  and  $\mathbb{R}_+^n$  are not forward invariant for the vector field in [47].

We present an alternative version of the autocatalytic mechanism, written within the chemical reaction network theory (CRNT) framework [30]. The MAK-ODEs induced by the mechanism displays multiplicity of equilibria and oscillatory behavior.

## 5.2 Proposed Kinetic Model

Let us consider the following kinetic mechanism (kinetic constants are omitted for brevity but they are considered along discussion within the text):



where  $S$  is the (constant) concentration substrate from which the cellular (healthy) protein  $X_1 = PrP^C$  is produced, and ultimately transforms into products,  $P$ .  $A$  incorporates all the metabolic processes leading to  $PrP^C$ . Reaction (5.2) accounts for isomerization of cellular prion  $X_1$  into the pathogenic prion  $X_2 = PrP^{Sc}$ . Irreversible autocatalysis (reaction (5.3)) stands for the self-replication of  $X_2 = PrP^{Sc}$  by interaction of more than one molecule with  $X_1 = PrP^C$ . After replication,  $X_2 = PrP^{Sc}$  infects healthy cells or tissue,  $X_3 = C$  (reaction (5.4)), which ultimately transforms into a metabolic product,  $P$  (reaction (5.5)). An alternative mechanism is derived by replacing reaction (5.2) with  $A \rightarrow X_2$ .

CRNT can be exploited to confirm the existence of positive steady states and determine their stability via the deficiency of a CRN,  $\delta$ . If multiple positive steady states are possible, then CRNT will provide kinetic constants consistent with them. To exploit this formalism we first need to write both modified mechanisms as CRNs.

In order to derive the CRN for both mechanisms, we stripped away species  $A$  and  $P$ , including them in the so called zero complex,  $\emptyset$ . We consider of interest species  $X_1 = PrP^C$ ,  $X_2 = PrP^{Sc}$  and  $X_3 = C$ , whose concentrations are denoted by  $x_1$ ,  $x_2$  and  $x_3$ , respectively. Hereafter, the CRN obtained considering reactions (5.1)-(5.5) will be denoted as  $\mathcal{N}$ , and  $\tilde{\mathcal{N}}$  for the CRN derived by considering reaction  $A \rightarrow X_2$  instead of reaction (5.2). Seeking clarity, species concentrations for  $\tilde{\mathcal{N}}$  will be denoted as  $\tilde{x}_i$ ,  $i = \{1, 2, 3\}$  along with its kinetic constants,  $\tilde{k}_j$ ,  $j = \{1, \dots, 6\}$ . Concentrations and kinetic constants are in arbitrary units.

5.2.1 MAK-ODES induced by  $\mathcal{N}$  and  $\tilde{\mathcal{N}}$  CRNs

For  $\mathcal{N}$  (see Figure 5.1) we obtain the following stoichiometric matrix,  $N \in \mathbb{R}^{3 \times 7}$ :

$$N = \begin{bmatrix} 1 & -1 & -1 & 1 & -1 & 0 & 0 \\ 0 & 0 & 1 & -1 & 1 & -1 & 0 \\ 0 & 0 & 0 & 0 & 0 & 1 & -1 \end{bmatrix} \quad (5.6)$$

and its MAK reaction rates vector:

$$v(x, k) = (k_1, k_2x_1, k_3x_1, k_4x_2, k_5x_1x_2^2, k_6x_2, k_7x_3)^T \quad (5.7)$$

where  $k_1$  includes the constant contribution of  $A$ . Then, the MAK-ODEs induced by  $\mathcal{N}$  are:

$$\begin{aligned} \dot{x}_1 &= k_1 - (k_2 + k_3)x_1 + k_4x_2 - k_5x_1x_2^2 \\ \dot{x}_2 &= k_3x_1 - (k_4 + k_6)x_2 + k_5x_1x_2^2 \\ \dot{x}_3 &= k_6x_2 - k_7x_3 \end{aligned} \quad (5.8)$$

subject to  $\mathbf{x}(0) \in \bar{\mathbb{R}}_+^3$ .

From Figure 5.2, we derive the corresponding stoichiometric matrix and MAK reaction rates vector for  $\tilde{\mathcal{N}}$ :

$$\tilde{N} = \begin{bmatrix} 1 & -1 & 0 & -1 & 0 & 0 \\ 0 & 0 & 1 & 1 & -1 & 0 \\ 0 & 0 & 0 & 0 & 1 & -1 \end{bmatrix}, \quad \tilde{N} \in \mathbb{R}^{3 \times 6} \quad (5.9)$$

$$\tilde{v}(\tilde{x}, \tilde{k}) = (\tilde{k}_1, \tilde{k}_2\tilde{x}_1, \tilde{k}_3, \tilde{k}_4\tilde{x}_1\tilde{x}_2^2, \tilde{k}_5\tilde{x}_2, \tilde{k}_6\tilde{x}_3)^T \quad (5.10)$$

where  $\tilde{k}_1$  and  $\tilde{k}_3$  include the constant concentration of  $A$ . Then, MAK-ODEs for  $\tilde{\mathcal{N}}$

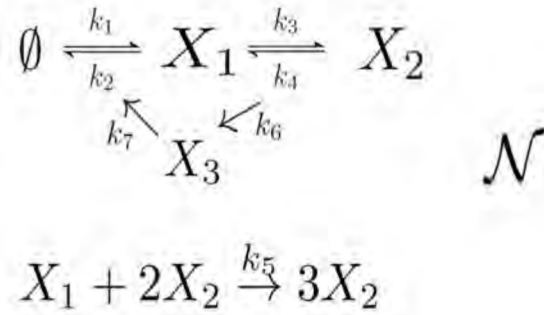


Figure 5.1:  $\mathcal{N}$  CRN which induced the MAK-ODEs (5.8).

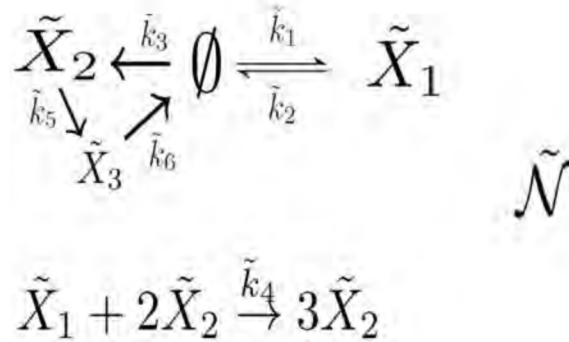


Figure 5.2:  $\tilde{\mathcal{N}}$  CRN which induced the MAK-ODEs (5.11).



has the form:

$$\begin{aligned}
 \dot{\tilde{x}}_1 &= \tilde{k}_1 - \tilde{k}_2\tilde{x}_1 - \tilde{k}_4\tilde{x}_1\tilde{x}_2^2 \\
 \dot{\tilde{x}}_2 &= \tilde{k}_3 + \tilde{k}_4\tilde{x}_1\tilde{x}_2^2 - \tilde{k}_5\tilde{x}_2 \\
 \dot{\tilde{x}}_3 &= \tilde{k}_5\tilde{x}_2 - \tilde{k}_6\tilde{x}_3
 \end{aligned}
 \tag{5.11}$$

subject to  $\tilde{\mathbf{x}}(0) \in \bar{\mathbb{R}}_+^3$ .

Now, we have the elements to compute the deficiencies associated to  $\mathcal{N}$  and  $\tilde{\mathcal{N}}$  CRNs. The set of complexes composing  $\mathcal{N}$  are identified from Figure 5.1 as  $\mathcal{C}_{\mathcal{N}} = \{\emptyset, X_1, X_2, X_3, X_1 + 2X_2, 3X_2\}$ ; thus  $|\mathcal{C}_{\mathcal{N}}| = 6$ . The linkage class set of  $\mathcal{N}$  consist of two set of complexes that are internally connected by reactions, while no reactions exist between elements of distinct sets:  $\mathcal{L}_{\mathcal{N}} = \{\{\emptyset, X_1, X_2, X_3\}, \{X_1 + 2X_2, 3X_2\}\}$ . Then,  $|\mathcal{L}_{\mathcal{N}}| = 2$ . In addition, both stoichiometric matrices,  $(N, \tilde{N})$ , have full row rank; i. e., no conservation relations exists. Thus, using (??), we have for  $\mathcal{N}$  that  $\delta_{\mathcal{N}} = 6 - 2 - 3 = 1$ . Following the same procedure for  $\tilde{\mathcal{N}}$ , it can be computed from Figure 5.2 that  $\delta_{\tilde{\mathcal{N}}} = 6 - 2 - 3 = 1$ .

According to the DOT [30, 31, 28], there are set of kinetic constants for which the MAK-ODEs induced by both  $\mathcal{N}$  and  $\tilde{\mathcal{N}}$  admit multiple positive steady states. Moreover,  $\mathcal{N}$  admits a degenerate steady state whereas  $\tilde{\mathcal{N}}$  does not. We use these set of kinetic constants along with the cubic equation, derived by setting to zero the left hand side of (5.8) and (5.11), to compute the full set of positive steady states for both  $\mathcal{N}$  and  $\tilde{\mathcal{N}}$ .

For  $\mathcal{N}$  we have the steady state cubic equation:

$$a_3x_{3,ss}^3 + a_2x_{3,ss}^2 + a_1x_{3,ss} + a_0 = 0
 \tag{5.12}$$

where

$$a_3 = 1 \quad (5.13)$$

$$a_2 = -\frac{k_1}{k_7} < 0, \quad \forall \mathbf{k} \in \mathbf{R}_{>0}^7 \quad (5.14)$$

$$a_1 = \frac{k_6(k_3k_6 + k_2k_4 + k_2k_6)}{k_5k_7^2} > 0, \quad \forall \mathbf{k} \in \mathbf{R}_+^7 \quad (5.15)$$

$$a_0 = -\frac{k_1k_3k_6^2}{k_5k_7^3} < 0, \quad \forall \mathbf{k} \in \mathbf{R}_+^7 \quad (5.16)$$

Additionally,

$$x_{1,ss} = \frac{k_1 - k_7x_{3,ss}}{k_2}, \quad x_{2,ss} = \frac{k_7x_{3,ss}}{k_6} \quad (5.17)$$

Meanwhile for  $\tilde{\mathcal{N}}$  we have:

$$\tilde{a}_3\tilde{x}_{3,ss}^3 + \tilde{a}_2\tilde{x}_{3,ss}^2 + \tilde{a}_1\tilde{x}_{3,ss} + \tilde{a}_0 = 0 \quad (5.18)$$

$$\tilde{a}_3 = 1 \quad (5.19)$$

$$\tilde{a}_2 = -\frac{\tilde{k}_1 + \tilde{k}_3}{\tilde{k}_6} < 0, \quad \forall \tilde{\mathbf{k}} \in \mathbf{R}_+^6 \quad (5.20)$$

$$\tilde{a}_1 = \frac{\tilde{k}_2\tilde{k}_5^2}{\tilde{k}_4\tilde{k}_6^2} > 0, \quad \forall \tilde{\mathbf{k}} \in \mathbf{R}_+^6 \quad (5.21)$$

$$\tilde{a}_0 = -\frac{\tilde{k}_2\tilde{k}_3\tilde{k}_5^2}{\tilde{k}_4\tilde{k}_6^3} < 0, \quad \forall \tilde{\mathbf{k}} \in \mathbf{R}_+^6 \quad (5.22)$$

and

$$\tilde{x}_{1,ss} = \frac{\tilde{k}_1 + \tilde{k}_3 - \tilde{k}_6\tilde{x}_{3,ss}}{\tilde{k}_2}, \quad \tilde{x}_{2,ss} = \frac{\tilde{k}_6\tilde{x}_{3,ss}}{\tilde{k}_5} \quad (5.23)$$

## 5.3 Dynamical scenarios

### 5.3.1 Dynamics for $\mathcal{N}$

The DOT [30, 31, 28] provides two set of kinetic constants for  $\mathcal{N}$  such that (5.8) admits multiple positive steady states. The steady states for  $\mathcal{N}$  and their stability are

resumed in Tables 5.1 and 5.2. Figure 5.3 shows that  $x_{1,ss1} < x_{1,ss2}$  and  $x_{2,ss1} > x_{2,ss2}$ . Furthermore,  $x_{3,ss1} > x_{3,ss2}$ . This means that, SS2 has the lowest concentration of infected cells,  $x_{3,ss2}$ , along with the lowest concentration of scrapie protein,  $x_{2,ss2}$ . Conversely, SS1 has the highest concentration of infected cells,  $x_{3,ss1}$ , along with the highest concentration of scrapie protein,  $x_{2,ss1}$ . In addition to these facts, the (local) stability of steady states SS2 and SS1 implies each one is attractive for any initial condition at the attraction basin and the concentrations hold on SS2 and SS1 along time. In other words, when a subject lies in an starting condition such that the concentrations  $x_1, x_2$  and  $x_3$  are within a healthy situation (*i.e.*, attraction basin of SS2), then time evolution of disease converges to the SS2. On contrary, as the starting condition of subject are within the progress situation (*i.e.*, attraction basin of SS1) the disease evolves towards the highest concentration of infected cells and scrapie protein.

**Table 5.1:**  $\mathcal{N}$  steady states and their stability for kinetic constants  $k_1 = 2.9872232$ ,  $k_2 = k_3 = k_7 = 1$ ,  $k_4 = 12.626548$ ,  $k_5 = 5.6433885$ ,  $k_6 = 0.85914091$ .

Steady State	$x_{1,ss}$	$x_{2,ss}$	$x_{3,ss}$	Eigenvalues
$SS_1$	1	2.3130	1.9872	(-1, -0.7534, -18.8184), stable
$SS_2$	2.7183	0.3130	0.2689	(-1, -5.4834, -0.9512), stable
$SS_3$	2.2562	0.8509	0.7311	(-1, 3.2646, -1.168), unstable

**Table 5.2:**  $\mathcal{N}$  steady states and their stability for kinetic constants  $k_1 = 11.107337$ ,  $k_2 = k_7 = 1$ ,  $k_3 = 0.17891084$ ,  $k_4 = 5.7767046$ ,  $k_5 = 1.0096634$ ,  $k_6 = 3.194528$ .

Steady State	$x_{1,ss}$	$x_{2,ss}$	$x_{3,ss}$	Eigenvalues
$SS_1$	10.1073	0.3130	1	(-1, -2.4352, -1.4249), stable
$SS_2$	3.7183	2.3130	7.3891	(-1, $0.9076 + 2.9339 i$ , $0.9076 - 2.9339 i$ ), unstable
$SS_3$	8.3891	0.8509	2.7183	(-1, 4.1455, -0.6119), unstable

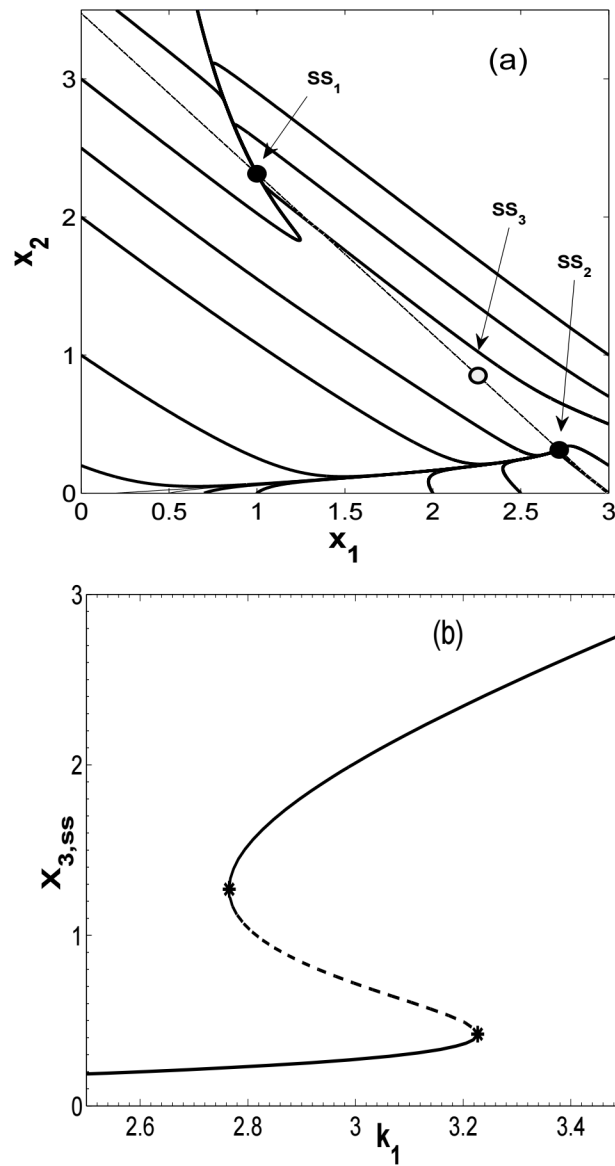


**Figure 5.3:** (a) Solid lines: solutions of (5.8) with different initial conditions. Set of kinetic constants as in Table 5.1. Black circle: stable steady state. White circle: unstable steady state. Dotted line: locus of equilibrium. (b) Equilibrium bifurcation diagram for  $x_3$  showing multiple steady states as  $k_1$  vary. Solid line: stable branch. Dotted line: unstable branch.

Moreover, a very interesting issue concerns a threshold which has to be reached to permit the disease progression. Actually the threshold for disease progression exists and regards both infected and healthy cell concentrations. In order to explain this, let us observe Figure 5.3. As discussed above, the disease evolves to SS2 or SS1 depending on the initial conditions of  $x_1$  and  $x_2$ . Note that the locus of equilibrium (dotted-line) connects to SS1, SS3 and SS2. The equilibrium SS3 plays the main role on the determination of the threshold. In fact, there is a region below the locus of equilibrium such that any initial condition converges to SS2 whereas a starting condition at other region above it leads to SS1. That is, in order to illustrate our point, consider two initial conditions  $(x_1(0), x_2(0)) = (0.5, 1.0)$  and  $(x_1(0), x_2(0)) = (3.0, 1.0)$ , then SS2 and SS1 are attractive for the former and the latter, respectively. The interpretation of this fact is as follows. Assume the system is at SS2 (*i.e.*, a healthy condition). If the concentration of  $x_2$  increases beyond  $x_2 \approx 0.5$  by means of a possible metabolic change (related to sporadic manifestation) or the external addition of scrapie protein (related to infectious manifestation), then the time evolution of disease converges to SS1 with the consequent disease progression. Thus, once the threshold is surpassed the system could not return to SS2.

Figure 5.4 shows that, if external factors changes the rate of reactions (*e.g.*, an immune action from the host) in such a way that  $x_1$  grows faster from substrate while the replication processes diminish (see  $k_1, k_2$  in Table 2) the disease does not progress

A description of the oscillatory behavior is supported by  $\mathcal{N}$  for the set of kinetic constants  $k_1 = 3$ ,  $k_2 = k_7 = 1$ ,  $k_3 = 0.5$ ,  $k_4 = k_5 = 6$ ,  $k_6 = 2$ , with a steady state of multiplicity of three from (5.12):  $\mathbf{x}_{ss} = (2, 0.5, 1)$ . Eigenvalues associated to this steady state are  $(-1, 1, 0)$ , indicating a (neutral) saddle-node [27]. Using  $k_1$  (substrate rate of production) as a bifurcation parameter, it can be seen that for  $k_1 = 2.89$  the system has one stable steady state for which  $x_{1,ss} > x_{3,ss} > x_{2,ss}$  (cf. Figure 5.5 a,b). Furthermore, if  $k_1$  increase, the system undergoes a super-critical

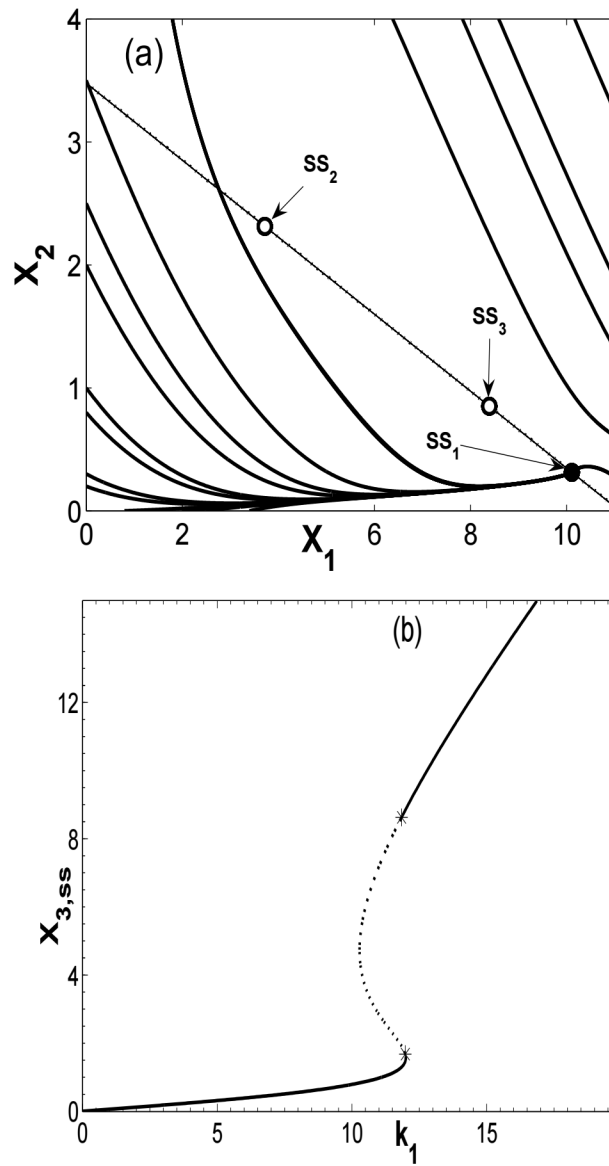


**Figure 5.4:** (a) Solid lines: solutions of (5.8) with different initial conditions. Set of kinetic constants as in Table 5.2. Black circle: stable steady state. White circle: unstable steady state. Dotted line: locus of equilibrium. (b) Equilibrium bifurcation diagram for  $x_3$  showing multiple steady states as  $k_1$  vary. Solid line: stable branch. Dotted line: unstable branch.

Hopf bifurcation close to the saddle-node as shown in Figure 5.5. Because the saddle is unstable and steady states are multiplicity of three, solutions of (5.8) steers to the stable limit cycle where they will remain confined.

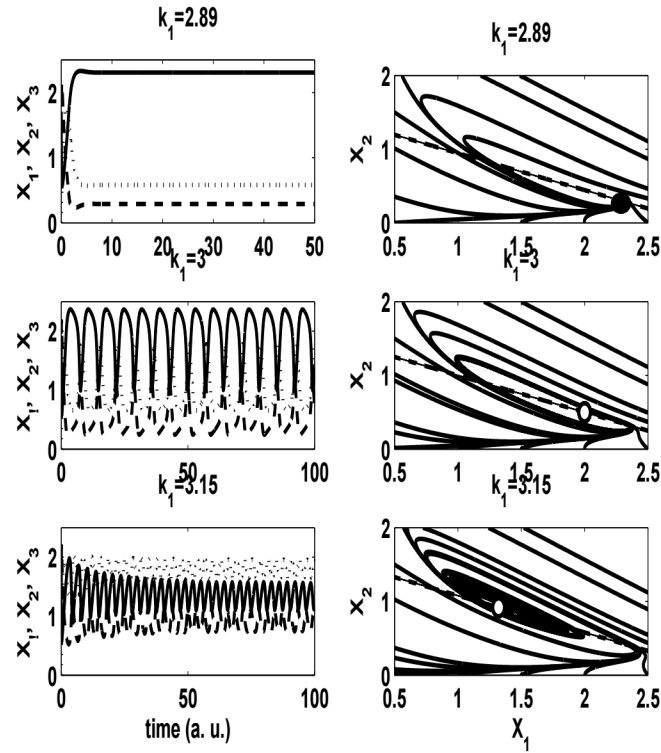


**Figure 5.5:** *Bifurcation scenario for degenerate steady state varying  $k_1$ : vector field (5.8) goes from a stable steady state (Figs. 5.5a,b) to an unstable saddle (Figs. 5.5c,d) which undergoes a supercritical Hopf bifurcation (Figs. 5.5e,f). Time evolution of species  $x_1$  (black line),  $x_2$  (dashed line) and  $x_3$  (dotted line). Black circle: stable steady state. White circle: unstable steady state.*

### 5.3.2 Dynamical scenario of $\tilde{\mathcal{N}}$

For  $\tilde{\mathcal{N}}$  the DOT gives a set of kinetic constants that enable (5.11) to exhibit one stable steady state and two unstable ones, as shown in Table 5.3 (see Figure 5.6). Despite  $\tilde{\mathcal{N}}$  foresee the formation of  $X_2 = PrP^{Sc}$  directly from the substrate at a constant rate, the existence of such a reservoir is not sufficient for the prion disease to progress (cf.  $\tilde{k}_1$  in Table 5.3). Note that the autocatalytic reaction rate takes place at a lower pace than the remaining reactions (cf.  $\tilde{k}_4$  in Table 5.3). Under these circumstances,  $\tilde{\mathcal{N}}$  is sufficiently robust against infection.

**Table 5.3:**  $\tilde{\mathcal{N}}$  steady states and their stability for kinetic constants  $\tilde{k}_1 = 15.696713$ ,  $\tilde{k}_2 = \tilde{k}_3 = \tilde{k}_6 = 1$ ,  $\tilde{k}_4 = 0.33799396$ ,  $\tilde{k}_5 = 4.8020616$ .

Steady State	$\tilde{x}_{1,ss}$	$\tilde{x}_{2,ss}$	$\tilde{x}_{3,ss}$	Eigenvalues
$\tilde{S}S_1$	5.5894	2.3130	11.1073	$(-1, 0.5645 + 2.1042 i, 0.5645 - 2.1042 i)$ , unstable
$\tilde{S}S_2$	15.1935	0.3130	1.5032	$(-1, -1.3101 + 0.1726 i, -1.3101 - 0.1726 i)$ , stable
$\tilde{S}S_3$	12.6106	0.8509	4.0862	$(-1, 1.8843, -0.6774)$ , unstable

## 5.4 Bifurcation analysis

The second dynamical scenario suggest the existence of a homoclinic orbit such that in a neighborhood of the saddle focus chaos might be present in the system if Shilnikov's condition hold. That is, when the steady state is a saddle focus with the eigenvalues  $(\mu, \rho \pm \omega i)$  satisfying the Shilnikov's condition  $|\rho/\mu| < 1$ , we know that there exists a chaotic set of trajectories near the homoclinic orbit [27]. Recall that the second dynamical scenario has a saddle focus with eigenvalues  $\Lambda_2 = (-1, 0.9076 \pm 2.9339 i)$ , for which Shilnikov condition hold.

Seeking for such a chaotic region, we performed a bifurcation analysis of every dynamical scenario. As bifurcation parameters we choose the pair  $(k_6, k_1)$  which stands



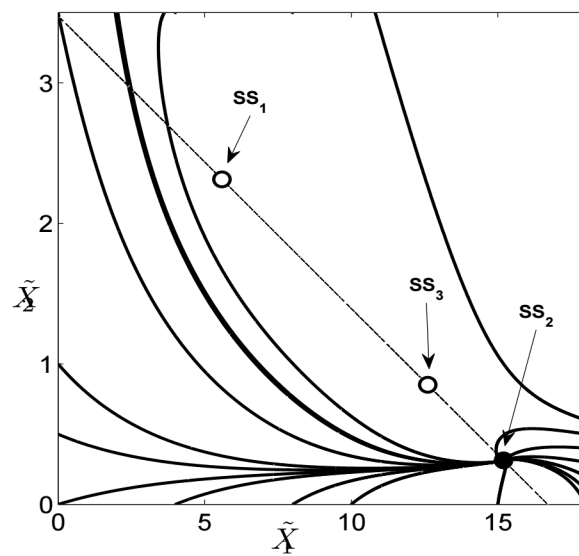


**Figure 5.6:** *Solid lines: solutions of (5.11) with different initial conditions. Set of kinetic constants as in Table 5.3. Black circle: stable steady state. White circle: unstable steady state. Dotted line: locus of equilibrium.*

for the rate of infection and the rate of production of healthy protein, respectively.

Continuation of  $x_1$  equilibrium using  $k_6$  from  $\mathbf{K}_1$  is shown in Figure 5.7. Three steady states are possible within the range  $k_6 \in (0.5, 1)$ , approximately. The continuation of equilibria in the  $(k_6, k_1)$  space leads to the following possible bifurcations (see Figure 5.8): Bogdanov-Takens(=BT), *i.e.* the critical equilibrium has a zero eigenvalue of (algebraic) multiplicity two. Coordinates:  $(k_6, k_1) = (1.100256, 3.122943)$ . At  $(k_6, k_1) = (1.231066, 3.298550)$  there is a Zero Hopf(=ZH) Neutral Saddle. A Cusp Point(=CP) is founded at  $(k_6, k_1) = (1.803793, 3.945468)$ , followed by another Zero Hopf Neutral Saddle located at  $(k_6, k_1) = (1.641215, 3.808766)$ . A second Bogdanov-Takens point is located at  $(k_6, k_1) = (1.366877, 3.594817)$ .

Figure 5.9 shows a very similar bifurcation diagram in the  $(k_6, k_1)$  parameter space using the set  $\mathbf{K}_2$ . Using the same nomenclature as in the previous paragraph: BT at  $(k_6, k_1) = (12.270874, 3.359119)$ ; ZH located at  $(k_6, k_1) = (15.593040, 5.354471)$ ; CP in  $(k_6, k_1) = (29.297191, 13.394117)$ ; second ZH at  $(k_6, k_1) = (6.2703, 1.4298)$ ; second BT at  $(k_6, k_1) = (5.616992, 1.181614)$ . Moreover, there is an oscillatory region (left to the CP point), which ends, due to numerical difficulties, in a Limit Point Cycle(=LPC). Figure 5.10 shows the oscillatory behavior at the left of the CP.

Varying  $k_6$  in the third dynamical scenario (degenerate steady state) we obtain Figure 5.11. From left to right: at  $k_6 = 1.862951$  we encounter a subcritical Hopf(=H) point, followed by a Neutral Saddle at  $k_6 = 1.994178$ . A second Neutral Saddle and a subcritical Hopf point are located at  $k_6 = 2$  and  $k_6 = 2.014358$ , respectively.

Following the Hopf point in the  $(k_6, k_1)$  parameter space, Neimark-Sacker(=NS) and Limit Point Cycles(=LPC) can be encountered. Quasi-periodic oscillations around the NS points are possible as suggested by Figure 5.13.

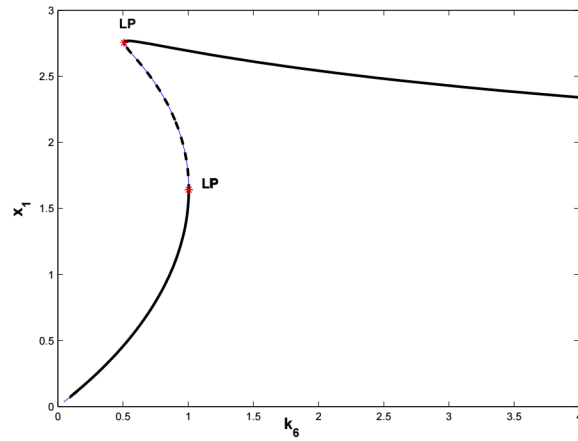


**Figure 5.7:** Continuation of  $x_1$  using  $k_6$  from the set  $\mathbf{K}_2$ . Solid line stable equilibrium. Dashed line unstable equilibrium. LP=Limit Point.

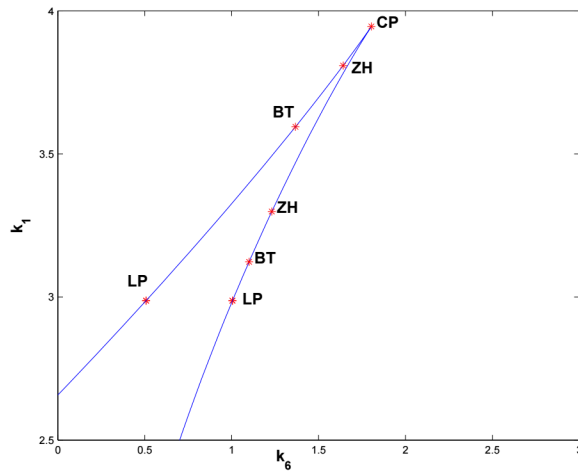


**Figure 5.8:** Bifurcation diagram in the  $(k_6, k_1)$  space from the set  $\mathbf{K}_1$ . LP=Limit Point. BT=Bogdanov-Takens. ZH=Zero Hopf(Neutral saddle). CP=Cusp Point.

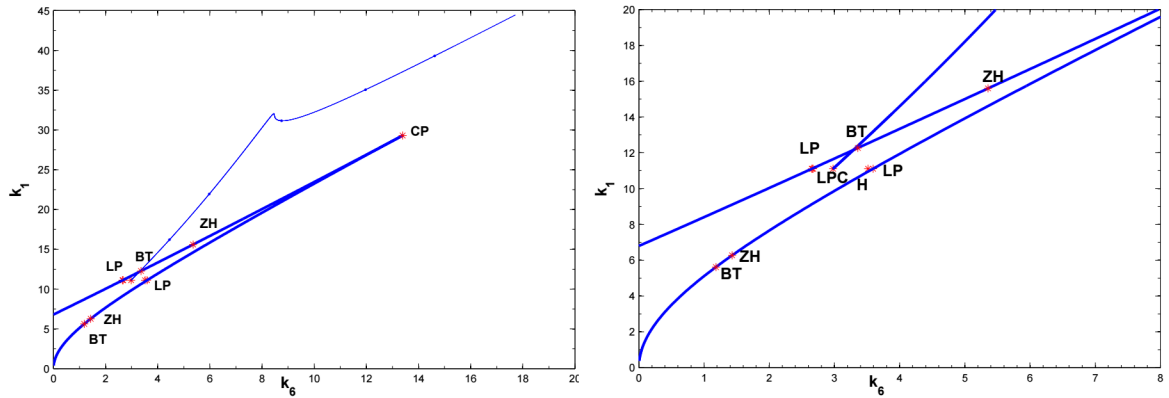


**Figure 5.9:** Upper panel: Bifurcation diagram in the  $(k_6, k_1)$  space from the set  $\mathbf{K}_2$ . Lower panel: augmented region to show the Limit Point Cycle (LPC). LP=Limit Point. BT=Bogdanov-Takens. ZH=Zero Hopf (Neutral saddle). CP=Cusp Point.

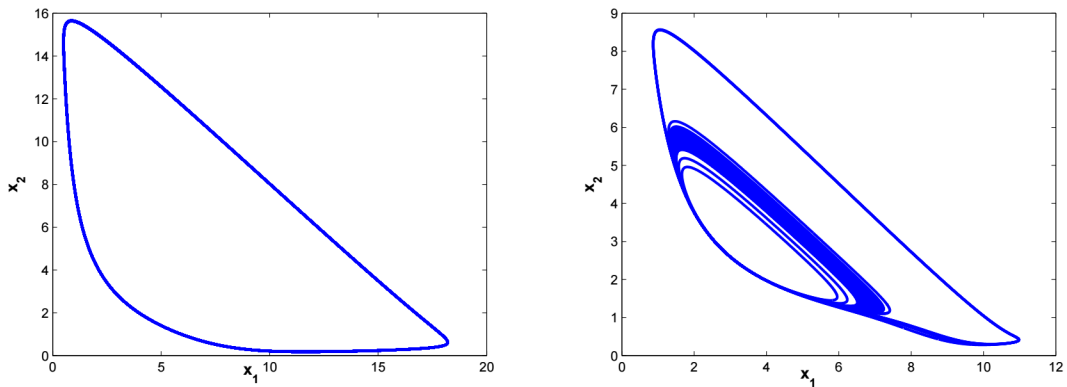


**Figure 5.10:** Two different oscillations projected in the  $x_1 - x_2$  space from the oscillatory region at the left of the Cusp Point in Figure 5.9. Upper panel:  $(k_6, k_1) = (8, 25)$ . Lower panel:  $(k_6, k_1) = (3.39, 12.46)$ ; remaining kinetic constants as in  $\mathbf{K}_2$

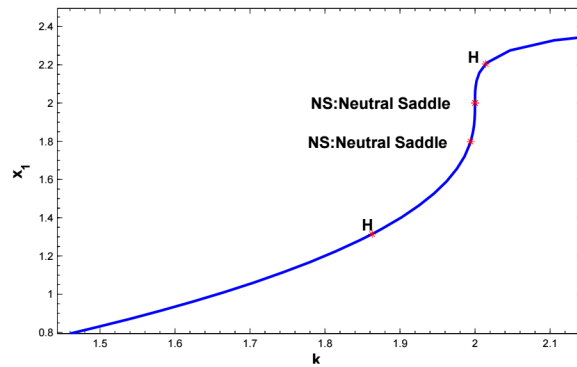


**Figure 5.11:** Bifurcation diagram for degenerate steady state varying  $k_6$  from set  $\mathbf{K}_3$ .  $H$ =Hopf.  $LP$ =Limit Point.

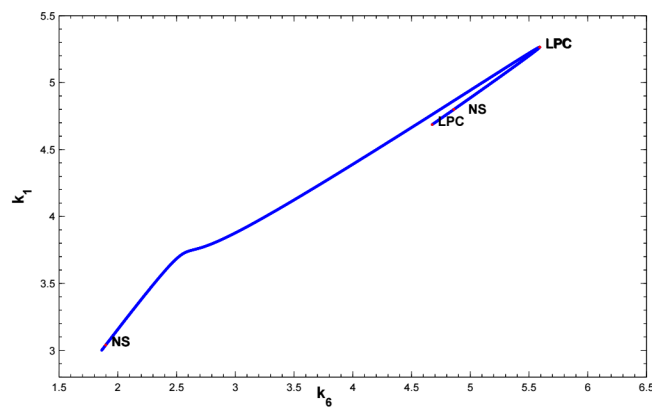


**Figure 5.12:** Bifurcation diagram for degenerate steady state in the  $(k_6, k_1)$  space.  $NS$ =Neimark-Sacker,  $LPC$ =Limit Point of Cycles.

## 5.5 Concluding remarks

It was assumed that every set of kinetic constants provided by the CRNT encodes possible changes within the metabolic process or external disturbances. In this sense,  $\mathcal{N}$  is able to exhibit three different dynamical scenarios for different sets of kinetic

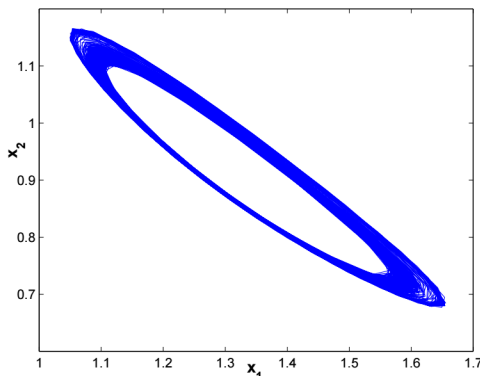


**Figure 5.13:** *Quasi-periodic oscillations in the  $x_1 - x_2$  plane at the Neimark-Sacker point  $(k_6, k_1) = (1.897181, 3.039192)$ .*

constants. The first dynamical scenario for  $\mathcal{N}$  is the bistability and shows that there exists an *infectious threshold* in terms of  $PrP^{Sc}$  concentration,  $x_2$ , for which the host can develop a higher concentration of infected cells,  $x_3$ , if it is surpassed by an external addition or sporadic appearance of  $PrP^{Sc}$  (see Figure 5.3). On the other hand, in the second dynamical scenario, the infectious threshold it is absent when two steady state become unstable.

We conjecture that the host is robust in face to both sporadic and infectious manifestations of the prion disease because is able to return to its stable steady state (see Figure 5.4). In terms of the kinetic rates, such a robustness might be achieved if we can managed to change the rate of reactions (*e.g.* an immune or inoculation action) in such a way that  $x_1$  grows faster from the substrate while the replication processes diminish (cf.  $k_1$ ,  $k_5$  in Table 5.2). In addition, regarding the third scenario,  $\mathcal{N}$  is able to exhibit sustained oscillations. In other words, oscillations in the protein concentrations (healthy and scrapie) and infected cells might be conjectured to be in a dormant progression state. This is suggested because of two facts: (i) prion

diseases are characterized by long incubation time periods [42, 50] and (ii) under oscillatory regime, high concentration of infected and healthy cells are alternately reached. That is, increments as well as decrements in  $x_3$  can be exhibited involving that, for instance, neural tissue regenerates at time intervals, which could be plausible from a biological perspective since neurogenesis is now an accepted phenomena [51, and references therein].

Regarding  $\tilde{\mathcal{N}}$ , where  $\text{PrP}^{\text{Sc}}$  can be yielded directly from substrate, the scenario that we found using CNRT displays no infectious threshold because there is only one stable steady state. Note this scenario for  $\tilde{\mathcal{N}}$  is equivalent to one of the scenarios (the second one) for  $\mathcal{N}$ .

The relation between these dynamics and a possible medical interpretation need to be investigated further. For example, the impact on the progression of the disease if external conditions onset (quasi)periodic oscillations in the concentration of proteins. This is not an easy task because the peculiarities of the Prion disease progression such as asymptomatic long incubation periods, lack of fast and reliable blood test for a prompt detection of the pathogen form of the Prion protein or to estimate the progression of the disease. Nevertheless, it has been reported that oscillations are related with flare-ups, *i.e.* the recurrence of symptoms or an onset of more severe symptoms [52]. It remains an open question whether or not oscillations can be tuned to induce a recovery or to bound the progress of the disease. Furthermore, the design of robust (non)linear state estimators to provide, with certain accuracy, the degree of disease progression to physicians, seems challenging.

Bio-inspired problems such as Prion diseases offer a good opportunity for the control community to develop or implement mathematical tools aimed to understand and, possibly, give some insights that lead to the cure of this kind of diseases.

## 6. Conclusions and Further Research

In this thesis, the concept of *dynamical equivalence* among chemical reaction networks has been addressed. The dynamical equivalence states that chemical species concentrations of one reaction network can be expressed via a suitable change of coordinates, as a function of a second reaction network: solutions, *i.e.* trajectories of ordinary differential equations, are mapped to an equivalent system. The change of coordinates is constructed via recursive Lie derivatives of an observable function along the vector field induced by the reaction network, endowed with mass actions kinetics or other kinetics, *e.g.* Michaelis-Menten.

This definition was motivated by the fact known in the chemistry literature as the fundamental dogma of chemical kinetics: more than one candidate chemical reaction networks can fit the experimental data. Candidate reaction networks not necessarily share the same number of chemical species or reactions. Moreover, their ordinary differential equations may or may not follow the mass action kinetic law. Thus, their associated set of dynamical equations will induce vector fields, *i.e.* the right hand side of the ordinary differential equations, with distinct dimension among candidate reaction networks and with different structure. These issues are particularly well illustrated by the Belusouov-Zhabotinsky (BZ) oscillatory chemical reaction.



## Conclusions and Further Research

---

The usual graph theoretical approaches such as the Chemical Reaction Network Theory (CRNT) [30, 32], *i.e.* deficiency analysis, and Stoichiometric Network Analysis [4], were implemented in order to find structural properties oscillatory reactions, *e.g.* Brusselator and Oregonator might share. The former being the first respectable oscillatory reaction network that showed the same qualitative dynamics as the BZ reaction, meanwhile the latter is considered as the minimal reaction network for the BZ reaction. Brusselator and Oregonator networks are endowed with mass action kinetics of different dimensions, two and three, respectively. It was shown in Section 3.1.1 they do not share the same deficiencies. Nevertheless, the 2-D Brusselator and 3-D Oregonator CRNs, represent a straight line in the reaction rate space (Section 3.1.2). The question to what extent both chemical oscillator can be equivalent, it was shown that through a transformation,  $T$ , of the Oregonator's jacobian is possible to obtain the same linear combination of convex coordinates as in the Brusselator's Jacobian entries. Nevertheless, such a transformation is not invertible.

Seeking invertible transformations a change of coordinates was proposed, such that chemical species concentrations of two different oscillatory CRNs, not necessarily of the same dimension, can be expressed as function of the other, and vice versa, through composition of diffeomorphic maps. These maps were constructed via Lie derivatives of a suitable observable (a measure chemical specie) along the vector fields induced by the set of MAK-ODEs. For a set of kinetic constants and a suitable initial condition states, was possible to map trajectories from Brusselator's space onto Oregonator's space, preserving the qualitative dynamical nature displayed by the Brusselator (cf. Section 3.2). Conversely, Oregonator's trajectories (solutions) onto Brusselator's was partially achieved for  $x_{1,BR}^*$ , thus both chemical oscillators can be regarded as *partially dynamic equivalent* for these chemical species. Conditions in parameters space that guarantee  $x_{2,BR}^* > 0$  cannot be fulfilled for typical values of both Brusselator and Oregonator CRNs. In this sense, a broad parametric search need

## Conclusions and Further Research

---

to be performed. This shows that there exist observable functions that lead, for some region of parameter space, to algebraic expressions where dynamical equivalence can adopt the form of free parameter equalities. For the case of Brusselator and Minimal-Mass-Action-Kinetic-With-Limit-Cycle reaction network, a mirror reflection of the dynamics was found, resembling a *chirality* phenomena previously reported in [40] within a reduced order synchronization context.

Chapter 4 shown that the deficiency is not an invariant among CRNs of distinct structure and dimension that stands for the same experimental reality, *e.g.* the set of GF CRNs for the BZ reaction. Dynamical equivalence between distinct dimensional oscillatory CRNs that stands for the BZ reaction and unrestricted to follow MAK, was explored together with Oregonator, a three dimensional CRN for the BZ reaction. Particularly, the case of dynamical equivalence between  $GF_D$  and Oregonator CRN lead to a highly involved algebraic relationship among states, *i.e.* chemical species concentrations. Only sufficient conditions which guarantee the existence of an inverse for the  $GF_D$  were given. Thus, in principle, the composition of Oregonator and  $GF_D$  is possible. It remains to derive from such composition conditions of non-negativeness. In this sense, perhaps the major drawback of the concept of dynamical equivalence is that the algebra of the composed maps  $\Phi^{-1}(\tilde{\Phi}(\tilde{\mathbf{x}}))$  and vice versa, is not trivial except for simple cases. Furthermore, is not clear to what extent the *nonlinear* mapping  $\Phi : \mathbb{R}^n \rightarrow \mathbb{R}^n$  can provide insight into the behavior of the reaction networks, even for the case where the dimension is the same: nonlinear mapping does nor preserve, in general, the form of the reactant complexes nor the behavior of the mass action network. It is paramount to derive conditions so that the set  $\bar{\mathbb{R}}_+^n$  be invariant for the composition of maps.

On the other hand, the CRNT is a powerful tool which theoretically enables us to study BCRNs for which kinetic constants are not fully available, such as in the neurodegenerative disease caused by Prions. Implementation of the CRNT on

## Conclusions and Further Research

---

a Prion disease autocatalytic CRNs in Chapter 5, shown the existence of bistability and sustained oscillations. Sustained oscillations of cellular and scrapie prion protein concentrations were conjectured to be related with flare-ups, *i.e.* the recurrence of symptoms or an onset of more severe symptoms [52]. Other tools from the control literature, such as the design of robust (*e.g.* against parameter uncertainty) state observers, can be fruitfully complemented with the CRNT to understand other diseases and provide insight to physicians.

# Bibliography

- [1] L. Gyorgy and R. J. Field. Simple models of deterministic chaos in the belousov-zhavotinsky reaction. *J. Phys. Chem.*, 95:6594–6602, 1991.
- [2] M. Eiswirth, A. Freund, and J. Ross. *Mechanistic classification of chemical oscillators and the role of species*, volume 80 of *Advances in Chemical Physics*. 1991.
- [3] I. R. Epstein and J. A. Pojman. *An introduction to nonlinear chemical dynamics*. Oxford University Press, 1998.
- [4] B. L. Clarke. *Stability of complex reaction networks*, volume 43 of *Advances in Chemical Physics*. 1980.
- [5] T. M. Leib, D. Rumschitzki, and M. Feinberg. Multiple steady states in complex isothermal cfsrs-i. general considerations. *Chem. Eng. Sci.*, 43(2):321–328, 1988.
- [6] A. Isidori. *Nonlinear control systems*. Springer–Verlag, 3rd. edition, 1995.
- [7] H. Nijmeijer and A. J. van der Schaft. *Nonlinear dynamical control systems*. Springer–Verlag, 3rd edition, 1995.
- [8] J. J. E. Slotine and W. Li. *Applied nonlinear control*. Prentice-Hall, 1991.

## Bibliography

---

- [9] P. Ellison and M. Feinberg. How catalytic mechanism reveal themselves in multiple steady-state data: II. an ethylene hydrogenation example. *Journal of Molecular Catalysis A: Chemical*, 154:169–184, 2000.
- [10] G. Craciun, Y. Tang, and M. Feinberg. Understanding bistability in complex enzyme-driven reaction networks. *Proceedings of the National Academy of Sciences of the USA*, 103(23):8697–8702, June 2006.
- [11] P. Ellison and M. Feinberg. How catalytic mechanism reveal themselves in multiple steady-state data: I. basic principles. *Journal of Molecular Catalysis A: Chemical*, 154:155–167, 2000.
- [12] D. L. Nelson and M. M. Cox. *Lehninger. Principles of Biochemistry*. W. H. Freeman, 4th edition, April 2004.
- [13] J. M. Méndez and R. Femat. Mechanisms of prion disease progression: a chemical reaction network approach. *IET Syst. Biol.*, 5(6):347–352, July 2011.
- [14] R. M. Noyes. Stoichiometric factor in the oregonator model. *J. Phys. Chem.*, 80:6071–6078, 1984.
- [15] Z. Noszticzius, H. Farkas, and Z. A. Schelly. Explodator: a new skeleton mechanism for the halate driven chemical oscillators. *J. Phys. Chem.*, 80:6062–6070, 1984.
- [16] I. Prigogine and P. Lefever. Symmetry breaking instabilities in dissipative systems. ii. *J. Chem. Phys.*, 48(4):1695–1700, 1968.
- [17] R. M. Noyes, R. J. Field, and E. Koros. Oscillations in chemical systems. i. detailed mechanism in a system showing temporal oscillations. *Journal of the American Chemical Society*, 94:1394–1395, 1972.

## Bibliography

---

- [18] R. J. Field and R. M. Noyes. Oscillations in chemical systems. iv. limit cycle behavior in a model of a real chemical reaction. *J. Chem. Phys.*, 60:1877–1884, 1974.
- [19] D. Zhang, L. Gyorgy, and W. R. Peltier. Deterministic chaos in the belousov-zhabotinsky reaction: experiments and simulations. *CHAOS*, 3(4):723–745, 1993.
- [20] G. Craciun and C. Pantea. Identifiability of chemical reaction networks. *J. Math. Chem.*, 44:244–259, 2008.
- [21] G. Szederkényi and K. M. Hangos. Finding complex balanced and detailed balanced realizations of chemical reaction networks. *J. Math. Chem.*, 49:1163–1179, 2001.
- [22] N. D. Evans, M. J. Chappell, M. J. Chapman, and K. R. Godfrey. Structural indistinguishability between uncontrolled (autonomous) nonlinear analytic systems. *Automatica*, 40:1947–1953, 2004.
- [23] S. Schnell, M. J. Chappell, N. D. Evans, and M. C. Roussel. The mechanism distinguishability problem in biochemical kinetics: the single-enzyme, single-substrate reaction as a case study. *C. R. Biologies*, 329:51–61, 2006.
- [24] M. D. Johnston and D. Siegel. Linear conjugacy of chemical reaction networks. *J. Math. Chem.*, 49:1263–1282, 2011.
- [25] G. Szederkényi, J. R. Banga, and A. A. Alonso. Inference of complex biological networks: distinguishability issues and optimization-based solutions. *BMC Systems Biology*, 5(177), 2011.
- [26] M. Feinberg. Complex balancing in general kinetic systems. *Arch. Rational Mech. Anal.*, 49:187–194, 1972.

## Bibliography

---

- [27] Y. A. Kuztenov. *Elements of applied bifurcation theory*. Springer, 2nd. edition, 1998.
- [28] M. Feinberg and P. R. Ellison. The chemical reaction network toolbox. Version 1.1a, <http://www.chbmeng.ohio-state.edu/~feinberg/crnt>, 2000.
- [29] O. M. Temkin, A. V. Zeigarnik, and D. Bonchev. *Chemical Reaction Networks: A graph-theoretical approach*. CRC, 1996.
- [30] M. Feinberg. Chemical reaction network structure and the stability of complex isothermal reactors-i. the deficiency zero and deficiency one theorems. *Chem. Eng. Sci.*, 42:2229–2268, 1987.
- [31] P. R. Ellison. *The advance deficiency algorithm and its applications to mechanism discrimination*. PhD thesis, University of Rochester, 1998.
- [32] M. Feinberg. Chemical reaction network structure and the stability of complex isothermal reactors-ii. multiple steady states for networks of deficiency one. *Chem. Eng. Sci.*, 43:1–25, 1988.
- [33] S. Klamt. Fluxanalyzer. Max-Planck Institut Magdeburg. An interactive program in Matlab, available upon request, 2002.
- [34] R. Gilmore and M. Lefranc. *The topology of chaos*. John Wiley and Sons, 2002.
- [35] G. Bastin and D. Dochain. *On-line estimation and adaptive control of bioreactors*, volume 1 of *Process Measurement and Control*. Elsevier Science, 1990.
- [36] D. Dochain and P. A. Vanrolleghem. *Dynamical modeling and estimation in wastewater treatment processes*. IWA Publishing, 2001.

## Bibliography

---

- [37] G. Nicolis and I. Prigogine. *Self - organization in non - equilibrium systems : from dissipative structures to order through fluctuations*. John Wiley and Sons, 1977.
- [38] J. Toth. Multistationarity is neither necessary nor sufficient to oscillations. *J. Math. Chem.*, 25:393–397, 1999.
- [39] A. Sensse. *Convex and toric geometry to analyze complex dynamics in chemical reaction systems*. PhD thesis, Otto-von-Guericke-Universitat Magdeburg, 2005.
- [40] R. Femat and G. Solis-Perales. Synchronization of chaotic systems with different order. *Phys. Rev. E*, 65, 2002.
- [41] T. Wilhelm. The smallest chemical reaction system with bistability. *BMC Systems Biology*, 3(90), 2009.
- [42] A. Aguzzi, C. Sigurdson, and M. Heikenwaelder. Molecular mechanisms of prion pathogenesis. *Annu. Rev. Pathol. Mech. Dis.*, 3:11–40, 2008.
- [43] F. E. Cohen and S. B. Prusiner. Pathological conformations of prion proteins. *Annu. Rev. Biochem.*, 67:793–819, 1998.
- [44] J. C. Watts, A. Balachandran, and D. Westaway. The expanding universe of prion diseases. *PLoS Pathogens*, 2:152–163, 2006.
- [45] J. Masel, V. A. A. Jansen, and M. A. Nowak. Quantifying the kinetic parameters of prion replication. *Biophys. Chem.*, 77:139–152, 1999.
- [46] M. Laurent. Autocatalytic processes in cooperative mechanisms of prion diseases. *FEBS Lett.*, 407:1–6, 1997.
- [47] V. Vitagliano and G. D’Errico. A simple kinetic model to describe the progression of prion disease. *Phys. Chem. Chem. Phys.*, 3:4547–4550, 2001.



## Bibliography

---

- [48] I. V. Baskakov, G. Legname, S. B. Prusiner, and F. E. Cohen. Folding of prion protein to its native  $\alpha$ -helical conformation is under kinetic control. *J. Biol. Chem.*, 276(23):19687–19690, 2001.
- [49] V. Chellaboina, S. P. Bhat, W. M. Haddad, and D. S. Bernstein. Modeling and analysis of mass action kinetics. *IEEE Control Syst. Mag.*, 29(4):60–78, 2009.
- [50] K. J. Ryan and C. G. Ray. *Sherris Medical Microbiology. An introduction to infectious diseases*. McGraw–Hill, 4th. edition, 2004.
- [51] B. D. Aguda and A. Friedman. *Models of cellular regulation*. Oxford University Press, 2008.
- [52] S. Iwami, Y. Takeuchi, Y. Miura, T. Sasaki, and T. Kajiwara. Dynamical properties of autoimmune disease models: Tolerance, flare–up, dormancy. *J. Theor. Bio.*, 246:646–659, 2007.
- [53] J. A. Bondy and U. S. R. Murty. *Graph theory with applications*. University of Waterloo Ontario, Canada, 1976.

## A. Research articles

The following publications describe portions of this dissertation:

1. J. M. Méndez and R. Femat. Mechanisms of prion disease progression: a chemical reaction network approach. *IET Syst. Biol.*, 2011, Vol. 5, No. 6, p. 347 – 352.
2. J. M. Méndez and R. Femat. Dynamical equivalence in tangent spaces from vector fields of chemical reaction networks. *Chem. Eng. Sci.*, in press, 2012.
3. J. M. Méndez and R. Femat, On Brussleator and Oregonator as chemical reaction networks: a graph approach, Proceedings of the Congreso Nacional de la Asociación de México de Control Automático, Zacatecas, Zac., México, 2009, J. A. Gallegos et. al. (eds).
4. J. M. Méndez and R. Femat, Toward a Dynamical Equivalence between Brusselator and Oregonator: A Lie based approach. Proceedings of the Congreso Nacional de la Asociación de México de Control Automático, Puerto Vallarta, Jalisco, México, 2010, p. 423 – 427.
5. J. M. Méndez and R. Femat. On bifurcation of a chemical reaction network for Prion disease. Proceedings of the Third IFAC Conference on Analysis and Control of Chaotic Systems, Cancún, México, 2012.

6. J. M. Méndez and R. Femat. On the controllability of two linear confoundable chemical reaction networks. Proceedings of the XXXIII Encuentro Nacional y II Congreso Internacional de la AMIDIQ, San José del Cabo, BCS, México, 2012, p. 2599 – 2603.



# Mechanisms of prion disease progression: a chemical reaction network approach

J.M. Méndez R. Femat

Laboratorio para Biodinámica y Sistemas Alineales División de Matemáticas Aplicadas, IPICYT, Camino a la Presa San José 2055, Col. Lomas 4a. sección C.P. 78216, San Luis Potosí, México  
 E-mail: rfemat@ipicyt.edu.mx

**Abstract:** Fatal neurodegenerative diseases such as bovine spongiform encephalopathy in cattle, scrapie in sheep and Creutzfeldt–Jakob disease in humans are caused by prions. Prion is a protein encoded by a normal cellular gene. The cellular form of the prion, namely  $\text{PrP}^C$ , is benign but can be converted into a disease-causing form (named scrapie),  $\text{PrP}^{\text{Sc}}$ , by a conformational change from  $\alpha$ -helix to  $\beta$ -sheets. Prions replicate by this conformational change; that is,  $\text{PrP}^{\text{Sc}}$  interacts with  $\text{PrP}^C$  producing a new molecule of  $\text{PrP}^{\text{Sc}}$ . This kind of replication is modelled in this contribution as an autocatalytic process. The kinetic model accounts for two of the three epidemiological manifestations: sporadic and infectious. By assuming irreversibility of the  $\text{PrP}^{\text{Sc}}$  replication and describing a first-order reaction for the degradation of cellular tissue, the authors explore dynamical scenarios for prion progression, such as oscillations and conditions for multiplicity of equilibria. Feinberg's chemical reaction network theory is exploited to identify multiple steady states and their associate kinetic constants.

## 1 Introduction

Prion diseases are infectious neurodegenerative diseases occurring in humans and animals with a lethal outcome (e.g. Creutzfeldt–Jakob and Gerstmann–Straussler–Scheinker diseases in humans). The key issue of prion diseases is at the misfolding of the prion cellular protein,  $\text{PrP}^C$ , into its pathogen form,  $\text{PrP}^{\text{Sc}}$  [1, 2]. The detailed molecular process that changes the structure of  $\text{PrP}^C$  into a rich and lethal  $\beta$ -sheet structure,  $\text{PrP}^{\text{Sc}}$ , and later replication, is not yet fully understood [3]. What is known is that the presence of  $\text{PrP}^C$  is absolutely required for disease progression [1, 2]. The characteristic event in prion diseases is the aggregation of  $\text{PrP}^{\text{Sc}}$  into large amyloid plaques and fibrous structures associated with neurodegeneration; that is, at sufficiently high concentration of  $\text{PrP}^{\text{Sc}}$ , it self-aggregates irreversibly [2]. Replication takes place by inducing the same transition in other pre-existing  $\text{PrP}^C$  molecules through an autocatalytic reaction scheme. By autocatalysis, the protein can self-replicate avoiding the usual process involving polynucleotides, be they RNA or DNA. Actually, the fact that  $\text{PrP}^{\text{Sc}}$  imparts its conformational information on  $\text{PrP}^C$  constitutes a new dogma in molecular biology [2]. Another unique feature of prion diseases is about their trimodal epidemiological manifestations [3], which can be

1. Sporadic: spontaneous misfolding of  $\text{PrP}^C$  into  $\text{PrP}^{\text{Sc}}$ .
2. Infectious: conversion of  $\text{PrP}^C$  to  $\text{PrP}^{\text{Sc}}$  takes place by a pre-existing seed of  $\text{PrP}^{\text{Sc}}$ .
3. Genetic: changes in the letters within the amino acid sequence that code for the  $\text{PrP}^C$  leads to the production of a mutant version of  $\text{PrP}^C$  that acquires the  $\text{PrP}^{\text{Sc}}$  properties.

Efforts to derive a model of  $\text{PrP}^{\text{Sc}}$  replication can be found in the literature [1, 2, 4, 5, and the references therein]. Among them, an autocatalytic mechanism of four species and five reactions that accounts for both sporadic and infectious manifestation was published in [6]. The mechanism exhibits multiple steady states: one unstable and two stable ones. In particular, for the concentration of  $\text{PrP}^{\text{Sc}}$ , one stable steady state does not support the prion disease progression; the second one evolves into the outbreak of the disease. This reaction mechanism is able to switch between the steady states depending upon external factors such as possible changes in metabolic processes (sporadic manifestation) or the external addition of  $\text{PrP}^{\text{Sc}}$  (infectious manifestation). Kinetic constants encode these external disturbances that influence the dynamical behaviour of the system. Although this mechanism mimics the progression of prion diseases [6], some assumptions are invalid at the light of experimental evidence probably unknown at the time of publication; for instance, the reversibility of the autocatalytic replication of the  $\text{PrP}^{\text{Sc}}$ . Once the  $\text{PrP}^C$  changes its natural conformation due to the interaction with  $\text{PrP}^{\text{Sc}}$  molecules, the latter holds up because it is thermodynamically stable [7]. Furthermore, assumptions in [6] lead to a polynomial differential equation that is not a valid mass action kinetic (MAK)-ordinary differential equation (ODE) [8]. Thus, there are non-negative initial conditions leading to negative concentrations, that is, the sets  $\mathbf{R}_{\geq 0}^n$  and  $\mathbf{R}_{> 0}^n$  are not forward invariant for the vector field in [6].

We present an alternative version of the autocatalytic mechanism, written within the chemical reaction network theory (CRNT) framework [9]. The MAK-ODEs induced

Contents lists available at [SciVerse ScienceDirect](http://www.sciencedirect.com)

Chemical Engineering Science

journal homepage: [www.elsevier.com/locate/ces](http://www.elsevier.com/locate/ces)

# Dynamic equivalence in tangent spaces from vector fields of chemical reaction networks

J.M. Méndez, R. Femat\*

IPICYT, División de Matemáticas Aplicadas, Grupo de Biodinámica y Sistemas Alineales, Camino a la Presa San José 2055, Col. Lomas 4a. Sección, C.P. 78216 San Luis Potosí, S.L.P., Mexico

## HIGHLIGHTS

- ▶ We use Lie algebra of derivations to construct diffeomorphic maps from reaction networks.
- ▶ We propose a definition of dynamical equivalence by composing diffeomorphic maps.
- ▶ Oscillatory chemical reaction networks as a proof of concept for dynamical equivalence.
- ▶ Dynamical equivalence among chemical reaction networks following mass action kinetics or not.

## ARTICLE INFO

### Article history:

Received 29 April 2011  
 Received in revised form  
 18 May 2012  
 Accepted 26 June 2012

### Keywords:

Autocatalytic kinetics  
 Nonlinear dynamics  
 Belousov–Zhabotinsky reaction  
 Lie algebra  
 Dynamic equivalence  
 Lie groups

## ABSTRACT

Distinct chemical reaction networks (CRNs) may lead to the same dynamics; this fact has been termed the fundamental dogma of chemical kinetics. We use Lie algebra of derivations to construct a tangent space along trajectories of vector fields, induced by CRNs, such that their dynamical structure is preserved via the construction of a diffeomorphic map  $\Phi$ . Thus, given two CRNs, it is possible to express the states (i.e. chemical species concentration) of one CRN as function of the other and vice versa, via the composition of their diffeomorphic maps. We call these map compositions the *dynamical equivalence*.

© 2012 Elsevier Ltd. All rights reserved.

## 1. Introduction

It is known in Chemical Engineering that more than one proposed chemical reaction network (CRN) may lead to the same dynamics (Hill, 1977). That is, two structural and parametrically different CRNs can stand for the same experimental reality. This lack of *uniqueness* has been termed the fundamental dogma of chemical kinetics (Craciun and Pantea, 2008, and references therein). Thus, it is natural to ask for the structural conditions that candidate CRNs need to satisfy in order to explain the experimental collected data.

Recently, necessary and sufficient conditions have been provided (Craciun and Pantea, 2008) such that two CRNs are capable of inducing the same mass action kinetics (MAK) ODEs under an appropriate selection of kinetic constants. Craciun and Pantea

(2008, see Theorem 4.4) named this feature “confoundability”, where the key point is that the vector space spanned by the linear combination of chemical species located at the left hand of the chemical arrow in both CRNs be no empty. Other contribution in this direction states that two structurally different CRNs are *dynamical equivalent* if they can give rise to the same MAK-ODEs (Szederkényi and Hango, 2001). A concept, technically suitable, is the *indistinguishability* (Evans et al., 2004; Schnell et al., 2006), which is focused on the state space in the sense that two trajectories cannot be distinguished for distinct initial conditions lying at the domain of state vector in a ODE describing chemical kinetics.

In this paper, we have chosen to borrow from geometric control theory a procedure for the construction of diffeomorphic maps,  $\Phi$ , (a differentiable homeomorphism along with its inverse) using Lie derivatives of the output function along the ODEs induced by the CRNs (Isidori, 1995; Nijmeijer and van der Schaft, 1995). We show that, if the inverse  $\Phi^{-1}$  exists, it is possible to map trajectories of one of the systems into the

\* Corresponding author. Tel.: +52 444 8342000; fax: +52 444 8342010.  
 E-mail address: rfemat@ipicyt.edu.mx (R. Femat).